UCRL-11420

University of California

Ernest O. Lawrence Radiation Laboratory

TWO-WEEK LOAN COPY

This is a Library Circulating Copy which may be borrowed for two weeks. For a personal retention copy, call Tech. Info. Division, Ext. 5545

THE INFLUENCE OF OXYGEN ON THE INTERNAL FRICTION OF HIGH PURITY (99.9999%) SILVER FROM 4° TO 1000°K

Berkeley, California

DISCLAIMER

This document was prepared as an account of work sponsored by the United States Government. While this document is believed to contain correct information, neither the United States Government nor any agency thereof, nor the Regents of the University of California, nor any of their employees, makes any warranty, express or implied, or assumes any legal responsibility for the accuracy, completeness, or usefulness of any information, apparatus, product, or process disclosed, or represents that its use would not infringe privately owned rights. Reference herein to any specific commercial product, process, or service by its trade name, trademark, manufacturer, or otherwise, does not necessarily constitute or imply its endorsement, recommendation, or favoring by the United States Government or any agency thereof, or the Regents of the University of California. The views and opinions of authors expressed herein do not necessarily state or reflect those of the United States Government or any agency thereof or the Regents of the University of California.

UCRL-11420

UNIVERSITY OF CALIFORNIA
Lawrence Radiation Laboratory
Berkeley, California

AEC Contract No. W-7405-eng-48

THE INFLUENCE OF OXYGEN ON THE INTERNAL FRICTION OF HIGH PURITY (99.9999%) SILVER FROM 4° TO 1000°K

Michael Wayne Guinan

(Ph. D. Thesis)

December 1965

THE INFLUENCE OF OXYGEN ON THE INTERNAL FRICTION OF HIGH PURITY (99.9999%) SILVER FROM 4° TO 1000°K

Michael Wayne Guinan

Inorganic Materials Research Division, Lawrence Radiation Laboratory, Department of Physics, University of California, Berkeley, California

December 1965

ABSTRACT

Using the resonant bar technique, the decrement and modulus of high purity, oxygen-free silver single crystals (ρ 293°K/ρ 4.2°K $\cong$ 2500) have been measured (at roughly 25 kc) over the range from 4° to 100°K at various strain amplitudes between 10^{-8} and 10^{-5}. The addition of 40 ppm of oxygen or less to high purity silver reduces the internal friction over most of this temperature range by almost two orders of magnitude. It further appears that oxygen can be removed from silver in a completely reversible manner by annealing in vacuo at sufficiently high temperatures. Such treatments not only restore the initial high damping level but also the temperature and strain amplitude dependence characteristic of the oxygen-free material. The kinetics of the desorption of oxygen in a vacuum of about 6×10^{-6} torr have been followed at temperatures between 870° and 1000°K by measuring the changes in the decrement and modulus with time in a crystal initially containing about 40 ppm oxygen. It is found that the decrement recovers in at least two separate stages, one having an activation energy of 0.67 ± 0.06 eV and the other an activation energy of 2.6 ± 0.4 eV. The presence of oxygen also results in a relaxation peak at 365°K, which is not present in oxygen-free silver. A theory is developed which relates the relaxation to the dragging of interstitial oxygen pinning points by moving dislocation. From the

interpretation of these results, the magnitude of the attractive interaction between oxygen and dislocations is estimated to be 0.25 ± .04 eV. The addition of oxygen, since it effectively eliminates dislocation contributions to the internal friction and modulus, proves of value in interpreting the observed behavior of high purity oxygen-free silver.

TABLE OF CONTENTS

Abstract		ii
List of Tables		vi
List of Figures		vii
I.	Introduction	1
II.	Experimental Apparatus and Procedures	19
	A. Apparatus	19
	B. Procedures	38
III.	Results	57
	A. Introduction	57
	B. Time-Dependent Effects	60
	C. The Temperature Dependence of the Damping in 6-9's Silver at Low Strain Amplitudes	67
	D. Influence of Oxygen on the Decrement and Modulus of 6-9's Silver from 4°K to 380°K	72
	E. Strain Amplitude Dependence	76
	F. Kinetics of Oxygen Saturation and Vacuum Desorption	79
	G. Miscellaneous Observations	84
IV.	Discussion	89
	A. Recovery after Mounting or Transfer	94
	B. Internal Friction at Low Temperatures	100
	C. Internal Friction at High Temperatures	146
	D. Internal Friction and Modulus Changes during Oxygen Saturation and Vacuum Desorption	159

TABLE OF CONTENTS, continued

V. Summary and Conclusions 166

A. Dislocation Contributions to the Modulus and Internal Friction of 6-9's Silver 166

B. Influence of Oxygen 169

Acknowledgements 172

References 173

Tables 182

Figures 189

I. INTRODUCTION

Internal friction generally refers to the dissipation of the mechanical energy of a vibrating solid which takes place even when the solid is completely isolated from its surroundings. The study of this internal conversion of mechanical energy to heat might then be expected to provide useful information about the structure of the solid, if the process giving rise to the dissipation can be identified. A number of sources of internal friction in metals have been recognized for some time and were finally put on a firm phenomenological basis by Zener[1] in 1948, prominent examples being the thermoelastic effect and the stress-induced ordering of solute atoms. As early as 1940 Read[2] recognized that the motions of dislocations represent a considerable and perhaps the major source of internal friction in metals. With the development of dislocation theory[3-5], a theoretical basis was later provided for the interpretation of dislocation contributions to internal friction.

Internal friction phenomena were comprehensively reviewed by Nowick[6] in 1953 and since have been the subject of a number of later reviews[7-11]. In particular, the review by Niblett and Wilks[10] was concerned with dislocation contributions to the internal friction in metals. Dislocation contributions to the internal friction in metals can

be broadly grouped into three categories[10,11]: 1) Peaks in the decrement as a function of temperature which presumably correspond to relaxation processes involving dislocations; 2) an amplitude-independent, frequency and temperature dependent 'background' component or components; 3) an amplitude-dependent component which depends on temperature but is at most only slightly frequency dependent. A brief description of the internal friction phenomena associated, directly or indirectly, with dislocations in metal crystals as well as some of the theoretical models advanced to explain them follows.

In the first category, the most obvious feature of the internal friction of deformed or even lightly handled materials is the appearance of a peak (or peaks) at low temperatures ($T < 200°K$). Such peaks were first observed by Bordoni[12] in several f.c.c. metals and later by others in b.c.c.[13] and h.c.p.[14] metals, as well as in ionic crystals[15]. All the experimental evidence indicates that these low temperature peaks, which are loosely termed Bordoni peaks, arise from a relaxation process in which dislocations play an essential role. Much of the interest in the Bordoni peak, both experimental and theoretical, arises from the possibility that the experimentally observed activation energy for the peak may, through a suitable theoretical model, be related to the magnitude of the Peierl's stress[16] in a given material. This possibility was considered in a

general sense by Bordoni[12], and a quantitative model was first proposed by Mason[17]. Mason considered the thermal activation of the entire free length of dislocation lying between pinning points across the Peierl's barrier into the adjacent potential trough to be the activated process. However, the large shift of peak temperature predicted by this model was not subsequently observed in experiment, and Seeger[18] proposed a more detailed model for the activation prosess. In Seeger's model the free length of dislocation moves over the Peierl's barrier by the thermal activation of a relatively short segment of dislocation followed by the lateral motion of the end configurations (kinks) of the segment under the applied stress. Seeger has shown that the kink pair is stable and will separate under the applied stress only if the kink separation is greater than some minimum value, d_{crit}. The barrier which must be overcome by thermal activation is then approximately the sum of the Peierl's energy of the segment, d_{crit}, and the energy required to form two half-kinks. The activation energy for the Bordoni peak, H_B, is then

$$H_B = W_P \, d_{crit} + U_k \qquad \text{(I-1)}$$

where W_P is the Peierl's energy per unit length, and U_k is the energy required to form a kink. The consideration of the thermal generation of kink pairs in detail by Donth[19] has led to a more refined theory[20] which has been able to account quantitatively for most of the experimental facts

relating to the Bordoni peak. Further refinements of the Seeger-Donth theory, in particular the influence of kink motion[21], kink-kink interactions[22], and internal stresses[23] on the relaxation process, which have been considered in an attempt to explain the remaining discrepancies between theory and experiment have not been entirely successful.

Of the various other mechanisms[24] proposed to account for the Bordoni peak, the kink diffusion theory of Brailsford[25] and the dislocation-dipole reorientation theory of Gilman[26] appear on the basis of present experimental evidence to be as reasonable, at least qualitatively, as the Seeger-Donth theory.

Unlike Seeger, who considered a kink to make the transition from one Peierl's valley to the next over a large distance compared to the interatomic spacing, Brailsford[25] has assumed that kinks are abrupt, and that the transition is made in a distance of the order of one atom spacing along the dislocation. Brailsford then shows that the thermally-activated lateral motion of such abrupt kinks under an oscillating stress leads to internal friction of the relaxation type. Again, in contrast to the Seeger-Donth treatment, the kink diffusion model makes use of the dislocations which do not lie along close-packed directions (i.e., those which contain a number of intrinsic or built-in kinks).

Gilman[26] has noted that a prominent feature of the structure of deformed materials is the existence of edge-dislocation dipoles (debris dipoles), which consist of two dislocations of opposite sign on separate glide planes. Such a configuration has two positions of stability, separated by an energy maximum, for which the line between the pair makes an angle of 45° with the slip direction. Small segments of the pair can reorient from one stable position to the other by thermal activation and thus lead to a relaxation type internal friction.

All three of the above theories are possible dislocation relaxation mechanisms in plastically strained solids, and all depend primarily on intrinsic properties of dislocations themselves. The configurations required by each theory, i.e., close-packed dislocations, non-close packed dislocations, and dipoles, are all known to exist in deformed materials. It is possible that all three mechanisms may contribute to anelastic behavior in a single material, although not necessarily in comparable strengths. As regards the Bordoni peak, only further refinement of both theory and experiment can lead to any positive identification as to the mechanism responsible in any given material.

In the temperature range between 100°K-300°K Hasiguti[27] has observed several additional peaks in the

internal friction of a large number of metals immediately following deformation, which appear from his work to be relaxation peaks. From the annealing behavior and activation energies observed, Hasiguti[28] has concluded that dislocations associated with point defects are responsible for the peaks and has proposed a model which is based on the motion of dislocation kinks which are trapped by point defects, and which leads to a relaxation type of internal friction. Observations of internal friction peaks in this temperature range have not been widespread, possibly due to the rapid annealing reported at room temperature.

In deformed b.c.c. metals with interstitial impurities an internal friction peak is observed in the temperature range 100°C-500°C. It is apparent that the presence of both interstitial impurities and dislocations are requisite for the observation[29-31] of the peak which is usually referred to as the cold-work peak (CWP). The activation energy for the peak, in all systems investigated, is about 0.5 eV higher than the activation energy for bulk diffusion of the interstitial which causes the CWP. Of the several theories[9, 30-34] advanced to explain the CWP, only the more recent theories of Boone[31] and of Schoeck[30] appear to be adequate to account for the experimental observations on the peak. Boone and Wert[35] have proposed that the stress induced relaxation of ordered interstitial clusters in the

immediate vicinity of dislocations gives rise to the CWP. Since a detailed treatment of such a model would involve both the size and assumed geometry of the clusters, this theory is necessarily only qualitative. Schoeck[30], on the other hand, has proposed a detailed atomistic model for the CWP, in which the relaxation arises from the motion of dislocations which, in order to move, must drag bound interstitial impurities with them.

A detailed theory of internal friction which falls into both the second and third categories was given by Granato and Lücke[36] (G-L) in 1956. Their model, which is based on earlier ideas put forth by Koehler[37], assumes that dislocations in a metal are pinned by impurities (point defects) with an average spacing L_c and by the nodes of the dislocation network with a spacing L_N. Under a small alternating stress the dislocation segments bow out between pinning points and their motion, which is damped, is like that of a vibrating string and has a resonance character. For most crystals this dislocation resonance is of the order of 100 mc; at much lower frequencies Granato and Lücke have shown that the decrement due to the bowing out of loops is

$$\Delta_I = (120\Omega\Delta_0\Lambda\omega B / \pi^3 C) \cdot L^4 \qquad \text{(I-2)}.$$

where Ω is an orientation factor relating the applied stress to the resolved shear stress on the slip plane; ω, the applied angular frequency; B, the damping constant;

C, the dislocation line tension; Λ , the dislocation density; $\Delta_o = 8Gb^2/\pi^2 C$; G, the shear modulus; and L, the average loop length, is

$$1/L = 1/L_c + 1/L_N.$$

Since the motion of the bowing loops under an applied stress results in an additional non-elastic strain, a modulus defect is also present and is given, according to G-L, by

$$(\Delta E/E)_I = (6\Omega\Delta_o\Lambda/\pi^2) \cdot L^2. \qquad \text{(I-3)}$$

As the stress is further increased, a point is reached at which the force on some pinning point within a network length L_N, arising from the dislocation line tension, exceeds the binding force between this point and the dislocation. Since the force exerted on a pinning point is proportional to the length of adjacent loops, breakaway occurs for all pinning points within the network length, and the dislocation then bows out with a length L_N. As the stress is decreased, the loops, now of length L_N, collapse until they are repinned. This, then, results in a closed, static hysteresis loop every half-cycle, and thus gives rise to an additional amplitude-dependent, but frequency-independent, contribution to the internal friction. By assuming a constant L_N and a Poisson distribution in L_c corresponding to a random impurity distribution along the dislocation line, G-L obtain

$$\Delta_H = (c_1 / \epsilon_0) \exp(-c_2 / \epsilon_0) \tag{I-4}$$

where

$$c_1 = (\Omega \Delta_0 \Lambda L_N^3 / \pi^2 L_c) \cdot c_2 \tag{I-5}$$

and

$$c_2 = (\pi / 4bRE) F_m / L_c, \tag{I-6}$$

In the above expressions, b is the lattice constant, R is a resolved shear stress factor, and F_m is the maxiumum binding force between a dislocation and an impurity pinning point. The degree to which this theory has been substantiated by experimental observations is discussed in detail by Niblett and Wilks[10], and by Gordon[38]. In particular, the L^2, L^4 relation between $(\Delta E/E)_I$ and Δ_I has been well verified[39,40], and the dependence of Δ_H on ϵ_0 given by (I-4) has been observed in a great number of experiments. More recently the vibrating string model has had considerable success in explaining the annealing response of Δ_I in neutron irradiated copper[41]. The major discrepancy between theory and experiment is that the frequency dependence of Δ_I predicted by Eq. I-2 has not been observed at frequencies below 100 kc. This discrepancy may be due in part to the fact that at lower frequencies thermal depinning may cause the effective loop length to increase[42].

A somewhat different view of the role played by impurities with respect to internal friction arising from

dislocation motion has been given by Weertman and Salkovitz[43] and Weertman[44,45]. This theory applies the Mott-Nabarro theory[46] of solid solution hardening to the motion of dislocations under an alternating stress. In this view impurities give rise to a stress field with a wavelength $\lambda = b/c^{1/3}$, where b is the atomic spacing and c is the atomic fraction of impurities. Under an applied stress, dislocation loops can overcome the smallest of the barriers presented by the stress field and thus move a distance of the order of λ. For an alternating stress their motion is hysteretic and for small amplitudes leads to an internal friction[43] of the form:

$$\Delta = \Delta E/E \propto 10^{-2} \Lambda a^2 / (\eta c)^{4/3} \qquad \text{(I-7)}$$

where Λ is the dislocation density, and η is the Cottrell misfit parameter. The model thus leads to an amplitude and frequency independent contribution to the internal friction. In the past there has not been a great deal of experimental support for this view; in particular, the internal friction is usually much more sensitive to the concentration of point defects than Eq. I-7 would indicate. More recently, however, several investigators[47-49] have found some experimental support for certain features of this model.

At high temperatures most metals exhibit an internal friction which rises exponentially with temperature. The experimental observations can be roughly separated into two

groups. The observations which fall into the first group are characterized by relatively high activation energies, of the order of 1-2 eV, and an inverse frequency dependence. Theoretical explanations for this type of internal friction can generally be described in terms of the thermal activation of dislocations over internal stress barriers. The exponential temperature dependence and inverse frequency dependence are then readily explained as the result of a very long relaxation time for the activated process. Dislocation climb[45], vacancy production at dislocation jogs[50], vacancy creep of subgrain boundaries[51], and the formation of jogs by the mutual intersection of dislocations[52, 53] have all been considered as the activated process. The wide range of activation energies observed, 0.8-2.1 eV in copper, for example, suggest that a number of thermally activated processes may contribute to the internal friction at high temperatures.

The second group comprises those observations for which the apparent activation energy is considerably smaller (of the order of a few tenths of an eV). There is also some evidence that this internal friction is independent of frequency[8]. Mason[8,54] has named this type of internal friction "temperature activated hysteresis" and has proposed a model in which the internal friction arises from the exchange of energy between adjacent vibrating dislocation

loops when their mutual pinning point is momentarily lost. The observed activation energy is then the binding energy between the dislocation and the pinning defect. A similar interpretation of these relatively low activation energies can also result from a consideration of the effects of temperature on the models, proposed by Granato and Lücke[36] and Weertman and Salkovitz[43], described previously. The effect of temperature on such models has been treated by Leibfried[55], Teutonico, Granato and Lücke[56], and Friedel[57] from somewhat different points of view.

This completes our not-so-brief account of the expected phenomena and some of the interpretations advanced for them. We would like now to present some considerations pertinent to the present investigation.

The present investigation was undertaken as part of a program to study the influence of oxygen on the mechanical properties of silver and dilute silver alloys[58-60]. There is evidence that oxygen, which is believed interstitial in silver (the activation energy for diffusion is 0.5 eV[61,62] as compared to values of ~2 eV for substitutional solutes) interacts strongly with dislocations as well as with impurities[63] and vacancies[64]. The addition of oxygen to silver thus provides one of the few systems with a face-centered cubic structure in which the interaction of interstitial impurities with dislocations can be studied.

Body-centered cubic metals, containing interstitial impurities have been studied extensively, and it has been found that the binding energy between dislocations and interstitial impurities (0.3-0.5 eV) is considerably greater than that estimated for substitutional impurities (0.1 to 0.2 eV). The increased binding of interstitials to dislocations in the b.c.c. structure arises from the fact that the distortions produced by interstitials have lower symmetry than the lattice and thus introduce a stress field with a shear as well as a hydrostatic component. In addition, the magnitude of the distortion arising from the presence of an interstitial is generally larger than that arising from a substitutional impurity. On the other hand, in the close-packed f.c.c. structure the only interstitial site (the octahedral position) large enough to accommodate an impurity has the same symmetry as the lattice. Furthermore, for silver the misfit of a neutral oxygen atom in this site is comparable to the misfit (~10%) of typical substitutional impurities. On this basis alone, we would not then expect oxygen to be more effective than an equivalent concentration of substitutional impurity in restricting the motion of dislocations in silver.

Experimentally, however, it is observed that oxygen has a much more pronounced effect on the mechanical properties of silver than substitutional impurities. It has

been found[60], for example, that the addition of as little as 100 ppm of oxygen to silver raises the yield stress of silver single crystals by about a factor of three and also results in the introduction of a sharp yield point. Furthermore, it has been observed[59] that the 'background' internal friction at $\sim$1 cps is lowered by more than an order of magnitude by the addition of only 30-50 ppm O_2. The experimental results for other metals and the theories proposed to account for these results indicated that the use of internal friction might provide useful information concerning the interaction of oxygen with dislocations in silver.

Of the various internal friction phenomena, it is apparent that the amplitude-independent 'background' and the amplitude-dependent damping will be most sensitive to the addition of impurities or point defects. In particular, interpretations of experiments on aluminum[65], lead[66], and copper[67, 68] in terms of the theory of Granato and Lücke for the amplitude-dependent component indicated it might be possible to obtain an estimate of the binding energy of oxygen to dislocations by making such measurements over a wide temperature range. Since oxygen is quite mobile in silver, this would require that the measurements be made at temperatures well below room temperature. Additional information on the interaction between oxygen and dislocations

might also be expected from a study of the 'background' internal friction during the addition or removal of oxygen. Such measurements would have to be made at relatively high temperatures.

The primary objective of this investigation, then, is to determine what effect, if any, the addition of oxygen has on both the amplitude-independent and amplitude-dependent components of the internal friction of silver over the temperature range from 4°K to 1000°K. Since a survey of the literature revealed that the relatively few measurements which had been made on silver were concerned with grain boundary relaxations[69-71] in polycrystaline material or with various relaxation peaks observed below room temperature in deformed samples[72-75], this necessarily involves the measurement of these same quantities in oxygen free silver. In addition, it was anticipated that measurements of this type might make it possible to obtain a quantitative estimate of the strength of the interaction between oxygen and dislocations.

A secondary objective of the investigation concerns the possibility of using oxygen, as irradiation-produced point defects have been used, to pin or otherwise restrict the motion of dislocations, thus providing a tool which can aid in interpreting the internal friction phenomena associated with dislocations in silver.

In order to carry out these investigations an apparatus has been designed and constructed to measure the internal friction and Young's modulus over the temperature range from 4°K to 1200°K. The resonant bar technique[6] has been employed because it is particularly suited for measurements over a wide range of strain amplitude. To avoid thermoelastic or grain boundary relaxation effects, single crystal specimens vibrating in a longitudinal half-wave mode have been employed. An electrostatic drive is utilized since this permits measurements to be made over a wide temperature range without the necessity of attaching other materials to the specimen. Because of the strong chemical affinity of oxygen to metallic impurities, silver of the highest purity available has been used, and extreme care has been taken to insure that contamination does not occur in the process of specimen preparation. A description of the apparatus and the experimental procedures followed in the preparation, mounting, and measurement of samples is given in Part II.

Throughout this paper, the logarithmic decrement, Δ, will be used as a measure of the internal friction. This quantity is defined by

$$\Delta = \ln (A_n / A_{n+1}) = dW / 2W \qquad \text{(I-8)}$$

where A_n and A_{n+1} are successive amplitudes of a body oscillating in free decay, dW is the energy dissipated per

cycle, and W is the energy stored in the body. Δ is related to the width of the resonance response curve of a specimen driven in forced oscillation by

$$\Delta = \pi (f_2 - f_1) / \sqrt{3}\, f_m \qquad \text{(I-9)}$$

where f_2 and f_1 are the frequencies at which the amplitude of vibration has fallen to 1/2 of its maximum at the resonant frequency f_m. These relations are valid when the damping is small and independent of amplitude, and must be modified otherwise[6]. They may, however, be used as a good approximation provided the amplitude dependence is not very great, as was the case in the present experiments.

Since internal friction arises from the fact that real materials do not exhibit perfectly elastic behavior, the measured elastic modulus is always lower than the true elastic modulus by an amount ΔE. This difference is termed the modulus defect and is expressed as the ratio $\Delta E/E$. Most theories for the internal friction also lead to expressions for $\Delta E/E$ and, thus, as Nowick[6] emphasized, simultaneous measurements of both Δ and $\Delta E/E$ are of importance in comparing theory and experiment. In accord with the experimental observations, we have separated Δ into two components Δ_I and Δ_H and have taken Δ_I equal to the value of decrement at low strain amplitudes so that we can write

$$\Delta = \Delta_I + \Delta_H. \qquad \text{(I-10)}$$

A similar notation is also used for $\Delta E/E$, viz.

$$\Delta E/E = (\Delta E/E)_I + (\Delta E/E)_H. \qquad \text{(I-11)}$$

The results of the measurements are presented in Part III. In Part IV the results for pure silver and the influence of oxygen are discussed and compared to other experimental results, primarily for copper and aluminum, and, where possible, interpreted on the basis of current theories of internal friction.

II. EXPERIMENTAL APPARATUS AND PROCEDURES

A. APPARATUS

1. General Description. As mentioned previously, measurements are made on specimens vibrating in the half-wave extensional mode. The specimen, in the form of a rectangular bar, is supported vertically between two knife edges at the center, or nodal plane. The decrement is determined either by measuring directly the decay of free vibrations or by determining the width of the resonance response curve in forced oscillation.

An electrostatic drive[76] and an FM detection system are employed to excite and measure, respectively, the specimen vibrations. Both drive and detection are accomplished at one end of the specimen by the use of simple filter networks to separate the respective signals. This combination, first used by Bordoni[72] and later by others[77-79], has two obvious advantages: 1)nothing is attached to the specimen which could affect the measurements or possibly restrict the temperature range over which the decrement can be measured, and 2) only one end of the specimen is utilized thus greatly simplifying the design of the apparatus. The only major disadvantage is the precise alignment necessary for obtaining the required range of strain amplitudes.

With the present apparatus decrements as low as

$1x10^{-7}$ and as high as $5x10^{-2}$ can be measured at strain amplitudes from $5x10^{-9}$ to $1x10^{-5}$. However, the product of decrement and the strain amplitude is limited to a value of approximately $1x10^{-8}$ by the nature of the electrostatic drive system. This is discussed in more detail in part B, section 5.

A feature unique to this apparatus is the wide (2°K to 1200°K) temperature range which can be covered without remounting the specimen. This was made possible by using two separate electrode assemblies of basically similar design, one being employed with a furnace for measurements between 300°K and 1200°K, and the other with a cryostat for measurements from 2°K to 300°K. The specimen holder was interchangeable in the two assemblies, thus allowing the specimen to be transferred without being demounted from the knife edge supports.

2. Specimen Holder and Electrode Assembly. With the electrostatic drive and FM detection system, the driving force and detection sensitivity are both inversely proportional to the square of the specimen-electrode spacing. It is desirable, therefore, to: 1) operate at as small a spacing as possible, 2) maintain this spacing constant, and 3) keep the support losses negligibly small over a wide temperature range. The first requirement can be met only by precise alignment of the specimen and

electrode and the second by allowing for external adjustment of the spacing. In order to satisfy the third requirement without sacrificing the first two, the assembly was made as rigid as possible, taking care to insure that any apparatus resonances were far removed from the desired 10-40 kc operating range.

(a) Specimen Holder. A sketch showing construction details of the specimen holder is given in Fig. 1, and a photograph of a mounted specimen in Fig. 2. The holder is made of Type 304 stainless steel and is threaded for installation in either of the two electrode assemblies. The holder is slotted to accomodate the knife edges, which are held rigidly in contact with a hold-down ring by a pair of set screws. Positive alignment of the holder with respect to the electrode assembly is accomplished by the use of flat parallel ground alignment surfaces.

In the original design, the knife edges were also made of 304 stainless steel with a 45° blade angle. The edges were machined straight to within 0.001 in. and had a maximum edge thickness of 0.001 in. It was found, however, that specimens tended to loosen in these knife edges on being raised to high temperatures. Increasing the initial penetration of the knife edges into the specimen from 0.0005 in. to 0.0015 in. resulted in recrystallization in a narrow band (1/16-in. wide) at the

knife edges, and, in most cases, some loosening still occurred.

The difficulty was eventually traced to the differential thermal expansion between the 304SS knife edges and the 1/8-in. thick silver specimen, which amounts to about 0.001 in. over the temperature range from 300°K to 1000°K. To overcome this problem it was decided to make the knife edges out of a material with just slightly less thermal expansion than the 304SS holder, thus compensating for the higher expansion of the silver specimen. Type 310SS filled this need admirably, giving less than 0.0001 in. differential expansion over the specimen width from 4°K to 1000°K. At the same time, the blade angle was reduced to 25°, and a precision edge was ground to within 0.0002 in. with a maximum edge thickness of 0.0002 in. This was done in order to reduce the deformation caused when the blades are forced into the specimen during mounting. The resulting knife edges proved very successful in eliminating loosening as well as recrystallization. Completely satisfactory mounting was accomplished with an initial blade penetration of 0.0005 in.

(b) Electrode Assembly. The design of the electrode assembly is similar to that used by Fine[80]. A schematic diagram of the electrode assembly and support tube used in the high temperature apparatus is given in Fig. 3. The

assembly used for low temperature measurements differs only in minor details, such as in the design of the support used for the specimen holder. The electrode is held in an insulated holder which is incorporated in a flanged, water-cooled head. Provision is made for micrometer adjustment of the vertical position of the electrode as well as for tilting the electrode to secure optimum alignment with respect to the specimen. The electrode, the electrode holder, and the support tube are fabricated from Type 304SS, while the head assembly is of brass.

The electrode itself consists of a 1/2 in. dia. x 1/8 in. thick disc having a 1 in. long shank which is press fitted into a 5/16 in. dia. x 1/32 in. wall tube. The upper end of this tube is press fitted into an insulating (Lava-A) sleeve in the electrode holder. The vertical position of the electrode is adjusted by a standard micrometer head which can be read to the nearest 0.0001 in. A slotted key together with a ring and collar assembly, which couples the upper end of the electrode holder to the micrometer shaft, gives the electrode a 1 in. vertical travel without rotation. A vacuum tight seal is provided by a double O-ring groove in the water-cooled head. Electrical connection is made through a braided copper wire, insulated with ceramic beads, which is brought out of the system through a Stupekoff seal.

In the unit employed for high temperature measurements, the support tube for the specimen holder consists of a 1½ in. dia. x 0.065 in. wall stainless steel tube approximately 16 in. long, which threads into the brass head. The lower end is also threaded to accommodate the specimen holder, and the threads are polished to eliminate sticking.

A platinum/platinum-10% rhodium thermocouple is introduced through a Stupekoff seal in the brass head. The thermocouple wires, insulated and supported by two-hole alundum spaghetti, are brought down the inside wall of the support tube. Just above the specimen holder the wires are bent so that the thermocouple junction is positioned close to (i.e., within 1/8 in.) but not in contact with the specimen.

Near its lower end, the electrode passes through a close fitting polished alundum collar which is supported horizontally by three set screws threaded into the support tube. Adjustment of the relative positions of the three set screws allows the collar to be positioned off center by as much as 1/8 in. in any direction. This makes it possible to apply a slight tilt to the electrode in order to correct for any misalignment of the specimen.

In the low temperature apparatus the 304SS support tube is 1 in. in diameter and 30 in. long with a 0.028 in.

wall. Vertical alignment of the electrode is provided by a 1 in. long Teflon collar, which fits snugly into the support tube and is attached to the electrode near the lower end. The upper end of the support tube is silver soldered into a brass collar which threads into the electrode assembly. The lower end is silver soldered into a heavy-walled copper can 2 in. in diameter and 5 in. long into which the specimen holder is threaded. After the specimen is installed, a vacuum tight seal is made by soldering a copper lid to the base of the can with Woods metal. Two 1/8 in. dia. holes were drilled approximately 1/2 in. deep into the upper portion of the can to accommodate the Au-2.1%Co/Cu thermocouples used to measure the temperature. The beads of these thermocouples were imbedded in small copper junctions which fit snugly into the 1/8 in. dia. holes. This allowed the thermocouples, which change calibration when heated above about 30°C, to be removed during soldering. Good thermal contact between the copper junction and the specimen can is obtained by securing the junction with a set screw.

3. Vacuum Furnace. To carry out the high temperature measurements, the electrode assembly was inserted in an evacuated stainless steel tube equipped with water-cooled flanges; this tube, in turn, was surrounded by a

resistance wound furnace. The high temperature electrode assembly described above mated with the upper flange, and a connection to the vacuum system was made at the lower flange. This arrangement and some of the details of the furnace construction are shown schematically in Fig. 4.

The 18 in. long furnace was supplied with three independent windings on a 3¼ in. ID alundum tube. The central winding, which was 12 in. long, was of Kanthal while the two end windings were of Nichrome. The latter were approximately 4 in. long and hence they overlapped the center winding by approximately 1 in. at either end.

Preliminary measurements of the vertical temperature gradients showed that, while these could be eliminated by a suitable adjustment of the power in the end windings, the gradients were quite sensitive to the power adjustment. Since the planned experiments included warmup runs over the range from room temperature to 800°C or 900°C, as well as runs at constant temperature, additional thermal ballast was needed. This was provided by placing a copper sleeve (1/2 in. thick x 16 in. long) inside the alundum furnace tube. Subsequent measurements showed that the temperature gradient could be reduced to within 1°C over a central 8 in. length with only crude adjustment of the power input to the end windings. However, the furnace now had a high thermal inertia which proved

somewhat disadvantageous in making rapid changes of temperature.

Chromel-alumel thermocouples placed at the center of each of the three windings near the outer surface of the copper sleeve were used for control purposes. Because of the large thermal mass of the sleeve, a simple on-off controller of the moving vane type, together with an Xactline modulator in series with the control thermocouple (to artificially shorten the control cycle), was found to provide better control than more sophisticated proportional control systems. For periods up to 24 hours the temperature remained constant within ±0.5°C; control within ±1.5°C could be achieved for periods up to two weeks. The end windings were supplied with power continuously, the settings being manually adjusted every 25°C to 50°C to the optimum values determined by the previous gradient measurements.

The controller used, namely a Brown type K pyrometer, was modified by the addition of a clock drive to the control point setting. This made it possible to sweep continuously through the temperature range from 50°C to 800°C at a rate of about 30°C per hour.

The vacuum system consists of a 2½ in. oil diffusion pump backed by a 5 cfm Duo-seal forepump. The diffusion pump is trapped using a liquid nitrogen reservoir equipped

with an automatic fill. A gate valve and roughing manifold allow the system to be pumped from 1 atm. to 10^{-5} mm Hg in approximately 10 minutes. Typical pressures obtained were 6×10^{-6} mm Hg at 750°C with a sample in place and 2×10^{-6} mm Hg at room temperature.

Originally, it was planned to carry out anneals in an inert atmosphere in the hope that the rate of evaporation of silver from the sample might not be too excessive at temperatures up to 900°C. To provide pure, dry helium for this purpose, as well as for use as an exchange gas, a helium purification train was constructed, which consists of three components in the following sequence: 1) a molecular sieve-type drying unit operating at tank pressure, 2) a titanium furnace operating at 800°C, and 3) a liquid nitrogen cooled silica gel trap. Provision for storing the purified helium was also made. However, it was found that, although the actual loss of silver from the sample was negligible, deposition of silver on the electrode surface prevented measurement of specimens which had been held above 750°C for even short periods. This then determined the high temperature limit (1000°K) for measurements on silver.

4. Cryostat. A 4 in. ID stainless steel liquid helium Dewar, obtained from Cryenco, formed the basis of the cryostat. The construction of this Dewar along with

various modifications which were made is illustrated in Fig. 5. The inner 4 in. ID x 36 in. long chamber is double walled and vacuum insulated over the lower 24 in. The inner wall is of stainless steel while the outer wall in contact with the liquid nitrogen reservoir is of copper. The upper 12 in. long section is fabricated from single walled 0.015 in. thick stainless steel. A Styrofoam plug with a central opening large enough to accommodate the 2 in. diameter specimen chamber is inserted in the upper thin-walled portion to prevent its collapse when evacuating the chamber.

The entire chamber is suspended from the top of the 25 liter capacity outer Dewar by a stainless steel collar which is tapped and supplied with an O-ring groove to accommodate a 1/2-in. thick brass cover flange. This flange was machined to provide an O-ring seal for the electrode assembly. It was also equipped with vacuum tight heater and thermocouple feed-throughs as well as fittings for filling and evacuating the inner Dewar.

A Nichrome heater, approximately 8 in. long and capable of supplying up to 100 watts, is placed inside the inner Dewar in order to provide a means for controlling temperature and the warmup rate. This heater is wound in the form of a 3 in. diameter helix on a threaded nylon frame which rests on the bottom of the inner chamber.

When positioned in the cryostat, the bottom of the specimen chamber is located 1½ in. above the base of the inner Dewar and is centered with respect to the heater coil.

With the specimen chamber installed, approximately two liters of liquid helim were required to cool the cryostat from 78°K to 4°K and an additional one liter to cool the transfer tube. The usual practice was to transfer approximately five liters in all so that, after equilibrium was established, the helium level was approximately 2 in. above the top of the specimen chamber. Under these conditions the specimen chamber could be maintained at 4.2°K for more than 24 hours if desired. The temperature could be lowered to approximately 2°K by pumping on the inner Dewar with a mechanical pump.

In making a warmup run, the usual procedure was to reduce the temperature to 2°K and start the warmup with the pump running by supplying power to the heater. With proper manual adjustment of the heater current, the warmup rate could be controlled at 10°K to 15°K per hour. When the last of the helium evaporated, usually somewhere between 30°K and 40°K, the pump was shut off and the pressure in the Dewar was adjusted to $\sim 500\mu$ of He so as to maintain exchange between the heater and specimen chamber. Under these conditions, the equilibrium temperature of the specimen chamber was 80°K. Warmup rates between 10°K and 30°K

per hour could also be maintained to 300°K by suitable control of the power input to the heater.

Above liquid nitrogen temperature, accurate temperature control could be achieved by using the output of the Au-2.1%Co/Cu thermocouple to monitor the power supplied by the heater. Control to within 0.1°K for a 24 hour period was accomplished using a Leeds and Northrup type G proportional control system. If desired, such long term temperature control could be obtained down to temperatures of about 55°K by pumping on liquid nitrogen placed in the inner Dewar.

5. Electronic Measuring Equipment. A block diagram of the equipment used for excitation, detection, and measuring is given in Fig. 6. The dotted lines in the figure indicate alternate signal routes. In part, the present system and those used by previous investigators[77-79] are quite similar, the main differences being in the methods employed in the measurement of the damping.

Three requirements governed the choice or design of the components: 1) low noise level, 2) ease and stability of calibration, and 3) linarity of response. The first requirement was essential if measurements were to be carried out at low ($\sim 10^{-8}$) strain amplitudes. It was also anticipated that the measurements would extend over long periods of time and that a large number of individual measurements

would be made. Hence, from the standpoint of convenience, it was considered desirable to eliminate, insofar as possible, frequent recalibration or tedious correction of the raw data. In the description that follows only those features which are unique to the present system or which were designed to circumbent some experimental difficulty will be described in detail.

(a) Excitation. A General Radio 1301B beat frequency oscillator, capable of supplying up to 50 volts RMS to the specimen, was employed as the source of the drive signal which was applied between the specimen and electrode through a low pass filter. In order to provide the necessary frequency sweep, a clock motor and a ten turn Helipot were coupled to a linear (±0.1 cycle) frequency vernier on the oscillator by means of gear trains. A fixed DC bias across the Helipot yielded a DC signal proportional to the position of the vernier, which covered a 200 cycle frequency range. Through a suitable choice of gears, this same arrangement could also be used to drive the main tuning dial so as to give a wider frequency sweep.

Two alternate methods were employed for exciting the specimen vibrations:

(i) Pure AC Drive. The signal from the oscillator is fed to an amplifier capable of supplying up to 650 volts RMS into the load presented by the low pass

filter and the specimen. In this case, the vibrational frequency of the driving force acting on the specimen is twice that of the oscillator. This is because the driving force is proportional to the square of the potential between the specimen and electrode.

(ii) DC Biased Drive. Up to 1000 volts DC bias obtained from batteries was applied across the electrode along with the AC signal available from the oscillator. In all cases in which this method of excitation was used, the ratio of the DC to the RMS AC signal was greater than 20. Under these conditions the frequency of the driving force is that of the oscillator. The 1000 volt limit on the DC bias or peak AC signal corresponds roughly to the potential at which discharge occurs between the specimen and electrode in vacuum when the normal gap of 0.001 in. is employed.

(b) Detection. The specimen-electrode gap was incorporated, through a high pass filter, in the tank circuit of a conventional 5 mc electron-coupled Hartley oscillator, which is thus frequency modulated by the specimen vibrations. The signal is then amplitude limited and demodulated by a Foster-Seely discriminator. The discriminator balance is indicated on a microammeter ($\pm 10 \mu a$) coupled to the output by an audio filter.

The audio signal, which is proportional to the

specimen amplitude, is amplified and fed through a Krohn-Hite 300 AB variable band pass filter. This filter was usually set to give a 2 kc band width. The RMS value of the resulting signal is measured with a Hewlett-Packard 400D VTVM. Details of the response of the various components and noise levels are given in part B, sections 2 and 5.

(c) Measurement of the Decrement and Resonant Frequency. As mentioned previously, both the resonance method and the decay method were utilized, the former for decrements above about $5x10^{-4}$ and the decay method for measurements of Δ below $5x10^{-4}$. The resonance method can be used at damping levels as low as $1x10^{-4}$, and the decay method up to $1x10^{-2}$; however, above about $5x10^{-4}$ the resonance method gives higher resolution.

(i) The Resonance Method. The 400D VTVM provides an AC output proportional to the scale reading on all ranges. This signal was amplified, rectified, and filtered to give a DC output proportional to the full scale reading and linear down to 1% of full scale. In order to tobtain this degree of linearity with the available 10 volt RMS full-scale signal, a full wave bridge was constructed using Hoffman Uni-tunnel diodes which begin to conduct in the forward direction at less than 50 mv. Trial variation of the bridge load and the full scale input level

resulted in the desired linearity.

This DC signal was applied to the Y-axis of an Electro-Instruments Model 500T X-Y recorder, while the X-axis was driven by the oscillator sweep. Use of the range switch on the VTVM then allowed the strain amplitude at resonance to be varied continuously without falling below about 1/3 of full scale on the VTVM.

Once the initial calibration of the oscillator sweep and rectifier outputs had been made, all of the information (i.e., strain amplitude, resonant frequency, and resonance half-width) required is obtained by sweeping through the appropriate frequency range to record the resonance curve and measuring the oscillator frequency at any convenient point on the X-axis. The oscillator frequency is measured to the nearest 0.1 cycle by taking a 10-second count on a Hewlett-Packard Model 521C counter.

(ii) The Decay Method. Two additional pieces of equipment were built in order to make measurements of the damping in free decay, namely an amplifier with variable 0-20 db. gain (in 1/2 db. steps) and a decay gate. The amplifier provided a constant output to the decay gate for any desired strain amplitude (to the nearest 1/2 db.). The circuit diagram of the transistorized decay gate is given in Fig. 7. Basically, it consists of upper and lower pulse height discriminators which are followed by

an anti-coincidence circuit. The latter is so designed that an output pulse is delivered only when the input pulse height falls between the levels determined by the discriminators.

Both discriminators are continuously variable from 1 v to 10 v. The unit operates satisfactorily from 5 kc to 100 kc and shows little or no drift. Discrimination is extremely good with less than 1% change in signal required at either gate to go from "no count" to "full count." In operation the gates are usually set in the ratio $e^{-1/2}=0.606$ and, prior to decay, the sample amplitude is adjusted just above the upper gate.

With the specimen vibrating at resonance at the desired strain amplitude, the oscillator frequency is recorded as before. The counter input is then switched to the decay gate output, and the drive turned off by a relay which also operates the external gate of the counter. The counter then records the number of oscillations made by the specimen as its amplitude falls by $e^{-1/2}$. If n is number of such counts, the decrement is simply 1/2n. It was found, however, that for values of the decrement of 10^{-5} or lower, the above procedure was inconvenient. At these damping levels the resonance is less than 1 cycle wide which makes adjustment to resonance difficult, especially when changing temperatures at 20°K to 30°K per hour.

Therefore, a phase detector was constructed which, in conjunction with a voltage variable capacitor (Semicap) installed in the oscillator, continuously maintained the specimen at resonance. A circuit diagram of this arrangement is given in Fig. 8. It should be pointed out that the operation of the phase detector depends on comparing the phase of the specimen signal to that of the drive oscillator and, hence, it can only be used with the DC biased drive method described above. The circuit operation is as follows: The reference signal from the General Radio BFO is first fed through a simple phase shift network to allow adjustment for phase shift in the apparatus. The output of the IN1305 transistor used for phase detection is amplified by a Philbrick P-2 solid state DC amplifier and applied across a type 6.8SC20 semicap incorporated in the tank circuit of the variable 200 kc oscillator used in the BFO. A microammeter ($\pm 10\mu a$) in the output circuit provides a visual indication of deviation from balance. Since the circuit is capable of adjusting the oscillator frequency by 50 cycles for a 0.1 cycle deviation from resonance at decrements up to 10^{-4}, only intermittent manual frequency adjustments were required to keep the resonance within the control range.

B. PROCEDURES

1. Specimen Preparation and Handling. Single crystals of both <100> and <111> orientations were grown from "oxygen free" 99.9999% silver* in high purity graphite crucibles by a modified Bridgman technique. After a long high temperature anneal in argon, the crystals were carefully removed from the mold and cut to the desired length by spark erosion. They were then given a light etch to eliminate any surface contamination, after which their weight and dimensions were measured. The specimens were then either stored under argon for future use or transferred to a special mounting jig in which the crystal could be accurately aligned and mounted in the specimen holder. Throughout all of the above procedures elaborate precautions were taken to avoid contamination or deformation of the specimens. For example, the specimens were never picked up by hand or treated in such a way that they were subject to a bending moment. They were always supported horizontally along their entire length when being mounted or otherwise handled, and, once mounted in the specimen holder, they were carried or transported in a vertical position.

*Oxygen-free 69 grade silver supplied by Consolidated Mining and Smelting Co. of Canada Ltd., Electronic Products Division, Spokane, Washington. Their analysis specified less than 0.7ppm oxygen and approximately 0.1ppm Cu, Pb, and Bi as the only detectable impurities.

(a) Growth of Single Crystals. All melting and crystal growing operations were carried out under a dynamic vacuum of approximately 10^{-6} mm Hg in thoroughly outgassed ultra-high purity graphite crucibles.* For this purpose the crucibles were supported vertically inside a long Vycor tube which formed part of an induction heated zone melting unit. Stock material was first prepared by casting the 69 grade Ag into bars of appropriate size and shape. Prior to casting, the graphite mold was outgassed for several hours at 1300°C with the charge suspended above by means of a winch. The charge, previously etched in hot dilute HNO_3 to remove any surface contamination, was then lowered into the crucible and cast into 1/4 in. x 1/8 in. x 5 in. long bars. The silver was held molten under vacuum for about 1/2 hour and then directionally solidified by slowly raising the induction coil.

The resulting bars of silver, along with 2 in. long seed crystals of the desired orientations, were etched in dilute HNO_3, washed, dried, and loaded into machined channels in a previously outgassed split graphite crucible. Crystals were then grown by passing a molten zone vertically through the charge at a rate of about 1 in. per hour. The seed crystals had been prepared in a similar manner from

*Supplied by United Carbon Products, Bay City, Michigan, who specify less than 10 ppm total metallic impurities.

a suitably oriented spherical seed. Four single crystal bars 1/4 in. x 1/8 in. in cross-section and approximately 12 in. long were grown simultaneously, two each of the $\langle 111 \rangle$ and $\langle 100 \rangle$ orientations. Seed orientations were selected so that the 1/4 in. wide surfaces of the crystals were parallel to $\{110\}$ in both cases. The orientations were subsequently checked by the standard Laue back reflection technique and found to lie within $\pm 2°$ of the desired orientations.

Before being cut to appropriate length, the as-grown crystals were annealed in high purity argon for 5 days at 900°C and furnace cooled at 20°C per hour to room temperature. This was accomplished by placing the graphite crucible containing the crystals in a fused quartz tube which was subsequently outgassed to 1×10^{-7} mm Hg at 300°C, flushed and filled with Linde research grade argon. The quartz container was then inserted in a vertical, resistance-heated furnace in which the temperature gradient along the length of the specimens was maintained at less than $\pm 3°C$.

(b) Specimen Preparation. The annealed crystals were now transferred from the split mold to a slotted aluminum tray for cutting. This was done by gently placing the tray over the two crystals in one half of the mold and inverting both the tray and mold as a unit. The

mold then was carefully lifted off leaving the two 12 in. long crystals resting on the tray. Next, the crystals were slid gently into place against the alignment lips on either side of the tray, and Duco cement was applied to hold them firmly in place.

The tray containing the crystals was then inserted in a machined track which was mounted in a "Servomet" spark cutter. This track had previously been aligned so that it was precisely perpendicular to the cutting blades. Several cuts were made simultaneously on the finest cutting range, three 2½ in. long specimens suitable for the internal friction measurements being obtained from each bar. The original seeds and other sections removed were used for orientation and residual resistivity measurements. The Duco cement was dissolved by immersing the tray and the crystals in acetone, and the specimens were then transferred to supporting slings fashioned from 0.001 in. thick Mylar sheet. Transfer was accomplished by gently sliding the Mylar between crystal and tray.

With the specimens now supported in the Mylar slings, they are given a light etch in 50% cold HNO_3; this is followed by a half-hour rinse in distilled water and finally by an acetone rinse. After drying, the crystals are weighed to within 0.05 grams and placed on a traveling stage microscope, which is used to measure the specimen

length to the nearest 0.0001 inch. The specimens are then stored, still supported in the Mylar slings, in an argon-filled box or else mounted directly in the specimen holder.

(c) Specimen Mounting Procedure. In order to mount the specimens in the knife edges with a minimum of handling and still obtain the precise alignment which is required, a special mounting jig was constructed. A photograph of the jig is given in Fig. 9. The specimen holder itself is located in a split collar in which the two opposing micrometer heads, used to adjust the knife edges, are inserted. The vee blocks are of Teflon and serve to maintain the specimen axis accurately perpendicular to the alignment surfaces on the specimen holder. Adjustment of the position of the crystal between the knife edges to within 0.0001 in. is accomplished by using the micrometer at one end of the vee blocks.

Mounting is carried out as follows: A polished dummy steel specimen is placed in the vee blocks, and the specimen holder is rotated inside the collar until the knife edges are accurately parallel to the wide specimen dimension. The holder is then clamped in place by tightening down the collar. This done, the knife edges are temporarily retracted and clamped lightly in place against the holding ring with the set screws. The dummy is now removed

and the silver crystal is transferred from its Mylar sling to the vee block. After positioning the specimen with the end micrometer, the opposing micrometer heads are now used to bring the knife blades up to the specimen surface until a diffraction pattern is observed between the specimen and either knife edge. The knife edges are then alternately adjusted in 0.0001 in. steps until each has been advanced by 0.0003 or 0.0004 in. The set screws holding the knife edges are then tightened and the micrometers retracted. Finally, the jig is turned on end into a vertical position and the specimen holder is carefully removed from the collar and inserted in one of the two electrode assemblies.

2. Strain Amplitude Calibration. In this section the method used to determine the detection sensitivity, i.e., the output signal at the VTVM for a given specimen strain amplitude, will be described and a calculation will be given of the strain amplitude to be expected for a given drive voltage. For convenient reference, the symbols and units employed in this and the following sections are listed below:

C_g = specimen-electrode capacitance ($\mu\mu f$)

C_o = effective oscillator capacitance ($\mu\mu f$)

d_g = specimen-electrode spacing (cm.)

L = specimen length (cm.)

A = cross-sectional area of end of specimen (cm^2)

f_H = FM oscillator frequency (cps)

G = system gain

v_d = discriminator output voltage (volts)

v_o = voltage measured at VTVM (rms volts)

ϵ_o = maximum specimen strain amplitude

m = specimen mass (grams)

ρ = specimen density (g/cc)

V_o = drive voltage at specimen (rms volts)

f_m = specimen resonant frequency (cps)

V_D = DC bias between specimen and electrode (volts)

Δ = logarithmic decrement of specimen

E_m = Young's modulus of specimen

The maximum strain amplitude, which occurs at the center of the specimen for the half-wave extensional mode, is given by

$$\epsilon_o = \pi \, \delta L/L \qquad \text{(II-1)}$$

where δL is the displacement of the end of the specimen from its equilibrium position. If we now assume that C_g can be regarded as a parallel plate capacitor with an area equal to the cross-sectional area of the specimen (this assumption was verified by direct measurement), then

$$C_g = 0.569 \, A/d_g \qquad \text{(II-2)}$$

and

$$\delta d_g = -0.569 \, A \;\; \delta C_g \, / \, C_g^2. \qquad \text{(II-3)}$$

The frequency change, δf_H, of the FM oscillator

is related by δC_g by

$$\delta C_g / C_o = -2 \ \delta f_H / f_H. \qquad \text{(II-4)}$$

Equation (II-4) will be taken as the definition of C_o. Noting that

$$\delta L = \delta d_g$$

and substituting Eqns. (II-3) and (II-4) into (II-1) gives

$$\epsilon_o = (1.73 \pi A C_o / L f_H G C_g^2) \gamma v_o , \qquad \text{(II-5)}$$

where the constant γ is defined by

$$\delta f_H = \gamma v_D = \gamma \sqrt{2} v_o / G. \qquad \text{(II-6)}$$

The effective oscillator capacitance, C_o, was determined by measuring f_H with known capacitances ($\pm 1\%$) replacing the specimen-electrode gap, and γ was evaluated by measuring the discriminator output, v_D, as a function of f_H. The linear relationship, (II-6), was found to hold over a ± 100 kc range with $\gamma = 0.304$ mv/cycle. The frequency of the FM oscillator could be tuned over a 500 kc range by means of a ten-turn Duo-dial coupled to the tank capacitor. In operation the oscillator was tuned for zero DC discriminator output, for which $f_H = 5.005$ mc.

A detailed calibration plot of the oscillator dial reading at balance vs. the known capacitance across the specimen-electrode gap provides a quick means of evaluating the specimen-electrode capacitance. Calibrations of this type, as well as determinations of C_o, were carried out

separately for both electrode assemblies. Thus, with a specimen of given length and cross-sectional area mounted in the system, the strain amplitude calibration is made by noting the dial reading at balance with the electrode retracted, and then lowering the electrode until balance occurs at the dial reading corresponding to the desired value of C_g.

In order to provide an independent check or alternate calibration method, the strain amplitude expected for a given value of the damping was calculated from the measured drive voltage, V_o. The equation of motion of the specimen can be written[81]

$$\frac{\partial^2 u(x,t)}{\partial t^2} - \underline{E}\,\frac{\partial^2 u(x,t)}{\partial x^2} = \delta(x-L/2)\,\sigma(t), \qquad \text{(II-7)}$$

where $u(x,t)$ is the displacement from equilibrium at time t of an element of the specimen located at position x with respect to the center, $\sigma(t)$ is the stress applied at one end of the specimen and $\underline{E}$ is the effective modulus. For a simple harmonic driving stress, $\sigma(t) = \sigma_o\, e^{i\omega t}$, and with the boundary conditions

$$u(0,t) = 0 \quad \text{and} \quad \left.\frac{\partial u(x,t)}{\partial x}\right|_{x = L/2} = 0,$$

the steady state solution to equation (II-7) can be shown by the usual method of separation of variables and eigenfunction expansions to be

$$u(x,t) = \sum_{n=0}^{\infty} \mathrm{Re}\left\{ A_n \sin(a_n x) e^{i\omega t} \right\} \qquad \text{(II-8)}$$

where

$$A_n = \left[a_n^2 (\underline{E}/\rho) - \omega^2 \right]^{-1} \sigma_o / L \qquad \text{(II-9)}$$

and

$$a_n = (2n + 1)\pi/L. \qquad \text{(II-10)}$$

If the driving frequency is equal to that of one of the normal modes, i.e.,

$$\omega = \omega_n = \sqrt{a_n^2 \ \underline{E}/\rho} \ , \qquad \text{(II-11)}$$

and we allow for the presence of damping[6] by substituting

$$\underline{E} = E_o \ (1 + i \ \Delta/\pi) \qquad \text{(II-12)}$$

Eq. II-8 becomes

$$u(x,t) = (\pi\sigma_o/\omega_n^2 \ L\Delta)\sin\left[(2n+1)\pi x/L\right].\sin\omega_n t. \qquad \text{(II-13)}$$

For the fundamental mode (n=0) the solution at resonance is then

$$u(x,t) = (\sigma_o/4\pi L f_o^2 \Delta)\sin(\pi x/L)\sin(2\pi f_o t). \qquad \text{(II-14)}$$

Since $\epsilon(x,t) = \partial u/\partial x$, the maximum strain amplitude is

$$\epsilon_o = (1/4f_o^2 \ L^2\Delta) \ \sigma_o. \qquad \text{(II-15)}$$

We must now express σ_o in terms of the drive voltage. The stress at the end of the specimen for an applied voltage, V, of angular frequency ω_D, is

$$\sigma = V^2 \ / \ (9\text{x}10^4)8\pi d_g^2, \qquad \text{(II-16)}$$

where

$$V = V_D + \sqrt{2}\, V_o \sin \omega_D t,$$

so that

$$V^2 = (V_D)^2 + V_o^2 + 2\sqrt{2}\, V_D V_o \sin\omega_D t - V_o^2 \cos 2\omega_D t. \qquad \text{(II-17)}$$

It is seen that for $V_D=0$ the dominant term is $-V_o^2 \cos 2\omega_D t$, whereas, for $V_D \gg V_o$ the term $2\sqrt{2}\, V_D V_o \sin\omega_D t$ predominates. Thus, for the pure AC drive we have, in terms of measured parameters,

$$\sigma_o = (8.77 \times 10^{-6}) V_o^2\, c_g^2 \,/\, A^2. \qquad \text{(II-18)}$$

For any given specimen, Eqs. II-5 and II-15 can be written in the form

$$\epsilon_o = \alpha\, v_o \,/\, c_g^2\, G \qquad \text{(II-19)}$$

and

$$\epsilon_o = \beta\, c_g^2\, V_o^2 \,/ \Delta f_o^2 \qquad \text{(II-20)}$$

where α and β are constants which depend only on the specimen dimensions and the fixed parameters of the system, namely, C_o and γ. These expressions can be combined to give

$$\Delta = \beta G c_g^4\, V_o^2 \,/\, \alpha\, v_o f_o^2 \,. \qquad \text{(II-21)}$$

The decrement was calculated periodically from this expression and compared with the measured decrement to be sure that the system response had not changed. Agreement within a few per cent was generally obtained. The calibration was rechecked if the calculated and measured

values did not correspond within ±4%.

The long term stability of the system response was found to be very good with the exception of the variable band pass filter. The insertion loss of this unit was quite sensitive to small changes in the characteristics of tubes employed and to the band pass settings. Therefore, before each run the band pass was adjusted for a constant insertion loss of 2 db. over a 1 kc wide range; this corresponded to a 4-6 kc band width setting.

3. Temperature Measurements.

(a) High-Temperature Apparatus. The output of a calibrated Leeds and Northrup platinum/platinum-10% rhodium thermocouple is recorded by a type G Speedomax equipped with automatic cold junction compensation and having a full scale sensitivity of two millivolts. This allowed the thermocouple EMF to be read to the nearest 1 μv, giving a sensitivity to temperature change of 0.1°K. No differences within ± 2μv could be detected between the recorded EMF and that measured with a potentiometer using a distilled water-ice bath reference. The calibrated output of the thermocouple agreed with the standard tables to within 0.5°K over the range from 300°K to 1300°K.

The largest source of uncertainty in the measurement of the specimen temperature arises from the fact that

the thermocouple is not in actual contact with the specimen. On continuous heating or cooling in vacuum ($\sim 10^{-6}$ mm Hg) at about 30°K per hour it was established, by hysteresis measurements, that the specimen temperature lags behind or leads that of the thermocouple by approximately 1.5°K. Below about 500°K the temperature lag in vacuum was somewhat greater; hence, in this range, a low pressure of He was used as an exchange gas.

(b) Low Temperature Apparatus. The output of the calibrated Au-2.1%Co/Cu thermocouple, which measures the temperature of the copper specimen can, was displayed on the same recorder described above. This provided a sensitivity to temperature change of ±0.5°K between 2°K to 6°K, and better than ±0.05°K above 15°K. The thermocouple was calibrated at the boiling points of He (4.2°K), H_2 (20°K), and N_2 (78°K) using ice-distilled water reference bath as a standard. The measured outputs were compared with those tabulated by Powell et al[82]. It was found that good agreement with the published table was obtained for each of the three calibration values when the corresponding tabulated values were multiplied by 97.47 ±0.01%. Using this conversion, a new table was then constructed from which thermocouple EMF could be converted directly to temperature.

It is known that the Au-2.1%Co alloy used is not

stable when heated above about 325°K. Therefore, to avoid recalibration before or after each run, the thermocouple junction was never heated above this temperature; only rarely, in fact, was it warmed above 300°K. Nevertheless, it was recalibrated after a period of six months, and it was found that the EMF at 4.2°K (with a 0°C reference) had changed by only 6 μv out of 9.6 mv. A trial warmup run was also made using a dummy silver specimen to which a second calibrated Au-2.1%Co/Cu couple was attached. With approximately 20 μ of He exchange gas in the specimen chamber, no lag was observed between the temperature of the specimen and the can up to 40°K when the warmup rate was maintained at 20°K per hour. At the same warmup rate the lag was less than 1°K in the range from 40°K to 300°K. Similar results were obtained from hysteresis measurements at temperatures above 80°K. Hence, even without corrections for lag, the maximum uncertainty in the measurements of the specimen temperature is believed to be only ± 2°K.

4. Operating Procedures. In most cases, the decrement and the resonant frequency were measured as a function of time for several hours to as long as several days after the specimen was mounted in the high temperature apparatus. This was done at various temperatures between room temperature and 150°C in order to follow the so-called Köster effect, the recovery of Δ and f_o after deformation.

The first measurement could generally be made within about 10 or 15 minutes after mounting at room temperature. At higher temperatures, the specimen did not reach equilibrium until 10 to 20 minutes after it was inserted in the pre-heated furnace, so that the first measurement was made approximately 1/2 hour after mounting.

Using either apparatus, the decrement could conveniently be measured as a function of time, and hence temperature, during a continuous warmup or cooling run. The time corresponding to each measurement was determined to the nearest 0.1 minute using a digital clock which was synchronized with the strip chart on which the furnace or cryostat temperatures were recorded. Generally, only about 30 to 40 seconds were required to measure both the decrement and the resonant frequency by either the decay or resonance methods. Measurements could, therefore, be made as close together as 1/2°K, if desired, even at warmup rates of 30°K per hour. An exchange gas was used in all runs made in the low temperature apparatus. Measurements of Δ as a function of the pressure of the exchange gas showed that acoustic radiation losses contributed less than 1×10^{-7} to the decrement at pressures up to 1000 μ.

In the low temperature apparatus, the FM oscillator frequency, with the electrode retracted, was independent of temperature over the whole range. However, in the high

temperature apparatus the oscillator frequency decreases with increasing temperature, probably due to changes in C_o associated with the temperature dependence of the dielectric constants of the insulators employed. Several dummy runs were made, and the effect was found to be quite reproducible. Appropriate corrections could, therefore, be applied to the oscillator setting so as to maintain the strain amplitude calibration during a continuous heating or cooling run.

Measurements of the strain amplitude dependence at a fixed temperature were usually made starting at the lowest amplitude and going on up to the maximum attainable. The specimen was never excited at high amplitudes for more than 10 to 15 seconds during these runs. Immediately after the highest amplitude was reached (e.g. within 30 seconds) repeat measurement was made at lower strain amplitudes to check for any permanent changes or time-dependent effects. Measurements at close intervals of strain amplitude could be made over the entire range in approximately one hour.

Oxidation treatments were carried out in the measuring apparatus with the specimen in place. The crystals were saturated with oxygen under static conditions at oxygen pressures up to 1500 mm Hg and temperatures up to 850°K. It was originally planned to make measurements of the decrement and resonant frequency during saturation as

well as during subsequent removal of the oxygen in a high vacuum. However, it was found that it was impossible to make measurements with oxygen in the system at temperatures above approximately 500°K due to ionization. Thus, the specimen could only be measured at close intervals of time during the desorption process.

5. Limits on Range and Accuracy.

(a) Temperature. The operating range of the apparatus, as designed, is from 2°K to about 1200°K. However, as was pointed out earlier, the evaporation rate of silver is such as to preclude measurements at temperatures much above 1000°K. Although the absolute accuracy of any single temperature measurement is ±2°K, the relative specimen temperatures determined during any individual run are known to be better than ± 0.2°K.

(b) Strain Amplitude. In evaluating the strain amplitude from Eq. II-5, the largest source of error arises from the uncertainty in value chosen for C_g. It is estimated that this quantity can be determined to within ± 3% so that the absolute accuracy of strain amplitudes quoted herein is ±6%. However, relative strain amplitudes, such as are obtained during measurements of Δ as function of strain amplitude, are reliable to better than 0.5%. The strain amplitude range which can be covered depends on the

noise level, the specimen-electrode spacing, and the value of the decrement at the highest strain amplitude used. It was found that reproducible measurements could not be made for signal-to-noise ratios less than five. This limited the lowest strain amplitudes obtainable with a 0.001 in. gap to about 10^{-8}. However, on a few particularly well-aligned specimens, measurements have been made at strain amplitudes as low as 3×10^{-9}. As noted previously, the upper limit on the strain amplitude is usually determined by breakdown discharge across the specimen-electrode gap. For a 0.001 in. gap in a vacuum of the order of 1×10^{-5} this occurs at $\sim$1000 volts. Consequently, the product $\Delta\epsilon_o$ is limited to values less than about 1×10^{-8} depending on the type of drive used.

(c) Decrement. The precision with which the decrement can be measured is better than $\pm 1\%$ when the signal-to-noise ratio exceeds a value of 5. The figure $\pm 1\%$ represents the actual reproducibility of duplicate measurements by the resonance method or of successive measurements by the decay method. In the range in which precise measurements could be obtained by both methods, agreement between the two was generally within $\pm 2\%$. However, if the decrement is markedly strain amplitude-dependent, the disparity in the two sets of measurements can be as high as 10%.

It is difficult to determine experimentally what portion of the measured decrement is due to support losses and what portion is contributed by the specimen itself. However, it was found that the decrement of one silver specimen dropped from about $3x10^{-3}$ to $5x10^{-6}$ when it was saturated with oxygen at 450°C while mounted in the apparatus. The value $5x10^{-6}$ then represents an upper limit to the external losses at 450°C. Decrements as low as $1x10^{-6}$ have been measured at low temperatures on an internally oxidized Ag-1%Mg specimen. Thus, for pure silver, which exhibits minimum damping values of $\sim 5x10^{-4}$, we can safely assume that the external losses are negligible. If we assume that the external losses simply add to the specimen damping, then, with the resolution of ±1% obtained, any features greater than $\sim 1x10^{-7}$ in the decrement of the oxygen-saturated material would have been visible.

III. RESULTS

A. INTRODUCTION

The results of this investigation have been assembled under six general headings: 1)Time-dependent effects in 6-9's silver including a description of the annealing behavior at high temperatures; 2) the variation of the damping and modulus with temperature at low ($\sim 2\times10^{-8}$) strain amplitudes in oxygen-free 6-9's silver from 4°K to 1000°K; 3) the effect of oxygen on the damping and modulus over this same temperature range; 4) the strain amplitude dependence of the damping at various fixed temperatures in oxygen-free 6-9's silver and in 6-9's silver containing approximately 40 ppm oxygen; 5) the changes in the damping and modulus with time during oxygen saturation and during subsequent vacuum desorption at temperatures between 715°K and 1000°K; 6) miscellaneous observations which do not conveniently fit into any of the above categories.

The logarithmic decrement, Δ, has been used throughout as a measure of the internal friction. Changes in the modulus are usually expressed directly in terms of the measured resonant frequency, f_m. However, in cases where it is desired to compare the magnitude of the modulus change with the corresponding change in Δ, as a function of strain amplitude, for example, the data are given in terms of the fractional change in modulus $\Delta E/E$. Since

the modulus is proportional to the square of the resonant frequency, $\Delta E/E$ is simply related to the change in f_m by

$$\Delta E/E = 2\ \Delta f_m / f_m. \qquad \text{(III-1)}$$

The results reported here comprise over 10,000 separate measurements of the damping and resonant frequency on a total of six separate crystals. More than half of these measurements were made on a single specimen, for which data have been obtained over the entire temperature range in both the oxygen-free and oxygen-saturated condition. A summary of the measurements carried out on each crystal and the sequence in which they were made is given in Table I.

The impurity contents quoted in the table for 6-9's silver refer to the spectrographic analysis provided by the supplier along with the starting material. The crystals grown from this material have not been analyzed directly. However, in order to obtain some indication of the purity level, the residual resistivity ratio $\rho_{273°K} / \rho_{4.2°K}$ was determined on the as-received material, on one of the vacuum cast rods from which the crystals were grown, and on a representative single crystal from the same batch of specimens as those listed in Table I. These measurements were made by the eddy current decay method[83]. The observed resistivity ratios were 4200 for the as-received silver ingot, 2500 for the vacuum cast rod, and 2600 for

the single crystal. Thus, it appears that only minor contamination has been introduced by the melting and crystal growing operations.

It should be mentioned in this connection that the measurement on the as-received material was made on an ingot having a cross section of approximately 3/4-in.x3/4-in. for which the decay time at room temperature was considerably longer than the "ring-time" of the coils employed; in contrast, the other measurements were made using 1/4-in. x 1/8-in. rods for which the decay times at room temperature were only of the order of 1.5 to 2 times the ring-time. Consequently, the resistivity ratios obtained for the vacuum cast rod and for the single crystal definitely represent lower limits, and it is probable that the total impurity concentration does not exceed that of the original silver ingot by more than a factor of two at the very most.

Facilities for measurement of the oxygen content were not available, and, considering the nature of the present experiments, it was felt that the effort needed to develop a suitable analytical technique would probably not be justified. For this reason, the oxygen concentrations quoted throughout this paper were calculated from the solubility data of Eichenauer and Müller[61], whose results have recently been confirmed by Podgurski and Davies[62].

All specimens of any one orientation, although ob-

tained from different bars, were actually grown from portions of the same seed crystal. In the tables and figures which follow the same letter identification is applied to all crystals cut from a single bar. All data reported, with the exception of the strain amplitude dependence measurements at room temperature on specimen 12A, were obtained on <111> oriented specimens. When 12A was annealed at high temperatures extensive recrystallization occurred, which prevented further measurement. Previous examination of the <100> specimens had shown them all to be badly striated, i.e., these crystals generally contained several low-angle grain boundaries running parallel to the growth direction. It is possible that a connection exists between these striations and the extent of recrystallization observed. In any case, it was felt that little would be learned concerning any possible orientation dependence until <100> specimens of perfection comparable to the <111> specimens could be grown.

B. TIME-DEPENDENT EFFECTS

The time-dependent phenomena reported below are of three general types: 1) effects associated with excitation of the specimen at high strain amplitudes, 2) the recovery of the damping and modulus after mounting or transfer, and 3) changes in the damping with time during cyclic annealing

at high temperatures.

1. Effect of Excitation at High Strain Amplitudes. Repeated checks have failed to reveal any pronounced time-dependent effects due to excitation at high ($\sim 5 \times 10^{-6}$) strain amplitudes in 6-9's silver, such as have been observed by other investigators in copper[67], aluminum[65], and lead[84]. An attempt was made, for example, to induce such effects by allowing a specimen to oscillate at $\epsilon_0 = 5 \times 10^{-6}$ for nearly one hour at 400°K. During excitation, the damping at both the high and low amplitudes increased slowly by about 10% and was observed to decay back to its original value in a few hours after excitation was discontinued. It was therefore concluded that time-dependent effects of this kind are not of major consequence and, indeed, cannot be conveniently studied in the 6-9's silver. On the other hand, a pronounced time-dependence was observed in measurements made at 715°K on a specimen containing about 20 ppm oxygen. Since the damping in this crystal was essentially independent of strain amplitude below $\sim 1 \times 10^{-5}$, the result was that the limit $\Delta \epsilon_0 = 10^{-8}$ was reached almost immediately after breakaway, and hence the time dependence could not be followed.

2. Recovery after Mounting. In all specimens of 6-9's silver the damping at low strain amplitudes was observed to decrease, and the modulus, as indicated by the

resonant frequency, to increase progressively with time after mounting. A similar effect, although somewhat reduced in magnitude is observed on transferring the specimen from one apparatus to another. The first measurements after mounting were usually obtained within 15-30 minutes, and the recovery of the damping and modulus was then followed for periods up to three days at various temperatures from room temperature to about 380°K. A typical plot of the recoverable part of the damping, $\Delta_I(t) - \Delta_I(\infty)$, and the change in resonant frequency during recovery, Δf_m, at room temperature is shown in Fig. 10. A similar plot of $\Delta_I(t) - \Delta_I(\infty)$ vs. t at 377°K is given in Fig. 11. When the difference in the values $\Delta_I(t)$ obtained 12 hours apart was less than 3%, the recovery was assumed completed and this value of Δ was taken as $\Delta_I(\infty)$. As can be seen from these figures, the recovery times are of the order of 50 hours at 293°K and 4 hours at 377°K.

The magnitude of this recovery effect was found to vary considerably from specimen to specimen. Thus, the ratio of the initial value of the decrement to that measured after recovery was essentially complete, ranged from 2 to 6 after mounting and from 1.5 to 3 after transfer. It also appears that, in addition to the initial relatively rapid decay of the mounting or transfer damage, a considerably slower recovery process is taking place which leads to

a further reduction in the damping at room temperature by as much as a factor of 50% after times of the order of two months. A summary of all observations of this type is given in Table II. It is considered significant that neither the specimen containing 40 ppm O_2, nor the 1% Mg alloy crystal showed any measurable change in either the damping or modulus after mounting or transfer.

Since the time dependence of the recovery is of some interest, an attempt was made to fit the data to a variety of functional relationships (see Part IV-Section A). The data seem to be best represented by the Granato-Hikata relation[85],

$$\Delta_I(t) - \Delta_I(\infty) = \alpha (1 + \beta t^{2/3})^{-4} . \qquad \text{(III-2)}$$

The full lines drawn in Figs. 10 and 11 are plots of Eq. III-2 using the values of the constants α and β listed in Table II.

2. Annealing at Higher Temperatures. As the temperature is raised to about 320-340°K, after first allowing the crystal to recover at room temperature, the damping is observed to decrease to a level approximately half of the recovered room temperature value. This decrease was at first attributed entirely to annealing but it was observed that, on subsequent cooling to room temperature, the damping was always higher than the value obtained at the annealing temperature by about 20-50%. The results on several

specimens all showed that the damping attains a minimum value somewhere between room temperature and the highest annealing temperature employed. The general trend was for the minimum to shift progressively to higher temperatures as the annealing temperature was increased.

On further increasing the temperature, in steps of 50°K to 100°K, the damping is observed to rise monotonically. Holding at a given temperature for times of from 2 to 15 hours generally resulted in only a small reduction in damping of the order of 10%. The equilibrium values of the damping obtained in three such runs on separate crystals are shown as a function of 1/T°K in Fig. 12. The average holding time at temperature for each of the runs is indicated next to the specimen number. As can be seen from the figure, the data are fitted reasonably well by straight lines at higher temperatures, indicating that the damping at high temperatures can be described by an Arrhenius-type relation

$$\Delta = C e^{-H/RT} \qquad \text{(III-3)}$$

where C is a constant and H the activation energy. The values of H obtained from the slopes of the lines drawn in Fig. 12 are 0.22, 0.25, and 0.33 eV/atom for specimens 34D, 34C, and 23C respectively. Unfortunately, only the annealing run on specimen 34C could be continued beyond this point. It was not possible to carry out additional meas-

urements on crystal 23C because of extensive deposition of silver on the electrode at ~1100°K, while crystal 34D was severely damaged and misaligned when the electrode was accidentally brought into contact with it.

Since annealing at fixed temperatures up to 1000°K resulted in only relatively small decreases in the damping, it was decided to carry out a cyclic annealing treatment on specimen 34C in the region between 500°K and 1000°K. This seemed of interest, because it has been observed[86] by etch pit studies on copper that cycling of this kind results in a larger decrease in the dislocation density than can be produced by a long anneal at a fixed high temperature. The warmup run on specimen 34C was therefore interrupted at about 900°K, and the specimen was allowed to cool overnight to 550°K at roughly 40°K per hour. The values of Δ measured during subsequent heating and cooling cycles are shown in Fig. 13 as a function of 1/T°K. The full lines represent the measurements made on heating. In all cases the heating and cooling rates were maintained between 30°K and 40°K per hour with pauses of about 2 hours being made every 50-100°K in order that equilibrium measurements could be obtained. The dashed line labeled (1) represents the initial warmup. On the curves labeled (2) and (3) measurements were made as close together as every 4°K, while on later runs only the equilibrium points were measured. This

cyclic annealing operation was discontinued when virtually identical results, reproducible to within $\pm 5\%$, were obtained on three successive cooling cycles, numbers (6), (7), and (8). From studies of this type the following observations have been made:

1) The data for any one cycle can be represented as exponential in 1/T. The slope of log Δ vs. 1/T°K (Fig. 13) appears to decrease slightly with each succeeding cycle. Even after as many as eight complete cycles, however, the apparent activation energy, H, has only dropped from 0.25 eV to 0.22 eV.

2) Good reproducibility is achieved in any given cooling and subsequent heating cycle up to about 875°K. This is true both when the temperature is changed continuously or when the temperature is varied in step-wise fashion, and the crystal is held at each temperature for times as long as 4 hours.

3) After warming to temperatures above 875°K, the damping is observed to decrease with time, as indicated by the arrows in Fig. 13, and this annealing process sometimes continued for as long as 48 hours. For example, the annealing kinetics at 1000°K after cycle (3) are shown in Fig. 14, where the change in the decrement and the resonant frequency $\Delta_I(t) - \Delta_I(\infty)$ and $2\Delta f_m/f_m$ are plotted as a function of the time, t, after reaching 1000°K. $\Delta_I(\infty)$

corresponds to the value of Δ_I measured after t = 72 hours. Little can be said concerning the actual functional form of the time dependence since, as can be seen in Fig. 13, considerable annealing has taken place before reaching 1000°K. Thus, neither the initial level of damping, nor the equivalent time at 1000°K are known. However, the magnitude of the modulus change, 2 $\Delta f/f$, during annealing can be compared with the corresponding change in the decrement as is done in Fig. 15. The data appear to fall on a reasonably good straight line, and, since both scales in Fig. 15 are identical, the ratio of $\Delta_I(t) - \Delta_I(\infty)$ to 2 $\Delta f/f$ is nearly unity. This then would indicate that the annealing kinetics are the same for both the modulus and decrement.

4) A reasonably pronounced peak in the damping is observed at about 950°K on each cooling cycle. The nature of this peak is described in more detail in part C below.

C. THE TEMPERATURE DEPENDENCE OF THE DAMPING IN 6-9's SILVER AT LOW STRAIN AMPLITUDES

One of the primary objectives of this work was to obtain measurements over the whole temperature range on a high purity silver crystal in the <u>annealed</u> condition. Such measurements were actually carried out on specimen 34E. However, it is generally observed that the decrement is raised appreciably as a result of transfer, and does not

fully recover. We now believe that the low temperature measurements are really characteristic of very lightly deformed material. In fact, the present low temperature data on silver show a great similarity to previous measurements on other f.c.c. metals which had been lightly deformed. The results obtained at low temperature may, therefore, correspond to a considerably different dislocation structure than that prevailing in the well-annealed specimen measured at higher temperatures.

The manner in which the low amplitude, $\epsilon_0 = 3\text{x}10^{-8}$, decrement and the resonant frequency vary with temperature over the entire range investigated is illustrated in Fig. 16 for crystal 34E. The low temperature measurements shown in Fig. 16 were made five days after transfer of the annealed crystal from the high temperature apparatus to the cryostat. Also plotted in Fig. 16 are the corresponding low temperature measurements on this same crystal after saturating with oxygen at 820°K. Essentially the same general behavior is exhibited in Fig. 17, which represents a composite of the low temperature damping data on crystal 34D and high temperature measurements on crystal 34C.

For descriptive purposes the temperature range may be divided into four parts.

1. <u>4°K - 120°K</u>. From liquid helium temperatures to about 40°K the decrement increases nearly linearly with

temperature. Above this temperature it rises much more rapidly, reaching a plateau or broad maximum between 70°K and 110°K. Superimposed on this characteristic background rise, a number of small peaks or irregularities are evident; these are in general accompanied by steps, which may represent possible modulus defects, in the frequency vs. temperature curve. A summary of the various 'peaks' observed in this temperature range in 6-9's silver is given in Table III. The damping is quite reproducible in this range, and the measurements show little or no scatter.

An expanded plot of the data shown in Figs. 16 and 17 and the results of additional measurements on other crystals in this same temperature range are given in Figs. 19-21. Fig. 19 illustrates the overall reduction in Δ_I after successively longer anneals at room temperature following mounting. As indicated, the upper and lower curves refer to crystal 34C measured after 2 days and 8 weeks of recovery at room temperature, respectively. The middle curve corresponds to crystal 23C after one week at room temperature and is included for comparison. It appears that room temperature annealing has reduced the level of the damping above about 70°K by a relatively greater amount than that below 70°K. Nearly all of the 'peaks' listed in Table III are evident in the uppermost curve of Fig. 19. An expanded plot of f_m for this run is shown in

Fig. 20. Modulus steps corresponding to each of these 'peaks' can also be distinguished, the most noticeable being those at 21°, 43°, 82°, and 92°K.

Fig. 21 shows the results of measurements of the modulus and damping on crystal 34E. This specimen had undergone the cyclic annealing treatment described previously and was allowed to recover 5 days at room temperature after transfer. The low temperature damping spectrum is quite similar to that exhibited by crystal 23C which had received a comparable room temperature anneal.

2. 120°K - 300°K. At least four additional peaks at about 130°K, 170°K, 205°K, and 250°K are observed in this range (see Table III); however, the modulus data exhibit only an overall defect and separate, well-defined steps are not discernible. The measurements of Δ_I in this range seem to be somewhat erratic with variations of the order of $\pm 3\%$ not uncommon. The points plotted in Figs. 16 and 17, in fact, represent averages of 5 or more measurements within each 5° temperature interval.

3. 300°K - 550°K. In this range Δ decreases monotonically with temperature and reaches a minimum at $\sim$550°K as seen in Figs. 16 and 17. Certain irregularities in the damping are also evident. For example, on either heating or cooling several small spikes (these are described more fully in section G) were generally observed (see Fig. 17).

These spikes were not reproducible and were never observed on sweeping through the same temperature range again. They varied in width from as little as 5°K to 50°K. Morever, it was found that the background damping level was generally about 10% higher when this temperature range was traversed on cooling as opposed to heating.

4. 550°K - 1000°K. In this range the damping increases quite smoothly with temperature, and good reproducibility is obtained on heating and cooling if times of order of 12 to 15 hours are allowed for equilibration. This is true, however, only when cycling is carried out within this temperature range. If the specimen is held below 550°K for any length of time, the damping values measured on subsequent heating are invariably about 20% lower than would otherwise be obtained if the specimen were never cycled below 550°K.

A peak in damping is also observed at approximately 950°K, and a broad bulge is often found near 900°K which may correspond to still another peak. The damping behavior at high temperatures is shown in detail in Fig. 22. In this particular cycle, the data points above 825°K were obtained in a single continuous heating and cooling run at 33°K per hour.

The following observations have been made concerning the 950°K peak:

1) It is most pronounced when measurements are made on continuous cooling from temperatures above about 975°K;

2) the peak is only slightly in evidence when the measurements are made on continuous heating starting from a temperature well below the peak;

3) the peak is observed, although reduced in height, when equilibrium measurements (3-12 hour holding times) are made either in ascending or descending order;

4) the peak height on continuous cooling does not appear to depend on the time spent at temperatures above 950°K;

5) the peak temperature was never observed to have shifted by more than a degree or two under any conditions.

The characterization of the temperature dependence in this range is somewhat complicated by the presence of the peak. However, a log Δ_I vs. 1/T plot for all runs exhibit a reasonably linear portion in the range between 600°K and 950°K as shown in Fig. 13. This linear portion corresponds to an apparent activation energy of about 0.22 eV.

D. INFLUENCE OF OXYGEN ON THE DECREMENT AND MODULUS OF 6-9's SILVER FROM 4°K TO 380°K

The results of a low temperature run on crystal 34C after it was saturated with oxygen in the high temperature apparatus are presented in Figs. 23 and 24. Calculation

shows that this crystal contained about 40 ppm O_2 at equilibrium (825°K-2 atm. O_2).[61] In order to retain most of the oxygen in solution, the specimen was quickly withdrawn from furnace and allowed to cool in air. However, this procedure resulted in loosening and tilting of the specimen in the knife edges, thus necessitating that the crystal be removed and remounted before it could be measured. Prior to remounting, the crystal was etched deeply in an ammonium hydroxide-H_2O_2 mixture, approximately 0.002 in. of silver being removed from all dimensions; the specimen was then remeasured and weighed and, as indicated in Table I, it was also relabeled 34E.

Referring to Fig. 23, the main features apparent in the damping spectrum of the oxygen-saturated crystal below 100°K are: 1)A plateau extending from 4°K to 10°K, 2) a small peak at 42°K, and 3) a broader somewhat less pronounced peak at 75°K. However, compared to the damping in this same specimen in the oxygen-free condition (Fig. 21), the most striking difference is that the overall level of the damping has been reduced by more than two orders of magnitude. Furthermore, although the two peaks at 42°K and 75°K seem to be present in oxygen-free silver (see Fig. 21) as well, the measurements on 6-9's silver do not show any indication of a rise in Δ_I at the lowest temperatures, such as is seen in the oxygen-saturated specimen.

Fig. 24 gives the details observed from 100°K to 300°K on a more compressed vertical scale. The three small rather narrow peaks at 140°K, 148°K, 160°K, and the complex peak structure which exists above 200°K are to be noted. To establish whether or not these features were reproducible six separate runs were made both on heating and cooling through this range; one of these runs was also carried out at a much higher strain amplitude, namely, $\epsilon_0 = 5\times10^{-6}$. On each run every feature of the damping spectrum was duplicated to the minutest detail. In the run made at the higher strain amplitude, the three small peaks remained unchanged in magnitude and temperature, although they were now superimposed on a higher background. Above about 200°K, the high amplitude run coincided exactly with the previous run made at low amplitudes. This behavior is consistent with the observed strain amplitude dependence described in Part E.

After this last series of measurements, the oxygen-saturated specimen was transferred to the high temperature apparatus, and the measurements were extended to ~380°K. A relatively narrow, well defined peak in the damping was observed at 365°K (see Fig. 16) and a corresponding modulus defect was also present. The observed modulus defect was consistent with that expected[1] for a simple relaxation peak of the observed ($\Delta_{MAX} = 2.6\times10^{-3}$) height. It is obvious from Fig. 16 that a peak of this magnitude could not have

been present in the oxygen-free state.

Except in the vicinity of the peak near 365°K, the damping of the oxygen-saturated crystal at all temperatures is at least two orders of magnitude lower than that of 6-9's silver. It appears, in fact, as though the presence of oxygen has completely eliminated any dislocation contribution to the damping or modulus. If so, the modulus of the oxygen-saturated material at low strain amplitudes should actually represent or at least closely approximate the true elastic modulus of silver. A large plot was therefore made of f_{ox}^2 vs. T, based mainly on the data obtained below 300°K. It was found that the values of f_{ox}^2 above 120°K, as well as the three measurements made at 715°K, 770°K, and 820°K immediately after saturation, all fell on a good straight line, the deviation of any single point from this line being less than 2 cycles. An analytical expression was thus obtained from which the value of f_{ox}^2 could be calculated for temperatures above 300°K. This experession was then used to obtain the high temperature values of f_{ox} shown in Fig. 16. Since it was felt that the modulus data for 34E containing oxygen did approximate the true elastic modulus, the quantity $(f_{ox}^2 - f_m^2) / f_{ox}^2$ then represents the fractional dislocation contribution to the modulus. This quantity is shown for the frequency data of Fig. 16 in Fig. 18.

E. STRAIN AMPLITUDE DEPENDENCE

Detailed measurements of the strain amplitude dependence over the range from 10^{-8} to 10^{-5} were carried out on specimen 34D from 4°K to 300°K and on crystal 34C from 300°K to 1000°K. Similar measurements were made between 4°K and 300°K on specimen 34E containing 40 ppm of oxygen, and on crystal 34C after saturating with oxygen (~20 ppm) at 715°K. The results of these measurements are given in Figs. 25-28.

The absence of any pronounced time dependent phenomena, as noted in part B, made it possible to perform closely spaced measurements at high strain amplitudes. For the times (~10-20 seconds) involved in any one measurement, such small time-dependent effects as were observed could be considered unimportant. No hysteresis effects greater than a few per cent were observed on returning to low strain amplitudes after measurements at the highest amplitude attainable with the 6-9's silver specimens. Although the strain amplitude dependent damping in the well-annealed crystal (34C) did show considerable scatter near room temperature, this was neither systematic nor reproducible. The details of the observations can best be described separately for each of the specimens examined.

1) Specimen 34D - 4°K to 300°K. For this crystal, the strain amplitude dependence was determined at eight

temperatures spaced approximately 40°K apart. Most of the data obtained are presented in Fig. 25, although the measurements made at 155°K and 264°K have been omitted for the sake of clarity; the strain amplitude curves for these two temperatures are of essentially the same shape as that at 210°K. Obvious features displayed in Fig. 25 are the minimum observed in all the curves, together with the lack of any well defined "breakaway" point corresponding to the onset of amplitude dependence. It also appears that two separate processes are contributing to the strain amplitude dependence. This is particularly evident in the curve obtained at 210°K. Thus, it was found that all the strain amplitude curves could be resolved into three components: an amplitude independent background, Δ_I, corresponding to the observed minimum, and two additional strain amplitude dependent components, Δ_{H_1}, and Δ_{H_2}, both of which seem to obey the Granato-Lücke relationship[36]

$$\Delta_{H_i} = (C_{2i} / \epsilon_o) \exp(-C_{1i} / \epsilon_o) \qquad \text{(III-4)}$$

where C_{1i} and C_{2i} are constants independent of strain amplitude. The justification for such a separation as well as details concerning the method of analysis employed will be given below in Part IV-Section B. It might be mentioned, however, that both components appear to reach a maximum near 100°K. The behavior of both components as a function of temperature for various strain amplitudes can be seen

in Fig. 29.

2) Specimen 34C - 300°K to 1000°K. Measurements over this temperature range were made at approximately 50° to 100°K intervals. The strain amplitude dependence may be separated roughly into two regions, 300°K to 550°K and 550°K to 1000°K, and is illustrated in Figs. 26 and 27 respectively. The curves shown in Fig. 26 could not be fitted successfully using the two component scheme described above, and the data exhibit considerable scatter. Above 550°K the curves shown in Fig. 27 all reach an amplitude independent plateau at high strain amplitudes. The damping level corresponding to this plateau is observed to increase with temperature up to about 750°K after which it remains constant. At 1000°K the damping is amplitude independent, except for the slight rise observed at very low strain amplitudes.

3) Specimen 34E (40 ppm O_2) - 4°K to 300°K. The strain amplitude dependence of the oxygen-saturated crystal was studied at only a relatively few temperatures since the behavior, which is illustrated in Fig. 28, could not be characterized in any simple way. In addition, almost no amplitude dependence was observed above $\sim$200°K. In contrast to the behavior of all the oxygen-free silver specimens there is no indication of a rise in Δ at the lowest strain amplitudes. As with pure material, however, the

strain amplitude at which the decrement becomes amplitude dependent is nearly independent of temperature.

F. KINETICS OF OXYGEN SATURATION AND VACUUM DESORPTION

1. Saturation. As mentioned previously, changes in the damping could not be measured during saturation because ionization occurred in the specimen-electrode gap with oxygen in the system. However, the following observations can be made: 1) exposure to oxygen for times of 12 hours or less at 715°K causes a reduction in the damping of 6-9's silver, measured at this temperature, of more than two orders of magnitude, 2) this time is comparable to that required for oxygen to diffuse completely through the specimen, according to calculations based on the diffusion data of Eichenauer and Müller[61], and 3) the oxygen concentration needed to achieve this reduction in Δ_I is less than 40 ppm, as derived from recent solubility data[61, 62]. These observations are based on measurements made in vacuo on crystal 34C immediately following saturation at 715°K, 770°K, and 820°K at 2 atm. O_2. In addition, during an attempt to make measurements at lower temperatures and pressures, the damping was observed to decrease by more than 25% after only a 30 minute exposure to 100μ of O_2 at 600°K. The total amount of oxygen which could have been introduced under these conditions is calculated to be less

than 0.1 ppm. Thus it appears that only very small quantities of oxygen are required at these temperatures to reduce the damping to very low levels. This conclusion is confirmed by the desorption studies reported below.

2. Kinetics of the Recovery of the Damping during the Desorption of Oxygen in Vacuum. The initial experiments of this type were carried out on crystal 34C before it was remounted. It was found that after saturating with oxygen at 715°K the decrement measured immediately following evacuation of the system was $\sim 1\times10^{-5}$ as compared to $\sim 2\times10^{-3}$ before saturation. The damping remained at this low level for approximately 45 minutes, after which it increased rapidly (within <5 minutes) to about 8×10^{-5}. Over the next 30 hours the damping rose slowly but somewhat erratically to roughly 1×10^{-4}. The temperature was then raised at 50°K per hour to 770°K. During this heating period Δ was observed to decrease to a value of $\sim 2\times10^{-5}$ and then to remain sensibly constant at this level for several hours. Again, the temperature was raised at ~ 40°K per hour, this time to 1000°K, and the specimen left overnight in a dynamic vacuum of $\sim 7\times10^{-6}$ mm Hg. The initial high damping level, characteristic of oxygen-free silver before saturation, was completely recovered after this 12-hour vacuum anneal at 1000°K. The temperature was then cooled to 825°K in 50°K steps and it was found that previous

equilibrium measurements on crystal 34C in the oxygen-free state were also reproduced within close limits. It thus appeared that oxygen could be added to silver in order to eliminate dislocation contributions to damping and modulus and then removed in a completely reversible manner by a vacuum heat treatment. It was at this point that the specimen (34C) was resaturated with oxygen and cooled rapidly to room temperature.

When this crystal (now designated 34E) was eventually reheated to 1000°K and the oxygen pumped out, it was found that the decrement was nearly three times greater than the value measured (on crystal 34C) at the same temperature before saturating and remounting. This specimen was therefore cycled as described above (part C) in an attempt to reduce the damping. Although the behavior on cycling was similar in all respects to that observed previously, the final level of the decrement was still ~1.5 times that originally obtained on 34C.

Since prolonged exposure of the apparatus to oxygen at temperatures near 1000°K did not seem advisable, it was decided to carry out the kinetic studies by saturating at somewhat lower temperatures (i.e., 600°-700°K) and then desorbing the oxygen in a vacuum at temperatures between 850°-1000°K.* A standard annealing and saturation treatment

*It was not possible to carry out desorption experiments at lower temperatures because the kinetics were much too slow, as it turned out.

was adopted, viz., heating in vacuum ($\sim 7 \times 10^{-6}$ mm Hg) at 1000°K for ~12 hours, slow cooling (40°K per hour) to 770°K, and saturation with oxygen for 12 hours at 2 atm. pressure at 770°K; this treatment introduced approximately 40 ppm of oxygen into the crystal. Pumping was then started, and the temperature was raised rapidly (~200°K per hour) to the desired level, following which Δ and f_m were measured at close intervals of time. After each run below 1000°K, the crystal was heated to 1000°K and held there for 12 hours to insure complete removal of oxygen before beginning the next run.

The results of such kinetic measurements at 875°, 900°, 925°, 975°, and 1000°K are shown in Figs. 30-35. Plots of log Δ vs. log t at 875°K and 975°K are shown in Fig. 30. As can be seen, the recovery of the damping associated with the removal of oxygen from the crystal appears to proceed by a multi-stage process. In Fig. 30 the initial level portion of the kinetic curve at 875°K has been designated stage I, the next step has been labeled stage II, and the final recovery step, stage III. It is also possible that stage III actually corresponds to two separate stages. All three stages were visible at 875°, 900°, and 925°K, but at 975°K and 1000°K it appears that stage I and probably also stage II had already been completed before the first measurement could be made. In addition, a distinct break

seen in stage III at 875°K is only apparent as a slight change in slope at 975°K and 1000°K.

Since the level of the damping at the end of any given stage is itself a function of the temperature, the fractional recovery of Δ_I in stages II and III has been normalized and the data at all temperatures are thus replotted in Figs. 31 and 32 on a logarithmic time scale. The modulus data has been similarly analyzed and plotted in Figs. 33 and 34. An activation energy appropriate to stages II and III may then be determined from Figs. 31-34 using the method of cross-cuts[87]. A summary of the essential results is given in Table IV.

In all runs the damping was followed for as long as possible at three strain amplitudes: $3x10^{-8}$, $3x10^{-7}$, and $3x10^{-6}$. In the oxygen-free condition the damping is nearly amplitude independent over this range; similarly, little amplitude dependence was detected at any stage of the oxygen removal process. In a duplicate run at 975°K, however, a separate peak in Δ was observed at each strain amplitude as time proceeded. The peaks corresponding to each strain amplitude were well separated in time and occurred in order, the peak at the highest strain amplitude being the first to appear, etc. This behavior can be seen quite clearly in Fig. 35. Associated with each peak shown in Fig. 35 a step or defect was observed in the frequency

vs. time curve for which the relationship $\Delta_{MAX} = \pi/2(\Delta E/E)$ appears to hold.

G. MISCELLANEOUS OBSERVATIONS

1. Multiple Resonances. Well defined multiple resonances had been observed in a number of $\langle 100 \rangle$ oriented specimens at high temperatures during some of the initial runs made with poor knife edges. These effects could all be traced eventually to loosening of the specimens in the knife edges, or in one case, to extensive recrystallization. A transient triple resonance was observed, however, in the temperature range between 260°K and 280°K in specimen 34D which does not seem to be attributable to external causes. For example, the damping in this same crystal had previously been examined in detail without noticing anything unusual, and when the measurements were repeated immediately following the observance of the triple resonance they again failed to reveal any trace of this phenomena. During a continuous heating run, a small additional resonance appeared about 10 cycles below the specimen resonance; this additional resonance grew in amplitude with increasing temperature and was quickly followed by the appearance of a third resonance about 20 cycles below the main resonance. On raising the temperature further, a temperature was reached at which all three resonances became of equal

magnitude. Beyond this temperature the two higher frequency resonances were found to decrease in amplitude and finally disappear. The separation of the three resonances remained constant over the 20°K interval in which they occurred, while the frequency of the triplet shifted by approximately 100 cycles corresponding to the normal shift of resonant frequency with temperature. The decrement, as measured by the amplitude at a constant drive voltage, increased smoothly, reaching a maximum at the temperature at which all three resonances were of equal magnitude, and then decreased smoothly to a value compatible with an extrapolation of the data at lower temperatures.

Multiple resonances which do not appear to be due to external causes have been reported by a number of other investigators[23,88] but as yet no satisfactory explanation has been offered for this phenomena.

2. Peak at 42°K. The measurements reported above have revealed a peak in damping at about 42°K in both 6-9's silver and 6-9's silver containing 40 ppm of oxygen at a frequency of 27 kc. A peak at this temperature was also observed in the 1% Mg-Ag alloy specimen (crystal 23 AM). The damping of the Mg-doped crystal as a function of temperature from 4°K to 100°K is plotted in Fig. 23 along with the corresponding data for 6-9's silver containing oxygen (40 ppm). The peak at 42°K ($\Delta_{Max.} = 2x10^{-5}$) is quite well resolved

and occurs on a well defined linear background. This run on the Mg alloy crystal was made one day after the specimen was mounted.

3. Behavior below 10°K. In addition to the features described earlier, the low temperature measurements have revealed:

1) Indications of a peak at ~7°K in 6-9's silver (specimen 34D - Fig. 15), together with

2) a slight rise in the modulus below 7°k (34D - Fig. 16), and

3) a rise in the damping at low temperatures beginning near 10°K in silver containing 40 ppm of oxygen (34E - Fig. 23), which is absent in oxygen-free crystals of the same purity level.

We would like to simply add at this point two additional observations. First, careful examination of the measurements made on the 1% Mg alloy (23C - Fig. 23) has failed to show any anomalous behavior in this temperature range. Second, a rise somewhat similar to that found in the oxygen-saturated silver, although considerably greater in magnitude, has been observed in an internally oxidized Ag-1% Mg alloy.

4. The Occurrence of Spikes in the Damping during Heating or Cooling. During measurements in 6-9's silver, several spikes or sharp irregular peaks in the damping were observed, as mentioned in section C. Such spikes have also

been observed in the temperature range from 80°-300°K in an internally-oxidized 1% Mg-Ag alloy crystal. In this specimen the spikes were of the same order of magnitude (10^{-4} to 10^{-3}) as those observed in 6-9's Ag. However, the background level in the internally oxidized alloy is only of the order of 10^{-5}, and hence the spikes represent a prominent feature of the damping spectrum in this material. Some pertinent observations regarding the appearance of these spikes on heating and cooling are as follows:

1) The temperature at which the spikes occur is completely arbitrary and unpredictable;

2) the spikes frequently occur in groups of two or more at closely spaced temperature intervals;

3) in general the spikes are quite asymmetric, the damping often rising abruptly on one side and falling off more gradually on the other; contrary to the observations of Filmer et al.[89], however, the sense of the asymmetry is not apparently related to the direction of the change in temperature.

4) these spikes do not seem to represent discontinuous changes in the damping since up to 15 measurements per 1°K have been obtained on some spikes for which the decrement varied smoothly with temperature. Somewhat similar observations have been reported by other investigators in aluminum[50, 89] and copper[53, 88]. The nature of these spikes is

still in doubt. They may be due to transient changes either in the dislocation structure, or in the distribution of pinning points along the dislocations.

IV. DISCUSSION

Before considering the results of the measurements in more detail, a few general remarks may help in providing some overall perspective. The primary objective of these experiments was to establish the effectiveness of oxygen in pinning down dislocations in silver. From the results of measurements described above it is apparent that the presence of oxygen does indeed lead to a marked reduction in the internal friction of silver even at high temperatures. The interpretation of this observation, however, depends to a large extent on the manner in which dislocations contribute to the observed damping in the oxygen-free material. The discussion, therefore, is primarily concerned with interpreting the behavior of the oxygen-free material consistent with the fact that oxygen effectively eliminates dislocation contributions to the damping.

For this reason we have separated the discussion into sections based on the phenomena exhibited by 6-9's silver, i.e., recovery after mounting or transfer, dependence on strain amplitude, and the temperature dependence of Δ_I, while the final section is concerned with the kinetics of oxygen saturation and desorption.

A brief description of the internal friction phenomena associated with dislocation motion and the theories proposed to account for these phenomena has been given in the

introduction. As we shall see, a number of these models appear to account satisfactorily for the various contributions to the internal friction in 6-9's silver. However, in view of the absence of any previous work on silver single crystals, the interpretation of some of the observed phenomena in terms of a particular model is difficult since additional information (i.e., the effect of deformation or frequency on the observed behavior) which was not obtained from the present study would be required. The application of these models which treat dislocations as simple line defects to silver can be questioned since in silver dislocations are extended. The relatively low stacking fault energy of silver ($\sim$30 ergs/cm^2)[101] would lead us to expect[4] an equilibrium separation of partials of $\sim$ 20 Angstroms. However, most treatments make the reasonable assumption that both partials behave as if they were rigidly bound together and move as a unit.

At this point it will be convenient to consider a few general relations pertaining to dislocations in silver which will be needed in any comparison of theory and experiment.

In the f.c.c. silver lattice dislocations lie in $\langle 111 \rangle$ planes and slip occurs in the $[110]$ direction so that the magnitude of the Burgers vector, b, is $a/\sqrt{2}$ where a is the lattice constant. The value of the shear modulus,

G, appropriate to the $\{111\}$ planes is then $\frac{1}{3}(c_{11}-c_{12}+c_{44})$[8].

The effective line tension of a dislocation, C, is usually taken as $\sim \frac{1}{2}Gb^2$. However, Stern and Granato[90] have shown from the work of de Wit and Koehler[91] that to a good approximation the line energy (energy per unit length) of a dislocation can be written

$$E_L = (b^2/4\pi) \ln (R/r) \left[K_1 - K_2 \cos 2\phi \right] \qquad \text{(IV-1)}$$

where R and r are the usual cut-off radii of the elastic stress field, and ϕ is angle between the dislocation and its Burgers vector. The constants K_1 and K_2 can then be written in terms of the elastic constants by equating IV-1 with expressions developed by Foreman[92] for the line energy of a pure screw dislocation ($\phi = 0$) and a mixed dislocation ($\phi = \pi/3$). For silver at room temperature we obtain $K_1 = 3.55 \times 10^{11}$ dynes/cm^2 and $K_2 = 0.897 \times 10^{11}$ dynes/cm^2 using the values of the elastic constants[93] given below. The line tension, which is formally identified with $E_L(\phi)+E_L^{\prime\prime}(\phi)$ is then given by

$$C(\phi) = (b^2/4\pi) \ln (R/r) \left[K_1 + 3K_2 \cos 2\phi \right] . \qquad \text{(IV-2)}$$

The values of the dislocation line tension appropriate for pure screw (C_s) and pure edge (C_e) dislocations are given below using $R/r = 10^4$.

Since longitudinal stresses and strains are employed experimentally while theory is developed in terms of shear

stresses and strains on the slip plane, an orientation factor relating the longitudinal quantities to those in slip plane is required. The factor Ω appearing in Eqs. I-2 and I-3 can be shown[36] to be

$$\Omega = \frac{E(\Theta, \phi)}{G} \sum_i \frac{\Lambda_i}{\Lambda} R_i^2, \qquad \text{(IV-3)}$$

where $E(\Theta, \phi)$ is the modulus appropriate to the experimental mode employed, G the shear modulus appropriate to the slip plane, R_i the resolved shear stress factor, $\cos\Theta\sin\Theta\cos\phi$, of the ith slip system, Θ the angle between the specimen axis and the normal to the slip plane, and ϕ the angle in the slip plane between the projection of the specimen axis and the slip direction. If we assume all slip systems are equally populated, which is not unreasonable for undeformed crystals, Ω turns out to be nearly independent of orientation for extensional modes in f.c.c. crystals, the variation in E (Young's modulus) compensating for the variation of the sum. Values of Ω for $\langle 111 \rangle$ and $\langle 100 \rangle$ crystals are listed below, as well as the corresponding values of E and R (for these orientations R_i is either zero or R for each slip system).

For convenience then, we list numerical values for the following quantities which will be used throughout the paper:

a	$= 4.08 \times 10^{-8}$ cm	b	$= 2.88 \times 10^{-8}$ cm
c_{11}	$= 12.5 \times 10^{11}$ dynes/cm^2	E_{111}	$= 12.1 \times 10^{11}$ dynes/cm^2
c_{12}	$= 9.45 \times 10^{11}$ dynes/cm^2	E_{100}	$= 4.36 \times 10^{11}$ dynes/cm^2
c_{44}	$= 4.64 \times 10^{11}$ dynes/cm^2	G	$= 2.54 \times 10^{11}$ dynes/cm^2
R_{100}	$= \sqrt{6}/6$	Ω_{100}	$= 0.189$
R_{111}	$= \sqrt{6}/9$	Ω_{111}	$= 0.177$
C_e	$= 0.54 \times 10^{-4}$ dynes	C_s	$= 3.77 \times 10^{-4}$ dynes

In carefully prepared undeformed silver single crystals dislocations appear to be arranged in a random three dimensional network. In specimens which have dimensions comparable to those used here and which were prepared by essentially the same techniques described in section II dislocation densities are of the order of 5×10^6 to 2×10^7 as measured by etch pit counts[94]. The average length, L_N, of dislocations in such a network is related to the total dislocation density, Λ . For an f.c.c. lattice this relation is[5]

$$\Lambda L_N^2 \simeq 1 \ . \qquad \text{(IV-4)}$$

The mean free path of dislocations measured[94] in crystals with as-grown densities of 2×10^7 is $\sim 5\times10^{-4}$ cm. Since the network length is of the order of one-half the mean free path, we obtain $\Lambda L_N^2 \simeq 1.3$ in good agreement with IV-4. The value of the damping constant B, which is presumed to

arise from the scattering of thermal phonons by the stress field of the dislocation, has been given by Leibfried[95] as

$$B = 3\ kTZ/10\ a^2\ V_s \qquad \text{(IV-5)}$$

where V_s is the effective shear wave velocity and Z is the number of atoms per unit cell. For silver at 300°K we obtain 1.9×10^{-4}. There is some evidence (see Stern and Granato[90] for a discussion of this point) that IV-5 underestimates the phonon scattering by about a factor of five. For the sake of definiteness we will take the calculated value of

$$B = 0.63 \times 10^{-6}\ T\ (°K)\ \text{dyne-sec/cm}^2.$$

We will now consider the results of section III in more detail.

A. RECOVERY AFTER MOUNTING OR TRANSFER

As pointed out, especially by Nowick[96] and Van Bueren[9], two different types of recovery of the damping and modulus have been observed after small deformation; i.e., a strongly amplitude-dependent form of recovery seen at low and intermediate frequencies (1cps-50kcps) and an amplitude independent type which is manifest at intermediate and high frequencies (10 kc - 100 mc). These effects and those occurring at larger deformations have all been loosely termed the "Köster effect" after Köster[97], who first made

such studies in 1940. Granato et al.[85] have attempted to explain both types of recovery observed after small deformations in terms of the vibrating string model, on the assumption that the recovery is associated with the migration to and subsequent pinning of dislocations by deformation produced point defects. By further assuming that the rate of arrival of point defects at dislocations is governed by the Cottrell-Bilby relation[98] they derive relations for the change in Δ_H, Δ_I, and $(\Delta E/E)_I$ as a function of the time, t, after deformation. The relationships given by Granato et al. for the change in the damping and modulus are

$$\Delta_I(t) - \Delta_I(\infty) = \Delta_R\,(1 + \beta t^{2/3})^{-4} \qquad \text{(IV-6)}$$

$$(\Delta E/E)_I(t) - (\Delta E/E)_I(\infty) = (\Delta E/E)_R\,(1+\beta t^{2/3})^{-2} \qquad \text{(IV-7)}$$

where

$$\Delta_R = \Delta_I(0) - \Delta_I(\infty),$$
$$(\Delta E/E)_R = (\Delta E/E)_I(0) - (\Delta E/E)(\infty), \qquad \text{(IV-8)}$$

and the quantities Δ_I, $(\Delta E/E)_I$ are as previously defined (Eqs. I-2, I-3). The recovery parameter β is given by

$$\beta = (\sqrt{2}\,\pi\, c_o\, L_o / b^3) \cdot (bWD / kT)^{2/3} \qquad \text{(IV-9)}$$

where W = binding energy of the defect to the dislocation, D = diffusion constant for the pinning defect, and c_o =

atomic fraction of pinning defects in the lattice. The subscript zero on the loop length L denotes the value immediately after deformation. Granato et al. have been able to account satisfactorily for a number of previous observations using these relations, and other investigators[65,67,74,99] have also observed the predicted time dependence of one or more of the quantities Δ_I, $(\Delta E/E)_I$ and Δ_H.

Only Δ_I and $(\Delta E/E)_I$ have been measured in this investigation and then only under rather limited conditions. The present measurements are not ideally suited for comparison with the theory since 1) measurements could not be made immediately after mounting or transfer, and 2) the deformation itself is not necessarily uniform from specimen to specimen. Nevertheless, we have attempted to analyse the measurements reported here using the Granato-Hikata model, and a summary of the results is given in Table II.

As can be seen in Figs. 20 and 21, the fits are reasonably good. A variety of other functional forms were tried in an attempt to characterize the time dependence of Δ_I. These included e^{-t^n}, $(1+\beta t^n)^{-m}$ and simpler power laws, with n = 1/2, 2/3, 1, 2 and m = 2, 3, 4, 5. Neither the power law nor the exponential forms gave a satisfactory fit to the experimental data. The form $(1+\beta t^n)^{-m}$ was considerably better, and the best fits were obtained for

$n = 2/3$, $m = 4$.

By determining Δ_R, $(\Delta E/E)_R$, β and c_0 at various temperatures it should be possible to derive values of the diffusion coefficient, D, for the pinning defect and hence to estimate the activation energy for migration of this defect. Granato et al. have analysed the modulus data of Smith[100] on copper and obtained 1.0 eV for the migration energy, which they associate with that of a monovacancy in copper. We cannot, however, determine an activation energy from the present measurements since β is proportional to c_0, the bulk defect concentration and c_0, in turn, is related to the amount of deformation received which is not necessarily the same in each case. The migration energy of monovacancies in silver, 0.82 eV, as determined by quenching measurements [87], would require that the ratio $\beta_{333°K}/\beta_{293°K}$ be ~ 13, whereas the observed ratio is of the order of 2. Thus, c_0 in the two cases would have to vary by a factor of 7, which seems somewhat unreasonable, considering the small range of β for all measurements. An activation energy of 0.2 - 0.4 eV would appear to be much more in line with the observed temperature dependence of β.

The values of Λ and L_0 required in Eqs. I-2 and I-3 to account for the observed magnitude of Δ_R and $(\Delta E/E)_R$ are reasonable when we realize that only a relatively small fraction of the volume of the crystal near the

knife edges is involved. This is apparent from the fact that the magnitude of the recovery is nearly as large after transfer as after mounting. From Table II we see that L_0 is of the order (3×10^{-4} cm) of the expected network length L_N. This is to be expected since no matter how large a loop is generated by the deformation, the mean length between jogs produced by intersection with the existing network will determine L_0. The loop length would not be expected to be appreciably reduced by a random distribution of available pinning points. The impurity concentration is $\sim 10^{-6}$ and for an estimated 1-2% deformation the point defect concentration introduced[9, 87] is not expected to be much larger. Even if the total concentration is as high as 10^{-5}, the loop length determined by a random distribution is an order of magnitude larger than L_0.

If we assume only 2% of the total volume of the crystal is affected by deformation at the knife edges, then the density of fresh dislocations near the knife edges would be approximately fifty times the value ($\sim 6 \times 10^5$) given in Table II, or 3×10^7 / cm^2. An increase in dislocation density of this order is about that expected[94] for the estimated 1-2% deformation at the knife edges.

If we take c_0 as 10^{-6}, W as 0.2 eV, and assume $D = b^2 \nu_D e^{-E_m/kT}$, where ν_D is the Debye frequency ($\sim 10^{13}$ / sec), then, using the values of β and L_0 given in

Table II, solving IV-9 for E_M yields values of E_M ranging from 1.0 - 1.2 eV, while for $c_0 = 10^{-7}$ we obtain E_M = 0.9 - 1.1 eV. Thus the magnitude of β is clearly not consistent with an energy of migration for the pinning defect of 0.2 - 0.4 eV. The results here are inconclusive. Although the temperature dependence would indicate that, in silver, faster moving defects, such as interstitials or divacancies* may be involved in the pinning, the magnitude of β is not in agreement with this view. Before any interpretation can be made measurements would have to be made immedeately after deformation (to provide a more stringent test of the model) over this same temperature range. In addition, the deformation should be of a reasonably reproducible nature.

No changes are observed in Δ_I or f_m after mounting specimens containing 40 ppm O_2, and, of more significance, no change is observed on transfer. This would then indicate that no changes in the dislocation structure are introduced by mounting or transfer or, alternatively, that the damping associated with any changes is recovered quite rapidly (<10 min.). In either case the observations provide fairly direct evidence that oxygen is effective in restricting the motion of dislocations.

*The migration energy of divacancies in silver is estimated to be 0.57 eV from quenching experiments[87], while interstitials are presumed to migrate with a somewhat lower (0.1 - 0.3 eV)[9,87] energy.

B. INTERNAL FRICTION AT LOW TEMPERATURES

Although our intended purpose was to measure the internal friction of annealed single crystals of silver between 4.2° and 300°K, the results definitely show that despite great care in handling, permanent changes in the dislocation structure of the annealed specimens could not be avoided. This is apparent from the observation that the decrement increases on transfer and does not fully recover. Moreover, as will be seen, the damping behavior at low temperatures shows a much greater similarity to that of lightly deformed f.c.c. metals than to the behavior of well annealed crystals. Although a certain amount of handling damage was expected during mounting, the magnitude of the increase in Δ on transfer was somewhat surprising and points out the difficulty in making measurements on well-annealed crystals of high purity at low temperatures.

No measurements at low temperatures on annealed or lightly deformed Ag single crystals have been reported with which the present results can be compared. All previous work has been carried out on fairly heavily deformed silver of substantially lower purity, mostly on polycrystalline specimens. However, pertinent measurements have been made on copper, for which quite extensive low temperature data are available, and the results obtained on copper will, therefore, be used as a basis of comparison.

The experimental observations reported here (Figs.

16-21) indicate that the internal friction of 6-9's Ag at low temperatures can be characterized by: 1) A spectrum of discrete relaxation processes below 120°K (the evidence for this is based mainly on the modulus data--see Fig. 20); 2) a series of broad peaks between 120°K and 300°K, and 3) a relatively high 'background' internal friction on which 1) and 2) are superimposed. This 'background' rises fairly rapidly between 40°K and 100°K, reaches a broad maximum and decreases with temperature from 100°-300°K.

In the discussion to follow we will consider first the structure observed in the modulus and decrement of silver, which we believe to be associated with the various deformation produced peaks reported by other investigators. The discussion is limited primarily to a comparison with the results of other experiments, since neither the effect of varying amounts of deformation on the 'peaks' nor their frequency dependence was investigated.

The 'background' which accounts for the majority of the observed internal friction will be considered next. As will be seen, it appears that this contribution to the internal friction can be explained in terms of the lateral displacement of built-in dislocation kinks as treated by Southgate and Attard[102]. In the third section the results of the measurements of the amplitude dependence of the internal friction are discussed in terms of the interpretations

made for the low amplitude behavior.

In the fourth and final section we will discuss the effect of interstitial oxygen on the internal friction of 6-9's silver and in addition consider the possible mechanisms by which oxygen gives rise to those additional features observed in the internal friction which are not present in oxygen-free silver.

1. Structure at Low Temperatures. Deformation-produced relaxation peaks in the temperature range between 4°K and room temperature were first observed by Bordoni[12] in copper, silver, lead and aluminum. A great many experimental investigations have since been carried out on these peaks, mainly in Cu. No attempt will be made here to describe the experimental detail relating to these peaks. For these details the reader is referred to comprehensive reviews by Niblett and Wilks[10], and Sack[24] and to a number of papers presented at the recent International Conference on Lattice Defects in Tokyo.

However, the principal experimental observations may be summarized as follows: The Bordoni peak is observed in both deformed polycrystals and single crystals and does not anneal out until relatively high temperatures (700°K in copper). In addition to the main peak at ~80°K in copper, a subsidiary peak (the Niblett-Wilks peak) is observed at ~40°K at a frequency of 40KC. Both peaks are about four

times as wide as would be expected for a single relaxation process. For relatively large deformations (10%) the background is very low from 4° to 300°K. However, observations on copper[103, 104] indicate that in lightly deformed material these peaks are nearly obscured because they are superimposed on a relatively larger background damping. This background increases rapidly with temperature in the vicinity of the peaks, reaches a plateau, and then, in some cases, continues to increase and, in others, decrease with temperature up to 300°K. In annealed specimens, on the other hand, the damping is usually considerably lower and rises monotonically with temperature, the general trend being concave upwards. The peaks are reduced by the addition of impurities but not nearly to as large an extent as the background.

Relatively few measurements, all corresponding to fairly large deformations and all on material of nominal 99.99% purity, have been made on silver. Bordoni and coworkers[72] have investigated the damping in deformed polycrystals at frequencies between 10 KC and 1 MC. The measurements of Okuda[73] were made at about 1 cps on polycrystalline wires deformed at liquid helium temperatures, while those of Stern[74] were made at 15 MC and 65 MC on single crystals. Bordoni et al. and Stern observed only a single peak, somewhat wider than the corresponding Bordoni peak in

copper, while Okuda observed two peaks after deformation at 4.2°K which, however, were not resolvable after a prolonged room temperature anneal. The results of all these measurements, from which an activation energy of 0.098 ev, and a frequency factor of 6×10^{11} have been derived[73], would lead us to expect the Bordoni peak at 25 kc at about 75°K. Several irregularities in the damping and corresponding modulus defects have actually been observed near this temperature in 6-9's Ag. In addition, a rather broad peak at about 75°K is found in the O_2 saturated specimen which may correspond to the main Bordoni peak.

The present results on silver below 120°K exhibit many features in common with the observations made by Thompson and Holmes[104] on single crystals of copper (99.999%). Thompson and Holmes have found four distinct steps in the modulus-temperature curve for an "annealed" sample and seven such steps in a lightly (3.25%) deformed sample; corresponding irregularities or peaks superimposed on a sharply rising background were also observed. They analysed their results in some detail by assuming that each modulus step corresponds to a single relaxation process. By making the further assumption that the same attempt frequency applies for each process, Thompson and Holmes were able to calculate a relaxation spectrum from the usual relation (Zener[1]).

$$\Delta = \pi(\Delta E/E)\omega\tau/(1+(\omega\tau)^2). \qquad \text{(IV-10)}$$

The resulting sum of the individual relaxations was found to give a reasonable fit to the observed shape of the Bordoni peak in deformed polycrystalline copper. Thompson and Holmes have suggested that the separate relaxations may each correspond to a different possible dislocation configuration, i.e., to pure edge, pure screw, and the various mixed dislocations possible in an f.c.c. lattice. They have made tentative assignments based on arguments concerning the relative strength of the various components. Although we do not feel that the present measurements are precise enough to justify such a detailed analysis, the existence of at least five separate relaxations at 22°, 42°, 62°, 72°, 92°K (see Table III) seems to be indicated. These may correspond to heretofore unobserved structure of the Bordoni peak in silver, although this cannot be concluded with certainty on the basis of the present measurements. Further measurements of Δ, including closely spaced modulus measurements, on samples which have been deliberately deformed in a controlled manner might resolve this question.

Although the 'relaxations' appear grouped near 75°K, where at the measurement frequency we would expect to find the Bordoni peak, the component at about 42°K is a much more

persistent feature of the internal friction of silver. In the measurements on 6-9's silver containing ~40 ppm O_2, the peak at 42°K is much more prominent than the broad peak observed at 75°K, while in the 1% Mg alloy this peak is clearly resolved on a well defined background (see Fig. 41), whereas no peak is evident near 75°K. This behavior is just opposite to that observed in copper, in which low temperature annealing[103], the addition of impurities[88], and irradiation[104] all reduce the height of Niblett-Wilks peak with respect to the main Bordoni peak.

If we assume that the peak at 42°K arises from a single relaxation process, the activation energy can be estimated from the peak width, W, at half maximum using the relation[1]

$$W = (1/T_1 - 1/T_2) = 2.63\ k/H \qquad \text{(IV-11)}$$

where H is the activation energy and k is Boltzmann's constant. The value of the activation energy obtained is 0.05 eV ± 0.01 eV, which is of the same order (0.045 eV) as that quoted[73] for the Niblett-Wilks peak (at about 40°K) in copper.

As mentioned previously, Okuda[73] has observed two peaks in deformed polycrystalline silver at about 0.8 cps. We would expect to find the 42°K peak observed here at 23°K

at 0.8 cps, if H = 0.05 eV, and Okuda's data do indeed show an indication of a bulge at about this temperature. Immediately after deformation (16%) at 4.2°K, Okuda found a single peak at 37°K which decreased initially in height on room temperature annealing (40 hours) while a second peak appeared at 50°K. On prolonged (112 days) annealing at room temperature both peaks are observed to grow. Neither peak is shifted in temperature during annealing. In similar experiments on copper deformed at 4.2°K by Okuda[73] and also Bruner and Mecs[105], the Niblett-Wilks peak (21°K) decreases continuously without shifting while the Bordoni peak (46°K) first decreases and then increases and shifts to higher temperatures. This difference in annealing behavior might be explained if we assume that the main Bordoni peak in copper actually consists of two unresolved peaks which exhibit an annealing behavior similar to the two peaks observed by Okuda in silver.

From the present observation of a peak at 42°K and the results of Okuda's measurements, the existence of at least three separate relaxation peaks in silver in the temperature range of the Bordoni peak seems well established. The results obtained here also indicate that an even larger number of discrete relaxations might be involved. The observations of Thompson and Holmes and the observed annealing behavior of the main Bordoni peak in copper would indicate

that the same is also true of copper. It would appear then that attempts to explain the width of the Bordoni peak and shifts of peak temperature with annealing or alloying solely in terms of a broadened or changing distribution of relaxation times is not justified. It would also appear hasty at the present time to exclude the possibility that the observed multiplicity arises from two or more dissimilar mechanisms involving intrinsic dislocation properties.

Although the resolution is somewhat poorer at higher temperatures because of the observed (±3%) irregularity in the damping measurements, the existence of three or possibly four relatively broad peaks seems to be indicated at 130°, 170°, 205°, and 250°K, all ±10°K (see Figs. 16 and 18). A somewhat similar set of peaks has been observed at 144°, 153°, and 204°K by Papazian[59] at about 2 cps in 6-9's silver single crystals strained 2% at room temperature. Hasiguti[27] has also reported a set of peaks at 1 KC in cold-rolled polycrystalline silver (99.99%) at 173°, 200°, and 245°K, with activation energies of 0.22±0.02, 0.37±0.04, and 0.46±0.05 eV, respectively, which he has attributed to point defect dislocation interactions[28]. Because of uncertainties in the activation energies and peak temperatures it is not possible to decide whether there is any correspondence between the peaks found in the present experiments and those seen by Papazian or Hasiguti. However, the peaks

observed here as well as those reported by Papazian seem to be relatively stable with respect to room temperature annealing, while those observed by Hasiguti disappeared after one day at room temperature; this behavior could possibly be related to differences in the purity of the silver employed in the various experiments.

2.'Background' Internal Friction. The 'background' in 6-9's silver represents the majority of the damping observed below 200°K. Estimates based on the magnitude of the observed modulus steps (see Table III) indicate that the more or less discrete relaxations observed between 4.2°K and 120°K can account for at most 10-15% of the damping. Thompson and Holmes[104] have attributed the 'background' which in most of their specimens continues to increase with temperature above 120°K to the Δ_I of the Granato-Lücke theory. In their treatment the temperature dependence of Δ_I arises from the increase of dislocation loop length with temperature. But, as they point out, this explanation would not seem to be valid for specimens for which Δ decreases with increasing temperature. At present this decreasing type of 'background' has not been satisfactorily explained. In the discussion to follow we will attempt to show that the 'background' contribution to the internal friction arises from the motion of dislocations, and in particular from the lateral motion of built-in kinks.

The earliest model used to describe the motion of dislocations under very small oscillating stresses involved treating a dislocation as an extensible string. This analogy was first proposed by Koehler[37] and subsequently developed by Granato and Lücke[38]. The equation of motion of a dislocation in the KGL model is

$$A \frac{\partial^2 y}{\partial t^2} + B \frac{\partial y}{\partial t} - C \frac{\partial^2 y}{\partial x^2} = \sigma b \qquad \text{(IV-12)}$$

where A is the effective mass per unit length of dislocation, B is a damping coefficient, and C is the line tension. Granato and Lücke show that for a reasonable range of values of B the dislocation motion is overdamped, and the inertial term in Eq. IV-12 can be neglected.

For the boundary conditions appropriate to a dislocation of length L, the KGL model leads to

$$1/Q = \Delta/\pi = \Omega \Lambda \Delta_o L^2/\pi^2 \left[\omega\tau / 1 + \omega^2 \tau^2\right] \qquad \text{(IV-13)}$$

and

$$\Delta E/E = \Omega \Lambda \Delta_o L^2/\pi^2 \left[1 / 1 + \omega^2 \tau^2\right], \qquad \text{(IV-14)}$$

where

$$\tau = L^2 B / \pi^2 C \qquad \text{(IV-15)}$$

and the other symbols are as previously defined (see Page 7). For $\omega \ll 1/\tau$ Eqs. IV-13 and IV-14 are identical with the previous expressions (Eqs. I-2 and I-3) when the factors 51

and 31 resulting from an exponential distribution of loop lengths are taken into account.

While the extensible string analogy might be expected to provide a reasonable model of the actual motion of dislocations at high temperatures, the periodic nature of the lattice in which dislocations exist must be taken into account at low temperatures. If we then consider that dislocations lie preferentially in potential wells defined by the close-packed directions in the glide plane, then their motion in the glide plane will consist of the lateral motion of kinks which pass over the Peierls barrier from one potential trough to the next. As mentioned in the introduction, the relation between kink motion and internal friction has been considered by a number of authors. In particular Seeger, Donth, and Pfaff[20] have proposed that the thermal generation of kink pairs in loops lying entirely in the close-packed direction is responsible for the Bordoni peak, while Seeger and Schiller[22] and Brailsford[25] have treated the motion of intrinsic or built-in kinks in loops which lie at an angle to the close-packed direction. In what follows we will consider only dislocations which contain intrinsic kinks and will not expressly consider the thermal generation of kinks.

Although it is not obvious that a treatment of the motion of dislocations in terms of the lateral motion of

intrinsic kinks will lead to the same form for the internal friction as the KGL model, Southgate and Attard[102] have shown that both the theory of Seeger and Schiller and that of Brailsford can lead to an equation of motion for the dislocation of the same form as Eq. IV-12. In both cases the inertial term can be neglected for frequencies in the kilocycle range, and we are thus led to Eqs. IV-13 and IV-14 for the internal friction and associated modulus defect. Thus the motion of a dislocation by the lateral displacement of intrinsic kinks can be described at least formally, in terms of the motion of an extensible string. The actual physical interpretations given the damping coefficient B and the effective line tension C in the three models are considerably different. As we shall see below, these differences result in a considerable change in the predicted temperature dependence of the internal friction and modulus defect.

In the KGL model the line tension arises from the stress-field energy per unit length of the straight dislocation, while the damping coefficient, which in Eq. IV-12 is the damping per unit length of dislocation, arises from the scattering of thermal phonons by the moving dislocation line. In the model of Seeger and Schiller the line tension arises solely from the mutual inverse-square law repulsion of the kinks. The effective damping, which is again assumed

to arise from the scattering of thermal phonons, is larger than in the KGL model due to the higher velocity attained by the kinks for the same overall motion of the line. In contrast to Seeger and Schiller, Brailsford considers kinks to be abrupt and their lateral motion as thermally activated. The kinks have a mobility μ and a diffusion constant D. In the original treatment Brailsford did not consider the changes in the total elastic energy of the dislocation with kink redistribution. However, the model leads to an effective line tension arising from pressure on the kinks due to concentration gradients (or more precisely due to gradients in chemical potential). The damping coefficient for the dislocation is simply inversely proportional to the kink mobility.

In the table below the appropriate values of B and C in Eq. IV-12 for each of the models is given in terms of the lattice plane spacing a, the kink density p_0, the diffusion constant D, the mobility μ, the damping coefficient per unit length of dislocation arising from phonon scattering B_T, the line tension arising from the stress field energy of a straight dislocation C_0, and the line tension arising from the interaction of the stress fields of the kinks C_1.

	KGL	Seeger and Schiller	Brailsford
B	B_T	B_T / ap_0	$1 / \mu a^2 p_0$
C	C_0	C_1	$D / \mu a^2 p_0$

The stress field of a kinked dislocation is quite complicated but as a rough approximation to its energy we may take the sum of the energy of a straight dislocation passing through the end points and add to this the interaction energy of the kinks. The effective line tension is then $C = C_0 + C_1$, which is probably somewhat of an overestimate. From Foreman[92] for an isotropic crystal $C_0 = (Gb^2 / 4\pi)(1 - 2\nu)(1 - \nu)\ln(R/r)$ for an edge dislocation and $(Gb^2 / 4\pi)(1 + \nu)(1 - \nu)\ln(R/r)$ for a screw while from Southgate and Attard[102] $C_1 = (Gb^2 / 4\pi)(1 - 2\nu)(1 - \nu)(\ln p_0 L + \gamma)$ for screw kinks on an edge dislocation and $(Gb^2 / 4\pi)(1 + \nu)(1 - \nu)(\ln p_0 L + \gamma)$ for edge kinks on a screw dislocation. Thus

$$C_1 / C_0 = \frac{\ln(p_0 L) + \gamma}{\ln(R / r)} \qquad \text{IV-16}$$

for both edges and screws where γ is Eulers constant and the other symbols are as previously defined. For $R / r = 10^4$, $ap_0 = 3\times10^{-2}$ and $L = 3\times10^3 a$ the ratio $C_1 / C_0 = 1/2$. For a kinked dislocation in silver then we need to multiply the values quoted previously (p. 93) for the line tension by a factor of about 1.5.

For frequencies in the kilocycle range and loop lengths of $\sim10^{-4}$cm both the KGL theory and the theory of Seeger and Schiller as presented here will lead to values of τ (Eq. IV-15) at room temperature, which are small compared

to $1/\omega$, so that the internal friction would be expected to increase monotonically with temperature from 4°K to 300°K. If we assume then that the lateral motion of kinks is thermally activated with a diffusion coefficient of the form

$$D = D_0 \, e^{-H/kT} \qquad \text{(IV-17)}$$

and assume the validity of the Einstein relation $D = \mu kT$ then at temperatures below the maximum for which $\omega\tau \gg 1$ we would expect an internal friction from Eq. IV-13 of

$$\Delta = (8\Omega\Lambda Gb^2 D_0 a^2 p_0 / \pi\omega kT)\, e^{-H/kT} . \qquad \text{(IV-18)}$$

This is independent of both the loop length L and the effective line tension C. From Eq. IV-18 we see that a plot of $\ln(T\cdot\Delta)$ vs. $1/T$ should yield a straight line whose slope is equal to H/k. Such plots have been made for the available low temperature data (Fig. 19) for which the results are shown in Fig. 36.

From about 40°K up to the maximum or shoulder exhibited by the internal friction the data fits a straight line with a slope corresponding to an activation energy of H = 0.020 eV for each of the runs of Fig. 19. Below 40°K the internal friction decreases much less rapidly than Eq. IV-18 would indicate and remains substantially above apparatus background even at temperatures as low as 4°K. However, if the activation energy for kink motion is as small

as 0.02 eV, the zero point oscillations of the kinks themselves could give rise to an appreciable mobility independent of temperature. The classical result (Eq. IV-18) should apply to a temperature of approximately $h\nu_k / k$ where ν_k is the kink vibrational frequency. Although fairly localized, a kink would be expected to have a vibrational frequency somewhat lower than the Debye frequency, so that a departure at $\sim$40°K (which for silver is about one fifth of the Debye temperature) is not at all unreasonable.

The shift of the position of the maximum with room temperature annealing is considerable. A two-month anneal resulted in a shift of the maximum from 104°K to 68°K. We can make use of this large temperature shift to obtain an independent check on the activation energy through application of the model to the data of Fig. 36.

While we would normally expect room temperature annealing to result only in a reduction of the loop length, L, through pinning, in silver of the purity used here some rearrangement can take place in times of the order of months. While we do not expect any appreciable change in Λ, the average value of $\langle ap_0 \rangle$ might change considerably.

From Eq. IV-18 the internal friction at low temperatures (below the maximum) is $\Delta_{LT} \sim \langle ap_0 \rangle$ while the internal friction at the maximum is $\Delta_M \sim \langle ap_0 \rangle \cdot L^2$. At the temperature of the maximum internal friction, T_M, we have

$1/\omega = \tau \sim \frac{L^2}{\langle a\rho_0 \rangle} T_M \, e^{H/kT_M}$. Using the indices (1) and (2) to denote the runs corresponding respectively to one day and two months annealing at room temperature, we obtain the following relation

$$\ln\left[\Delta_M(1)\,\Delta^2_{LT}(2)\,T_M(1) \,/\, \Delta_M(2)\,\Delta^2_{LT}(1)\,T_M(2)\right] = (H/k)\left[1/T_M(2) - 1/T_M(1)\right] \qquad \text{(IV-19)}$$

Substituting the appropriate values from Fig. 36 we obtain $H = 0.018$ eV. This is in very good agreement with the value 0.020 eV derived from the low temperature slopes.

We can now consider the magnitude of the internal friction and the relaxation time to see if these lead to reasonable values of the parameters involved, namely Λ, L, ap_0, and D_0. For the lower curve of Figs. 19 and 36, setting $a = \frac{1}{2}\sqrt{3}\,b$, using the values given on P. 93 for the known parameters and the value $H = 0.02$ eV, Eq. IV-18 yields

$$\Lambda D_0 \langle ap_0 \rangle = 95 \text{ sec}^{-1}, \qquad \text{(IV-20)}$$

where all quantities are in cgs units.

For the concept of a kink density to make sense, we must have $ap_0 \gg a / L$, while the approximations made in obtaining the above expressions (neglect of second order terms in p) require $ap_0 \ll \frac{1}{2}$, which is the maximum for an f.c.c. lattice. Thus for typical values (10^{-4} cm) of L encountered we require $\frac{1}{2} \gg ap_0 \gg 3\times10^{-4}$. Eq. IV-20 assumes all dislocations contribute to the relaxation with $ap_0 = \sin\Theta$ = constant.

The only reasonable assumption we can make concerning Θ is that it is random. Thus $\langle ap_0 \rangle = \frac{6}{\pi}(1 - \cos\Theta_M) \simeq \Theta_M^2$. If kinks are not strictly abrupt but have a width w, then presumably dislocations for which $\sin\Theta > a/w$ will behave as strings rather than kink chains[114]. Thus the integration should be terminated at $\Theta_M = a/w$, and IV-20 becomes $\Lambda(a/w)^2 D_0 = 95$. If we take $\Lambda = 10^7$ and estimate $D_0 = \nu_k b^2$, where $(a/w)\nu_D < \nu_k < \nu_D$, we find $19a > w > 7a$. Thus we see that only ~10 per cent of the total dislocation density is effective in contributing to the internal friction, if we take $\Theta_M = 10^{-1}$.

From Eq. IV-13 the magnitude of the internal friction at the peak is, again integrating over Θ,

$$\Delta_{MAX} = 4\,\Omega G b^2 . \Lambda_E\, L^2 / \pi^3 C, \qquad \text{(IV-21)}$$

where $\Lambda_E = 8\Lambda\langle ap_0 \rangle$.

Before making numerical estimates from Eq. IV-21, we need to consider to what extent the line tension C arising from the stress field is increased by the kink gradient pressure term $D / \mu a^2 p_0$ in silver. Taking $\langle ap_0 \rangle = 10^{-2}$, $a = \frac{1}{2}\sqrt{3}\, b$, and making use of the Einstein relation $D = \mu kT$, we find $D / \mu a^2 p_0 = 4.78 \times 10^{-7}\ T(°K)$ ergs / cm. For the lower curve of Figs. 19 and 36, the contribution at the peak temperature (68°K) would be 0.33×10^{-4} erg / cm, compared to a contribution of 2.2×10^{-4} erg / cm arising from the stress field of a kinked 60° dislocation. Using the value 2.5×10^{-4} erg / cm for the total effective line tension at

68°K, $\Delta_{MAX} = 3.95 \times 10^{-3}$, $\Lambda = 10^7$, and the values given on p. 93 for the other constants, Eq. IV-21 yields a value for the loop length of $L = 1.6 \times 10^{-4}$ cm. This is about one-half the network length, L_N, expected for these specimens and seems consistent with the known purity and the fact that the specimen has been held for a considerable time (~two months) at room temperature.

Thus far we have assumed a delta function distribution of loop lengths. If instead we assume the loop lengths are distributed exponentially, the only modification to the discussion so far will be that the average loop length derived from IV-21 will be a factor of 2.1 smaller[90]. The internal friction is independent of the loop length distribution below the maximum. A distribution of loop lengths will, however, lead to a considerable broadening of the maximum. At 300°K, for the lower curve of Fig. 19, the model predicts an internal friction of 1.0×10^{-3} for a delta function distribution and a value 6.0×10^{-2} for an exponential distribution. A direct comparison with the measured value (2.7×10^{-3}) of the internal friction (Fig. 18) is not meaningful for a number of reasons.

First of all, the peak at about 250°K will make an unknown contribution to the internal friction at 300°K. Secondly, we expect a contribution to the internal friction from the scattering of thermal phonons. Using the values of the parameters derived above for an exponential loop length distribution and the value $B = B_T / \langle a p_0 \rangle$, this contribution

to the internal friction is 8.6×10^{-5} at 300°K.

A third objection to using this model at higher temperatures is the fact that we have not considered the effect of thermally generated kink pairs on the motion of the dislocation line. If we assume the losses associated with the thermal generation of kink pairs reach a maximum at the temperature of the Bordoni peak[20], then at 300°K thermal kinks can be generated in phase with the applied stress. We can roughly take this into account formally by replacing the average kink density, p_0, with an effective density, which increases with temperature. Finally, if the barrier to kink motion is as small as 0.02 eV, then at room temperature it is comparable to kT, and it is no longer clear how to calculate the kink mobility[119].

In determinations of B in the KGL model from internal friction measurements[10, 90] at room temperature, the value of B is invariably substantially larger than Leibfried's formula (Eq. IV-5) would indicate. Since at sufficiently high temperatures we expect the mobility to be determined primarily by phonon scattering, and an effective value of $\langle ap_0 \rangle \simeq a/w \simeq 10^{-1}$, this may be due to the effect of kinks. However, the fact that the internal friction is found to decrease up to 500°K in the present experiments would indicate that at room temperature the mobility is determined primarily by the presence of a finite Peierls

barrier for kink motion.

In summary, then, we see that the thermally activated motion of intrinsic kinks can account very satisfactorily for the magnitude and temperature dependence of the observed 'background' internal friction. The model leads to an activation energy for kink motion of 0.02±0.002 eV, and accounts satisfactorily for the breadth of the maximum as well as the large shift in the temperature of the maximum with room temperature annealing.

3. Strain Amplitude Dependence. We would now like to discuss the observed amplitude dependence (see Fig. 25) at low temperatures (T<300°K). Three features of the amplitude dependence should be noted: 1) All the curves show a rise at low strain amplitudes, or, alternately, a minimum in Δ as a function of strain amplitude; 2) Δ begins to increase with increasing strain amplitude at very low ($\sim 3 \times 10^{-8}$) strain amplitudes even at 4.2°K; 3) an inflection is observed in some of the curves of Δ vs. ϵ_0 at about $\epsilon_0 = 1 \times 10^{-7}$.

The rise in Δ at low strain amplitudes which is accompanied by an increase in modulus may possibly be evidence for the exhaustion of kink motion on dislocations lying at small angles to close-packed directions[115, 116]. This same effect has been observed over the entire temperature range (4.2°K - 1000°K) on all 6-9's silver specimens

studied. A similar rise has been reported in other metals by several investigators[53, 106, 107] at or above room temperature. At the present time any attempt at a quantitative discussion would not seem justified.

The first detailed treatment of the amplitude dependent internal friction is that of Granato and Lücke given in the introduction. As can be seen from Eq. I-4, a plot of $\ln(\epsilon_0 \cdot \Delta_H)$ vs. $1/\epsilon_0$ should yield a straight line having a slope c_1 and an intercept c_2. Such plots are generally referred to as Granato-Lücke plots. It is often observed that in high purity materials curved plots of this type are obtained[10], especially at the lower strain amplitudes. However, the G-L plots which have been prepared from the strain amplitude data given in Fig. 25 (taking the amplitude independent component Δ_I equal to the minimum observed value of the decrement in each case) are indeed good straight lines up to strain amplitudes of about 10^{-7} at all temperatures between 4.2°K and 300°K. (See Fig. 37.)

At approximately this same strain amplitude, some of the curves in Fig. 25 exhibit an inflection indicating a marked change in the amplitude dependence. Further evidence for this change in Δ_H is apparent when we consider the ratio of the amplitude dependent modulus defect $(\Delta E/E)_H$ to Δ_H. According to the Granato-Lücke theory this ratio, r, should

be a constant of the order of unity. A plot of $(\Delta E/E)_H$ vs. Δ_H is shown in Fig. 38 for the data at 4.2°K given in Fig. 25. As can be seen in Fig. 38, $(\Delta E/E)_H = 0.64\,\Delta_H$ initially. However, at higher values of Δ_H an almost discontinuous departure from this linear relationship is observed, which corresponds to the strain amplitude at which Δ_H departs from the G-L relationship (Eq. I-4). A similar result holds for the data at other temperatures. The value of r determined at each temperature is listed in Table V.

This suggests that there are two separate contributions to the observed strain amplitude dependence at low temperatures. One of these contributions, i.e., that observed at the lower strain amplitudes, appears to be adequately described by Eq. I-4 up to amplitudes of the order of 10^{-7}. Eq. I-4 would indicate that the internal friction will reach a maximum at $\epsilon_0 = c_2$ and decrease at higher amplitudes as $1/\epsilon_0$. Experimentally it would appear that the internal friction reaches an amplitude-independent plateau at which $\Delta_H = (c_1/c_2)e^{-1}$ corresponding to the maximum value of Eq. I-4. This component, which has been designated Δ_{H_1}, has been subtracted from the total observed amplitude-dependent decrement Δ_H, and the difference, denoted by Δ_{H_2}, has been replotted in Fig. 39 as $\ln \epsilon_0 \Delta_{H_2}$ vs. $1/\epsilon_0$. Again the data fall on a reasonably straight line, although the fit is somewhat poorer than that obtained

at lower strain amplitudes. It thus appears that both contributions initially obey the Granato-Lücke relation (I-4).

The presence of two components can be interpreted in terms of two separate systems of dislocations, each being characterized by different values of L_c, L_N, and F_m. Studies[90, 108] of irradiation pinning in copper single crystals also indicate that the irradiation data can best be accounted for by assuming two independent dislocation systems are contributing to Δ_I, although in the present case the possibility of a single system with both strong and weak pins cannot be ruled out.

While the experimental data appears to exhibit the predicted dependence on strain amplitude, the magnitude of the constant C_2 determined from the experimental data is two orders of magnitude smaller than one would expect for reasonable values of the parameters involved (Eq. I-6). Thus mechanical breakaway from pinning points cannot account for the observed amplitude dependence. In addition, from Table V in which the values of c_1 and c_2 corresponding to both amplitude dependent components are listed for each of the temperatures at which measurements were made, it is apparent that both Δ_{H_1} and Δ_{H_2} exhibit maxima as a function of the temperature. The Granato-Lücke theory as outlined in the introduction does not take into account the

fact that thermal energy may assist dislocations in breaking away from pinning points, nor does it allow for the possibility that L_c may also be a function of the temperature, i.e., that the number of pinning points may change with temperature. While we do not expect the pinning point distribution on the dislocations to change appreciably below $\sim 200°K$, the effect of thermal forces on the depinning process is expected to be large[55, 56]. The values of C_1 and C_2 determined may then only represent curve fitting. In this case C_2 represents the strain amplitude at which the internal friction reaches a maximum while the quantity $0.368\ C_1 / C_2$ gives the magnitude at the plateau.*

The thermal oscillations of a pinned dislocation have been considered by Leibfried[55] to a limited extent, while Friedel[57] has considered the effect of thermal breakaway on the amplitude dependent internal friction. Leibfried's treatment is concerned primarily with the oscillations of the line at zero applied stress, while Friedel's treatment is only valid over a severely limited range of both temperature and strain amplitude. Recently an attempt has been made by Teutonico, Granato and Lücke[56] (TGL) to include the effects of thermal activation in detail, but the

*The separation of Δ_H into two components would still seem justified, however, since the shape of some of the curves as well as the relation between Δ_H and $(\Delta E/E)_H$ indicate two components are contributing.

problem is quite complicated and has not yet been satisfactorily resolved to the extent that a direct quantitative comparison with experiment can be made. Their results do, however, predict that a stress threshold for depinning will still exist in the presence of thermal fluctuations. In addition, the results of Teutonico et al. indicate that Δ_H should go through a maximum as a function temperature for a given strain amplitude.

For a dislocation loop with a single pinning point TGL calculate the potential energy of the configuration as a function of the pin-dislocation separation using a linearized form of the Cottrell interaction[109]. They find that below a critical stress, σ_T, only a single energy minimum corresponding to the pinned state exists, while above a second critical stress, σ_B, again only a single energy minimum corresponding to the unpinned state exists. At intermediate stresses both minimums exist separated by an energy maximum. For a loop of length 2L with a single pinning point at the center, the mechanical breakaway stress, which is the same as in the original G-L treatment, is

$$\sigma_B = 2\sqrt{2}\,U_0 / 3r_o bL \qquad \text{(IV-22)}$$

where U_0 is the magnitude of the pin-dislocation interaction energy, and r_o is the distance of closest approach of

the pinning point to the dislocation. The lowest stress at which thermal breakaway is possible is given by

$$\sigma_T = 6\ Cr_0\ /\ bL^2. \qquad \text{(IV-23)}$$

For typical values of L we see that this leads to a critical strain amplitude $\epsilon_T = \sigma_T\ /\ RE$ of the order of magnitude of the observed minimum.

The TGL treatment may also account for the observed minimum, since at stresses lower than σ_T the displacement of the dislocation line near the pin is determined primarily by the line tension, and the pinning point is less effective in restricting the motion of the dislocation. Although we expect that kinks will modify the form of the interaction between the pinning point and the dislocation, the results of TGL will not be appreciably changed as long as the range and magnitude of the interaction is not greatly different than that given by the linearized Cottrell interaction.

The fact that appreciable amplitude dependence is observed at 4.2°K would, however, require that the kinks be considered expressly in any rate calculations. This does not completely rule out the interpretation placed on the 'background' internal friction, since the majority of dislocations will make appreciable angles with the close-packed direction. From the discussion in Section 2, the value of

$a/w \sim 10^{-1}$ derived from the 'background' insures that even at low temperatures ~90 per cent of the dislocations are mobile.

Let us assume then that dislocations which are mobile at low temperatures give rise to the observed amplitude dependence through depinning. Since we have ruled out the possibility of mechanical breakaway, the temperature, amplitude, and frequency dependence will all be determined by the rates at which thermal depinning and repinning occur.

In a subsequent paper Granato et al.[110] calculate the rate at which thermal depinning occurs using Vineyard's[111] treatment of absolute rate theory. They derive a rate constant for depinning of

$$\Gamma = \nu_{eff}\, e^{-\Delta U/kT} \qquad \text{(IV-24)}$$

where $\Delta U \simeq U_0$ for stresses well below the mechanical breakaway stress, and the "effective attack frequency" ν_{eff} is

$$\nu_{eff} = \prod_{i=1}^{N} \nu_i \Big/ \prod_{i=2}^{N} \nu_i' \qquad \text{(IV-25)}$$

where the ν_i + ν_i' are the eigenfrequencies of the crystal

with the dislocation in the pinned and saddle point configurations, respectively. Granato et al. treat the dislocation as a continuum string and cut the number of modes off at $N = 2L/b$. (It is assumed that the vibrational modes associated with the lattice cancel out in the ratio taken in IV-25.) By assuming the pin exerts a force on the dislocation at only one point, they are able to calculate the ν_i and ν_i' directly and evaluate ν_{eff}. They find ν_{eff} is independent of L and depends only on the magnitude and form of the interaction force. For the linearized Cottrell interaction they find

$$\nu_{eff} = (U_0 / 8Cb^2) \sqrt{G/\rho}. \qquad \text{(IV-26)}$$

Contributions to the internal friction can arise in a number of ways with depinning: 1) A dynamic hysteresis loss resulting from the phase lag between the dislocation strain and the applied stress; 2) an enhancement of other loss processes through an increase in the effective loop length at high strain amplitudes, and 3) a static hysteresis loss. The third case can only arise if we exclude the possibility of simultaneous breakaway from two or more pinning points and assume that breakaway from a single pinning point results in the breakaway of the whole network length. While we cannot make quantitative comparison with experiment even

in the relatively simple case of breakaway from a single pinning point, we would expect a contribution of type 1) to reach a maximum at a temperature for which $\omega \approx \Gamma'$. The observation of a maximum in the amplitude dependence at about 75°K and 105°K would imply (from Eqs. IV-25, 26) that U_0 was of the expected (0.1eV) order of magnitude for a pin-dislocation interaction[109].

Thus we see that the TGL theory can account semi-quantitatively for a number of features of the observed amplitude dependence, in particular: The appearance of amplitude dependence at very low amplitude; the relatively small temperature dependence of the amplitude at which the internal friction increases appreciably, and the fact that the magnitude of Δ_H passes through a peak at relatively low temperatures. On the other hand, the temperatures at which the two amplitude dependent components appear to reach a maximum coincide closely with temperatures at which there is evidence of structure at low amplitudes. The possibility that the observed amplitude dependence is indeed related to processes responsible for the structure can not be ruled out.

4. <u>Influence of Oxygen.</u> When we compare the internal friction of a crystal in the oxygen-free condition to that observed in the same crystal containing 40 ppm of oxygen (Fig. 16), it is apparent that the 'background' decrement has been reduced by nearly two orders of magnitude

to values less than 10^{-5}. While this reduction is substantially greater than that observed for considerably higher concentrations of substitutional impurities, it can be understood simply on the basis of the higher mobility of oxygen as compared to substitutional impurities.

On the basis of thermodynamic equilibrium, Cottrell[4] has shown that the atomic fraction of impurities at a dislocation is given by

$$c_d = c_0 \, e^{U_0 / kT} \qquad \text{(IV-27)}$$

where c_0 is the atomic fraction of impurities in the lattice far from the dislocation, and U_0 is the impurity-dislocation binding energy. This equation should apply[5] for values of c_d up to saturation for which $c_d = 1/2$. In order to reach equilibrium with respect to the dislocation, the impurity must diffuse distances of the order of the spacing between dislocations in times of the order of days. At low temperatures, then, the atomic fraction of impurities at a dislocation will be characteristic of the temperature for which the diffusion coefficient

$$D = D_0 \, e^{-H/kT} \qquad \text{(IV-28)}$$

is of the order $L_N^2 / 10^5 = 10^{-13}$ cm^2/sec. For oxygen ($D_0 = 3.66 \times 10^{-3}$, $H = 0.50$eV) this will be 240°K, while for typical substitutional impurities in silver[112] ($D_0 = \sim 1$, $H = 2.0$eV) this will be ~720°K. If we take $U_0 = 0.1$eV in Eq. IV-27 for both oxygen and substitutional impurities,

then, at low temperatures oxygen would result in 25 times as many pinning points as an equal amount of substitutional impurity. Taking U_0 = 0.2eV (which we believe to be the magnitude of the oxygen dislocation interaction) and assuming equilibrium is reached at ~250°K, Eq. IV-27 yields $c_d / c_0 = 10^4$. Thus, at low temperatures 40 ppm O_2 will reduce the average loop length to values less than 10^{-7} cm. On the basis of any of the models considered for the internal friction this will be sufficient to account for the observed reduction.

The amplitude dependent internal friction for the oxygen-saturated specimen (Fig. 28) is similarly reduced in magnitude, while the strain amplitude at which amplitude dependence appears is a factor of 50 higher. The magnitude of Δ_H (taken at the highest strain amplitude of 10^{-5}) appears to reach a maximum between 120°K and 166°K. No amplitude dependence is observed above about 220°K. There does not appear to be any evidence for two amplitude dependent components. The observed behavior is qualitatively what we would expect, on the basis of the TGL theory discussed above, for a ten-fold reduction in loop length if U_0 is 0.2 eV. However, for a binding energy of 0.2 eV, we expect that the dislocations are nearly saturated with oxygen so that the origin of this amplitude dependence is not at all clear. The lack of amplitude dependence above

220°K eliminates the possibility of obtaining information on the oxygen-dislocation binding energy through the study of amplitude dependence.

The structure observed in the internal friction of the oxygen-saturated specimen occurs generally in same temperature ranges in which structure was apparent in the unsaturated condition. It would appear that the structural features are less sensitive to a reduction in the loop length than the 'background' internal friction. This would indicate that oxygen may prove of value in revealing structural features obscured by a high 'background.'

Papazian[59] has observed in measurements on single crystals at 2 cps three peaks which are definitely associated with the presence of oxygen in silver. These peaks are found at 130°, 180°, and 260°K. The corresponding activation energies, derived from a Wert and Marx plot are 0.37± 0.04eV, 0.50±0.04eV, and 0.74±0.04eV respectively. Consequently, these peaks, if present, should be observed at 185°±10°K, 255°±10°K, and 370°±20°K in measurements at ~27 kc. The two lower temperature peaks which both depend on the square of the oxygen concentration, Papazian assigns to the stress induced reorientation of oxygen-pairs.

From Papazian's data we can estimate the peak heights expected in a ⟨111⟩ crystal containing 40 ppm O_2. For the 130° and 180°K peaks we would only expect heights of 5×10^{-6} and 2×10^{-5} respectively. Thus, they may represent part of

the structure observed here (Fig. 24) in this temperature range. The upper peak which was found to be nearly independent of the oxygen concentration may very well correspond to the peak seen at 365°K in the present experiment. This peak is clearly absent in the oxygen-free silver and constitutes the major feature of the damping observed in specimen 34E (Fig. 16) containing 40 ppm. O_2. From the shift in peak temperature with frequency, making use of Papazian's data, and assuming a simple relaxation, we obtain a value of 0.75±0.04eV for the activation energy associated with this peak. We can also estimate the activation energy from the half-width of the peak (Eq. IV-11) since it exhibits a modulus defect compatible with a single relaxation of the observed strength ($\Delta_{MAX} = 2.6 \times 10^{-3}$). From Eq. IV-11 we obtain an activation energy of 0.71±0.06eV from the half-width which agrees closely with the value of 0.75±0.04eV obtained from the temperature shift. Papazian's observation that the peak nearly disappears with deformation at 77°K and reappears following room temperature annealing would indicate that the relaxation arises from the presence of oxygen at the dislocations and that this peak is due to an oxygen dislocation interaction.

A model which leads to an internal friction peak of the relaxation type arising from the motion of dislocations with impurity atmospheres has been proposed by Schoeck[30] to

explain the cold-work peak observed in most b.c.c. metals containing interstitial impurities. Briefly, the model assumes that dislocations are pinned along their length at fixed points, (i.e., nodes or substitutional impurities) with an average spacing L_0, and that interstitial impurities, with an average separation $\delta L \ll L_0$, further pin down the dislocation to the extent that it can move only if the interstitials along its length diffuse with it. As we shall see below, the application of this model with some modification to silver containing oxygen can explain the experimental observations on the peak occurring here at 365°K and leads to a value for the binding energy between oxygen and a dislocation in silver of 0.25±0.06eV.

We will consider a length of dislocation L_0 pinned at the points $x = 0$, L_0 and designate displacement normal to the dislocation line by y. Each segment of this dislocation of length δL will contain by definition one oxygen atom. The force acting on such a segment δL, and thus on the oxygen atom, under an applied stress will be

$$F_{\delta L} = \sigma b \cdot \delta L - C\left(-\frac{\partial^2 y}{\partial x^2}\right)\delta L \qquad \text{(IV-29)}$$

The term $C\left(-\frac{\partial^2 y}{\partial x^2}\right)$ arises from the fact that the dislocation is pinned at $x = 0$, L_0 and thus must bow between these points resulting in a reaction force due to the curvature, i.e., increased length, of the dislocation. The velocity, v, of the

oxygen atoms, and, therefore, of the dislocation, is determined by the mobility of the oxygen. Since the mobility, μ , is defined as the velocity per unit force, we have

$$v = \frac{\partial y}{\partial t} = \mu F_{\delta L} \qquad \text{(IV-30)}$$

Thus, the equation of motion of the dislocation is

$$\frac{dy}{dt} = \mu \delta L \left(\sigma b + C \frac{\partial^2 y}{\partial x^2} \right). \qquad \text{(IV-31)}$$

We can rewrite Eq. IV-31 as

$$\frac{1}{\mu \delta L} \frac{dy}{dt} - C \frac{\partial^2 y}{\partial x^2} = \sigma b \qquad \text{(IV-32)}$$

which is the familiar string equation (Eq. IV-12) with $B = 1/\mu \delta L$. Assuming only one lowest energy site per atomic plane threaded by the dislocation, δL, is related to the atomic fraction of oxygen at the dislocation by

$$\delta L = a / c_d \qquad \text{(IV-33)}$$

where a~b is the atomic spacing along the dislocation line. Making use of the Einstein relation, $\mu = D/kT$, we have $B = kTc_d / aD$.

The solution to Eq. IV-32 is given by Eqs. IV-13, 14. We can now characterize the relaxation by the parameters

$$\Delta_{MAX} = 4Gb^2 \Omega \Lambda L_0^2 / \pi^3 C \qquad \text{(IV-34)}$$

and

$$\tau = kTc_d L_0^2 / \pi^2 bCD \qquad \text{(IV-35)}$$

where c_d is the atomic fraction of oxygen at the dislocations, D is the diffusion coefficient of the bound oxygen, and the other symbols are as previously defined. The atomic fraction of oxygen at the dislocations, c_d, is related to the atomic fraction in the lattice far from the dislocations, c_0, by Cottrell's relation

$$c_d = c_0 \, e^{U_0 / kT} \qquad \text{(IV-36)}$$

where U_0 is the binding energy between oxygen and the dislocation. Eq. IV-36 should apply as long as $c_d < 1/2$, and equilibrium between dislocations and the surrounding lattice can be maintained, and should thus apply in the present case.

Before we can apply the theory, we need to know the appropriate value of D for an oxygen atom bound to a dislocation. If we write

$$D = D_0 \, e^{-E_M/kT} \qquad \text{(IV-37)}$$

This requires specifying D_0 and E_M.

In applying this theory to the CWP in b.c.c. metals, Schoeck and Mondino[30] take E_M as the sum of the activation energy for diffusion in the bulk and the binding energy of the interstitial to the dislocation. According to Schoeck and Mondino, this is due to geometry of the b.c.c. lattice, which requires the interstitial to move out of the slip plane

of the dislocation line in order to follow its motion[113]. In the f.c.c. silver lattice the interstitial can move parallel to the slip plane, so that E_M can be taken equal to the activation energy for the migration of oxygen in the bulk, since we have no a priori reason for assuming otherwise as long as the oxygen remains bound to the dislocation.

As regards D_0, Schoeck and Mondino take D_0 appropriate to bulk diffusion of the interstitial without comment. In the case where the interstitial remains bound to the dislocation, Freidel[5] has pointed out, in considering a similar problem in relation to microcreep, the effective frequency at which the diffusion barrier is attacked is that appropriate to the dislocation rather than the interstitial. He takes the lowest frequency mode of dislocation,

$$b\nu_D / \delta L = c_d \nu_D, \qquad \text{(IV-38)}$$

as the effective frequency for which $D_0 = D_0(\text{interstitial})C_d$. This would eliminate the factor C_d in Eq. IV-35, giving a relaxation time independent of C_d. The dragging of an interstitial is essentially the same problem as the breakaway of the dislocation from its pinning point as treated by Granato et al[110]. The difference is in the form of the potential at the pinning point. In the treatment of Granato et al. ν_{eff} is independent of the loop length, and depends only on the force constants, $\partial^2 U / \partial^2 y$, at the saddle and equilibrium configurations.

The expression derived by Granato et al. for ν_{eff} (Eq. 34, p. 2738) is

$$\nu_{eff} = (s^{1/2}\, b\, \gamma \,/\, 10.8c)\, \nu_D \qquad \text{(IV-39)}$$

where $\gamma = -\partial^2 U / \partial y^2$ at $y = 0$ (equilibrium configuration), and s = ratio of γ_e / γ_s. The subscripts e, s refer to the equilibrium and saddle point configurations. Use of IV-39 with $U = E_M/2(1 + \cos 2\pi y/b)$, as a simple approximation to the diffusion barrier, yields $\nu_{eff} \simeq \nu_D$. Since this form undoubtedly underestimates ν_{eff} we will use $D_0 = D_0$ (oxygen). Inserting Eqs. IV-36 and IV-37 into Eq. IV-35 we see that the activation energy associated with the relaxation is

$$H = E_M + U_0, \qquad \text{(IV-40)}$$

assuming saturation does not take place.

For $U_0 = 0.25$ eV saturation will occur at 260°K for 40 ppm O_2. U_0 can be found assuming saturation at 260°K with $c_d = ½$. This is in agreement with Papazian's observation that the peak temperature is independent of the oxygen concentration for 45 - 600 ppm O_2.

From Eqs. IV-35, 36 we have, assuming $\Lambda_1 = \Lambda_2$,

$$\log(f_2 T_2 \Delta_2 / f_1 T_1 \Delta_1) = (E_M / k)\,(1/T_1 - 1/T_2) - \log 2c_0 - U_0 / kT_2 \qquad \text{(IV-41)}$$

where the subscripts 1 and 2 refer to 260°K and 365°K respectively. Eq. IV-41 then yields U_0 = 0.21 eV for the binding energy of oxygen to a dislocation.

However, there is a serious objection to the use of the model at such high interstitial concentrations, since it does not take into account the effect of line tension on the diffusion of a single interstitial. Consider the figure below.

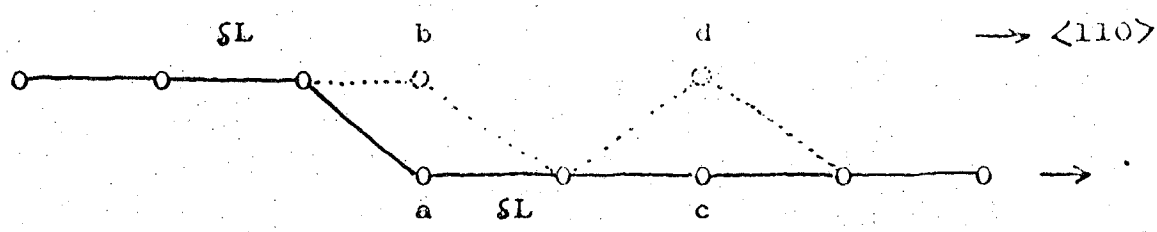

The circles represent interstitials along a dislocation with an average spacing $\delta L = b/c_d$. In an f.c.c. lattice the closest packing of interstitials is along ⟨110⟩ . The presence of a high concentration of interstitials will then lead to a situation somewhat analagous to a high Peierls stress. If we treat the segments between pinning points as a string, then the motion of the line can be described in terms of the lateral diffusion of kinks corresponding to a jump a→b. A jump of the type c→d, corresponding to kink pair generation, will not lead to a relaxation except in the presence of relatively large internal or applied stresses.[23, 114, 115] Since above room temperature we are dealing with well-annealed single crystals, we do not expect

any appreciable internal stresses. Therefore, the applied stress would have to be large enough to compensate for the difference in energy between states c and d arising from the increase in line length. From the figure above, the energy difference between c and d due to the line length change is

$$2\epsilon_k = 2C\left[\sqrt{\delta L^2 + a^2} - \delta L\right] \simeq Ca^2 / \delta L = Ca^2 c_d / b.$$

In order to have any appreciable relaxation, this must be balanced by the work done by the applied stress during the transition, $W = \sigma ab\,\delta L = \sigma ab^2 / c_d$. Thus, the applied stress must be at least

$$\sigma_R = Cac_d^2 / b^3. \qquad \text{(IV-42)}$$

If we compare σ_R with the minimum stress for thermal breakaway in the TGL theory, Eq. IV-23, we see they are comparable. Thus we do not need to consider either breakaway or jumps of the type c-d if $c_d > 5 \times 10^{-3}$, since the maximum applied stress in all the present experiments was less than $\sigma = 10^{-5}$ G.

We can describe the motion of the line then in terms of transitions of the type a→b (below 400°K, at least). The line tension will also cause the motional energy E_M to be lowered in a jump a→b, since the line will be shorter in the intermediate position. From the figure this amounts to a lowering of E_M by $a^2C\,c_d / 4b$. A slightly more detailed

calculation (taking into account the discrete geometry) gives nearly the same result so that E_M becomes

$$E_M' = H_0 - a^2 C\ c_d\ /\ 4b. \qquad \text{(IV-43)}$$

If we choose to describe the motion of the line in terms of the lateral diffusion of 'kinks', the diffusion coefficient of the 'kinks' is

$$D_k = (D_0\ /\ c_d^2)\ e^{-E_M'/kT} \qquad \text{(IV-44)}$$

where $D_0 = D_0$ (oxygen).

From our previous discussion (pp 110 ff) the relaxation time and peak height are given by*

$$\tau_k = \left[L_0^2\ kT\ c_d^2\ /\pi^2 C D_0 a\ (ap_k)\right]\ e^{E_M'/kT} \equiv \tau/\ ap_k \qquad \text{(IV-45)}$$

and

$$\Delta_{MAX} = 4\Omega G b^2 \Lambda\ L_0^2\ /\ \pi^3 C \qquad \text{(IV-46)}$$

where p_k is the density of a-b type configurations or 'kinks.' A little care is needed in relating ap_k to c_d and Θ, the angle between the dislocation and the close-packed $\langle 110 \rangle$ direction. For $\sin\Theta \geqslant c_d$ the dislocation will be able to accomodate all the interstitials without deviating from a straight line so that $ap_k = 0$. For $c_d \geqslant \sin\Theta \geqslant c_d\ /\ 2$ we will have one 'kink' for each excess interstitial, so that $ap_k = c_d - \sin\Theta$. For $0 \leqslant \sin\Theta \leqslant c_d\ /\ 2$ we will have one

*A more detailed treatment following the approach of Ninomiya et al.[117] yields identical results.

'kink' for each interstitial, so that $ap_k = \sin\Theta$. Since in the f.c.c. lattice $\sin\Theta \leq ½$, we will approximate $\sin\Theta \simeq \Theta$. Thus, if we write $\Lambda(\Theta)\, d\Theta$ as the dislocation density for which Θ lies between Θ and $\Theta + d\Theta$, we have for Δ,

$$\Delta = \Delta_{MAX} / \Lambda \int_0^{1/2} \Lambda(\Theta) \left[\omega\tau_k(\Theta) / 1 + \omega^2\tau_k^2(\Theta) \right] d\Theta \qquad \text{(IV-47)}$$

since $ap_k = 0$ for $\Theta \geq c_d$ and c_d is limited to a maximum value of ½, the upper limit in IV-47 becomes c_d. The integral will be split in two parts, $0 - c_d / 2$ and $c_d / 2 - c_d$ using the appropriate values of ap_k. With a change of variable in the second integral and a little algebra, we find

$$\Delta = \omega\tau\Delta_{MAX} / \Lambda \int_0^{c_d/2} \left[\Lambda(\Theta) + \Lambda(c_d - \Theta) \right] \frac{\Theta}{\Theta^2 + \omega^2\tau^2} d\Theta \qquad \text{(IV-48)}$$

where τ is defined in IV-45.

Before we can continue, we must make an assumption concerning the angular distribution $\Lambda(\Theta)$. Since we are dealing with a material with a low Peierls potential which was annealed at high temperatures, the only reasonable assumption is that Θ is random. Thus $\Lambda(\Theta)$ = constant = 2Λ. Thus IV-48 becomes

$$\Delta = c_d \Delta_{MAX} \left[x \log (1 / x^2 + 1) \right] \qquad \text{(IV-49)}$$

where $x = 2\omega\tau / c_d$. The function in brackets is similar to

the relaxation function with a maximum value of 0.8 at $x = ½$. We can then approximate IV-49 by a single relaxation function

$$\Delta = 2\Delta^{E}_{MAX}\,\omega\tau_E \,/\, (1 + \omega^2\tau_E^2) \qquad \text{(IV-50)}$$

where $\Delta^{E}_{MAX} = 0.4\ c_d\ \Delta_{MAX}$ and $\omega\tau_E = 4\omega\tau/\ c_d$. Thus we see that both the relaxation strength, Δ^{E}_{MAX}, and the relaxation time, τ_E, are proportional to c_d. Assuming as before that $c_d = ½$ at 260°K and Λ(2 cps) = Λ(28 kc), we find that our information on c_d at 365°K is included only in the change in E'_M with c_d. Thus the value derived for U_0 will be quite sensitive to the value taken for C in Eq. IV-43. Since our knowledge of C is somewhat limited, we have taken the value appropriate to an edge dislocation as a lower limit and twice this value as an upper limit. For those values of C we find U_0 = 0.22 eV and 0.28 eV respectively. We conclude the model leads to a value for the binding energy, U_0, of oxygen to an edge dislocation of 0.25±0.04 eV.

Using this value for U_0, we are in a position to compare the model with the experimental observations. In Fig. 40 the experimentally measured peak is compared with both Eqs. IV-49, 50. As can be seen, the approximate relation IV-50 fits the data quite well, while IV-49 leads to a somewhat broader peak. This may indicate that a slightly larger value of U_0 might be more appropriate. Substituting the observed values of Δ_{MAX} and τ(365°K) into IV-50, we

can solve for the quantities Λ and L_0^2 / C. The other parameters entering are all known and are listed on p. 93. We obtain

$$\Lambda = 2.8 \times 10^7 \text{ cm/cm}^3$$

and

$$L_0^2 / C = 4.6 \times 10^{-4} \text{ cm}^2 / \text{dyne}.$$

The value obtained for the dislocation density Λ is very reasonable, although it is a factor of 3 higher than that expected for these crystals (see pp. 93-94). For a value of C appropriate to an edge dislocation, we obtain $L_0 = 1.5 \times 10^{-4}$ cm. The value of L_0 would appear reasonable since it is of the order of the expected network length $L_N \simeq 1.9 \times 10^{-4}$ cm.

Although the experimental observations on this peak are rather meager, the present model appears to account quite satisfactorily for the available data. The model, suitably modified for a b.c.c. lattice, might also account quite directly for a characteristic feature of the CWP in b.c.c. metals, namely that the peak temperature and peak height both depend on the initial interstitial content for low concentrations. At higher concentrations the peak temperature and peak height are independent of the interstitial content in agreement with IV-50.

As regards alternate explanations for the present

peak, we can not rule out the possibility that ordered interstitial clusters at dislocations give rise to the relaxation. While this theory, due to Boone and Wert[35], is necessarily only qualitative, the present experimental observations are not in disagreement with such an interpretation. In fact, Papazian's observation of what appear to be oxygen pair peaks would suggest that the possibility of the formation of larger clusters definitely exists. The possibility that the relaxation arises from the alternate precipitation and solution of Ag_2O, after Mura et al.[33], can be ruled out due to the very large changes in volume required for Ag_2O precipitation internally in the silver lattice.

We would now like to proceed to a discussion of the data obtained at higher temperatures.

C. INTERNAL FRICTION AT HIGH TEMPERATURES

The most obvious feature of the damping in well-annealed 6-9's silver specimens (Figs. 16 and 18) is the pronounced minimum in Δ_I at about 550°K. It is further apparent (Fig. 13) that above this minimum the damping can be characterized as exponential in 1/T°K with an apparent activation energy of about 0.22 eV. In general, the magnitude of the damping at higher temperatures could be reduced by an order of magnitude by cyclic annealing without

appreciably changing the apparent activation energy, whereas the damping at room temperature was only slightly reduced by this annealing treatment. From observations of the annealing behaviour at low (~400°K) temperatures, we conclude that the major effect of annealing is to shift the position of the minimum to higher temperatures. It thus appears that two processes are contributing to the damping in 6-9's silver above room temperature, one process which gives rise to the decrease in damping at lower temperatures and a second for which the damping increases exponentially with temperature.

We will first consider the lower temperature region, in which the damping is decreasing. The only previous measurements on pure silver above 300°K are those of Köster[69], Pearson and Rotherham[71], and Nowick[70]. None of these investigations exhibited a minimum in Δ. All were made at relatively low frequencies on polycrystalline material and were concerned primarily with grain boundary relaxation phenomena. However, other investigators have found a minimum in the damping in this temperature range in copper single crystals. Pittenger[115] and Beshers[67] have both observed a minimum in the damping in high purity annealed copper crystals at about 500°K. Stevens[116] has observed similar minimums in impurity-doped copper crystals (0.05-0.5% Cu or Ni) for which a broad peak is observed just below room tem-

perature. While we feel this decreasing contribution to the internal friction is related to the decreasing 'background' observed here at lower temperatures, it is also conceivable that the observed decrease corresponds to the high temperature side of a peak just below room temperature. Since we were not able to make measurements below room temperature without the intervening transfer, we cannot decide between these. However, the fact that we do observe a damping which is decreasing with temperature for all specimens in both apparatus at 300°K, and considering that all of the peaks reported in pure f.c.c. metals in the range below 300°K are observed to anneal out well below the temperatures used here, we feel that the first possibility is the more likely. The observed decrease cannot be considered a hysteresis effect due to annealing, as suggested by Beshers, since the damping is reproducible on heating and cooling in this range. The possibility that the observed decrease in Δ is the result of a decrease in the average loop length, for example by the disassociation of pinning point clusters[41] into a larger number of individual pinning points, can be eliminated since the modulus defect increases over the entire temperature range.

At high temperatures the internal friction of most metals exhibits an exponential rise with temperature. From the discussion in the introduction it would appear that the

present results fall into the second category, i.e., the phenomena Mason[8] has named "temperature-activated hysteresis" resulting from the thermal depinning of dislocations.

In Mason's model the energy loss associated with the internal friction arises when two adjacent vibrating dislocation loops are momentarily freed from their common pinning point by thermal fluctuations. The resulting energy transfer between the two loops takes place irreversably and gives rise to the observed damping. Mason obtains

$$\Delta = (\sqrt{6}\, b^2 V_s / \pi)\, N_0 \exp(-U_0 / kT) \qquad \text{(IV-51)}$$

where b=Burger's vector of the dislocations, V_s is the shear wave velocity, N_0 is the total number of pinning points, and U_0 is the binding energy of the pinning point to the dislocation. Although IV-51 indicates a damping independent of frequency, Mason's model leads to an inverse frequency dependence. At one point in the derivation[8, 17] of IV-51, the logarithmic decrement is associated with $-(1/W)dW/dt$, where W is the stored energy. Since $-(1/W)dW/dt$ is twice the attenuation, $\alpha = f\Delta$, IV-51 should be corrected by a factor $1/2f$.

The same frequency and temperature dependence can also be obtained from models[43, 56, 57] which include the effect of temperature on the static hysteresis models of Granato and Lücke[36] or Weertman[44].

We do not feel that any of the above models are appropriate to the present case. From our attempts to measure the frequency dependence by exciting higher harmonics of the specimen, we concluded the damping is independent of frequency at best and more likely increases with increasing frequency. Secondly, all of the above models assume the concentration of pinning points is independent of the temperature. Even for the relatively high diffusion energies (1.5-2.0 eV) observed for substitutional impurities in silver[112], we expect that equilibrium between dislocations and the surrounding lattice could be maintained at temperatures as low as 550°K.

As we shall see, the present results can be satisfactorily explained from a consideration of the effect of a change in the average loop length, arising either from an increase in temperature or strain amplitude, on the damping arising from the scattering of thermal phonons.

The KGL (string) model predicts

$$\Delta_I(L) = (\Omega \Delta_0 \omega B / \pi^3 C)\ N(L)\ L^5 \qquad \text{(IV-52)}$$

and

$$(\Delta E/E)_I(L) = (\Omega \Delta_0 / \pi^2)\ N(L)\ L^3 \qquad \text{(IV-53)}$$

where $\Delta_0 = 8Gb^2 / \pi^2 C$ and N(L) is the loop length distribution function, i.e., $\int N(L)\ L\ dL = \Lambda$. The average loop length L_0 will be determined first by the network length

L_N and second by the additional pinning arising from a random distribution of point defects on the network. If the average number of point defects per network length, n, is large ($n > 5$), N(L) can be approximated by a Poisson distribution, independent of the distribution of network lengths. Integration over the loop length then gives Eqs. I-2 and I-3. In this case the average loop length is inversely proportional to the point defect concentration, c_d, at the dislocation. If equilibrium is maintained, c_d will be given by Eq. IV-27. Thus Δ_I will increase exponentially with temperature with an apparent activation energy of $4U_0$, while the modulus defect will rise with an apparent activation energy of $2U_0$, provided the applied stress is less than the minimum stress, σ_T(Eq. IV-23), required for thermal breakaway.

In the present case, the total impurity concentration, c_0, is less than 10^{-6}, so that at the lowest temperatures, 550°K, at which equilibrium is feasible, the concentration c_d is of the order of 10^{-4} for $U_0 = 0.2$ eV. This concentration corresponds to about one pinning point per network length. Since we expect the distribution of network lengths to be relatively narrow, N(L) will change considerably as pinning points evaporate. The simple interpretation given above for the apparent activation energy will then be incorrect.

As an approximation to the present case, let us take a delta-function distribution for the network lengths, L_N, and assume each network length has either one or no pinning points. In this case the distribution function N(L) will be

$$N(L) = \Lambda/L_N \left[(2f / L_N)\, H(L_N - L) + (1-f)\, \delta(L - L_N) \right] \qquad \text{(IV-54)}$$

where $\delta(x)$ = Dirac delta function, H(x) is the Heaviside unit function, and $f = c_d L_N / b$ is the fraction of network lengths which are pinned. With this form for N(L), integration of IV-52 and IV-53 yields

$$\Delta_I = (\Omega \Delta_0 \omega B / \pi^3 C) \Lambda L_N^4 (1 - 2f/3) \qquad \text{(IV-55)}$$

and

$$(\Delta E / E)_I = (\Omega \Delta_0 \Lambda L_N^2/\pi^2)(1-f/2). \qquad \text{(IV-56)}$$

Since we believe that the observed amplitude dependence arises from the effect on Δ_I and $(\Delta E/E)_I$ of an increase in loop length at high amplitudes, then for high amplitudes at 1000°K we expect f=0. Information on the total modulus defect is available for specimens 34C and 34E from oxygen saturation. In the table below the maximum measured modulus defect $(\Delta E/E)_N = \Omega \Delta_0 \Lambda L_N^2/\pi^2 = (\Delta E/E)_I + (\Delta E/E)_H$, and the total decrement, $\Delta_N = \Omega \Delta_0 \Lambda L_N^2 \cdot \omega B L_N^2 / \pi^2 C$, are

listed for both specimens in the annealed state as well as the derived quantities $\omega\tau_N = \omega B\, L_N^2 / \pi^2\, C$, Λ/B and $\Lambda L_N^2 / C$. Since $\Omega\Delta_0$ is proportional to E_{III} / C the value of E_{III} determined from the measurements at 1000°K was used in calculating the values of Λ/B and $\Lambda L_N^2 / C$.

Specimen	$(\Delta E/E)_N$	Δ_N	$\omega\tau_N$	Λ/B	$\Lambda L_N^2/C$
34C	1.58×10^{-2}	4.2×10^{-3}	0.26	1.2×10^{8}	7.1×10^{3}
34E	2.10×10^{-2}	6.2×10^{-3}	0.30	1.5×10^{8}	9.4×10^{3}

If we assume the value of B lies somewhere between the theoretical value at 1000°K (6.3×10^{-4}) and 5 times this value[90], then Λ for these specimens must be between 8×10^{5} and 5×10^{6}. These values are about an order of magnitude less than the estimated as-grown densities, and would appear reasonable in light of the expected effect of cyclic annealing. The significance of the last column depends on the value taken for C at 1000°K. While we might expect C to exhibit the temperature dependence of G, this turns out to be true only for C_s; C_E decreases considerably faster with temperature than G. The values calculated at 1000°K are 2.72×10^{-4} and 0.25×10^{-4} ergs/cm for C_s and C_E respectively. To be consistent with the model, we should assume $\Lambda L_N^2 = 1$. The resulting values of C from the table (1.4×10^{-4} and

1.1×10^{-4}) would appear closer to C_s.

Since the model appears to account satisfactorily for the high temperature limit of the decrement and modulus defect, we can now consider the temperature dependence. We expect the model to provide a reasonable approximation to the actual situation at higher temperatures. At lower temperatures the increased probability of more than a single pinning point per network length or the fact that equilibrium may no longer be reached can lead to large deviations. Unfortunately, due to the presence of the peak observed at ~950°K, we can not hope to gain any quantitative information on the temperature dependence of f from the measurements of Δ. However, the modulus defect data on 34E (Fig. 18) does not suffer from this objection, since repeated attempts have failed to reveal any modulus irregularities associated with this peak.

From Eq. IV-56 and the relation $f = (c_0 L_N / b) e^{U_0/kT}$ we see that a plot of $\log \left[(\Omega \Delta_0 \Lambda L_N^2 / \pi^2) - (\Delta E/E)_I \right]$ vs. $1/T$ should yield a straight line with a slope of U_0 / k and an intercept at $1/T = 0$ of $\Omega \Delta_0 \Lambda L_N^2 c_0 L_N / 2\pi^2 b$. Assuming first that the quantity $\Omega \Delta_0$ is independent of temperature (i.e., E_{III} / C_s is independent of T), the data of Fig. 18 does indeed yield a straight line from 1000°K to ~600°K. Below 600°K the measured modulus defect is larger than IV-56 predicts, possibly indicating multiple pinning or lack of equilibrium.

From the slope of the plot we find $U_0 = 0.17$ eV, and from the intercept $c_0 L_N / 2b = 1.4 \times 10^{-2}$. If, on the other hand, we assume that $\Omega \Delta_0$ exhibits a temperature dependence appropriate to E_{III} / C_E we again find a good fit over the temperature range 600°K to 1000°K with $U_0 = 0.13$ eV and $c_0 L_N / 2b = 1.9 \times 10^{-2}$. Thus in either case c_0 is certainly less than 10^{-6}, so that the impurities present can easily account for the observed effects.

Since the specimen will contain both edge and screw dislocations as well as the 30° and 60° mixed dislocations and several different impurities, we cannot attach any direct significance to the value of U_0 obtained. However, the values (0.13 - 0.17 eV) do appear to be of the right order of magnitude for an impurity-dislocation binding. For substitutional impurities in silver the only significant contribution to the binding energy arises from the size effect[98, 5], for which

$$U_0 = \left[(1 + \nu) / 3\pi(1 - \nu)\right] \cdot Gb' \Delta V' / R_0 \qquad \text{(IV-57)}$$

where R_0 is the distance of closest approach of the impurity to the dislocation with an edge component of the Burgers vector of b'. $\Delta V'$ is related to the difference in atomic volumes ΔV of the solvent and solute by[5] $\Delta V' = 3(1 - \nu) \cdot \chi_s \Delta V / \left[2(1 - 2\nu)\chi_i + (1 + \nu)\chi_s\right]$ where χ_s and χ_i are the

compressibilities of the solvent and solute respectively.

If we take $b' = R_0 = \sqrt{3}\, b / 3$ for a Schockley partial, then for the known impurities Cu, Bi, Pb Eq. IV-57 yields $U_0 = 0.20$, 0.42, and 0.35 eV respectively at room temperature. Since the interaction energy is elastic in origin, the measured values of U_0 will exhibit the temperature dependence[5] of $E_{III}V$, where V is the atomic volume. Thus the values calculated from IV-56 should be compared to 1.33 times the experimental value (0.13 - 0.17 eV).

The strain amplitude dependence observed at high temperatures (Fig. 27) would also seem to be in quantitative agreement with this model. From our previous discussion of the TGL model we associate the strain amplitude, ϵ_M, at which the minimum decrement occurs with the stress at which thermal breakaway is first possible, i.e., $RE_{III}\,\epsilon_M = \sigma_T$. From the data of Fig. 27 and Eq. IV-23 we find $L_N^2 / C = 2.6\times10^{-3}$, with $L = L_N / 2$ and $r_0 = \frac{1}{3}\sqrt{3}\, b$. For this same specimen (34C) the high temperature low amplitude data yielded $\Lambda L_N^2 / C = 7.1\times10^3$ and $\Lambda/B = 1.2\times10^8$. Thus we obtain $\Lambda = 2.7\times10^6$ and $B = 2.2\times10^{-3}$ at 1000°K.

We can also obtain information on the temperature dependence of f from the data of Fig. 27. We expect the internal friction on the high amplitude plateau, Δ_p, to be given by Eq. IV-55 with f = 0, while the internal friction $\epsilon_0 = \epsilon_M$ will correspond to the equilibrium value of f at

the temperature at which the strain amplitude measurements were made. Thus from Eq. IV-55 we have $f = 3/2\left[1 - \Delta(\epsilon_M) / \Delta_p\right]$. A log f vs. 1/T plot as before indicates $U_0 = 0.20$ eV and $2\, c_0 L_N / 3b = 3.1\times10^{-2}$ in very good agreement with values obtained from the temperature dependence of the modulus defect at low amplitudes, under the assumption that E_{III} / C is independent of temperature. This latter assumption is consistent with the observation that ϵ_M, which is proportional to C / E_{III} is very nearly independent of temperature.

The lack of any evidence for a pronounced temperature dependence of E_{III} / C would seem to indicate that relatively few dislocations lie along $\langle 112 \rangle$ directions, since we would expect approximately a third of such dislocations to be edge dislocations. This would seem to reenforce our conclusion, based on the small modulus defect at 4.2°, that in the cyclic annealed specimens nearly all the dislocations lie near $\langle 110 \rangle$ directions.

The fact that a net decrease of a factor of 3 in $(\Delta E/E)_I$ and more than an order of magnitude in Δ_I has occurred during cyclic annealing (Fig. 13) could be explained solely on the basis of a narrowing of the distribution of network lengths, L_N. The total dislocation density, Λ, and the average network length need not necessarily have changed. On the other hand, there is evidence from etch pit studies in copper[86] that similar cycling results in a

greater reduction in the dislocation density than that obtained solely by an anneal at a fixed high temperature.

However, the time-dependent effects, which have been observed during cyclic annealing, appear to be extremely complex and are difficult to interpret. The migration of excess vacancies introduced during cooling to dislocations might be expected to aid in dislocation rearrangement and annihilation, ultimately resulting in a lower dislocation density. If this is indeed the case, the fact that changes in Δ_I do not occur until the temperature is again raised above 900°K might be explained by a very high (~3 eV) activation energy for the rearrangement process. This, however, is highly speculative, since rearrangement processes are only poorly understood, particularly in the case of materials with low stacking fault energies, in which the climb of extended dislocations is involved.

The annealing behavior aside, it appears that the KGL model can quite successfully account for the temperature and strain amplitude dependence observed at high temperatures, and, as we shall see below, further evidence in support of our interpretation of the observations in terms of this model can be derived from the oxygen desorption studies.

We have not been able to establish the origin of the peak observed at 950°K. The details of our observations on

this peak were given in Section III, Part C-4. A careful study of the data on the resonant frequencies in this temperature range has failed to reveal a modulus defect associated with this peak. We, therefore, feel that this peak may not correspond to a relaxation process. On the other hand, its appearance at a single well-defined temperature and the fact that it is observed on heating as well as cooling, provided sufficient time is allowed for equilibration, indicate that this peak cannot be attributed to a simple hysteresis effect. A number of investigators[67,53,116] have reported a peak at about this temperature in copper, although no details have been given.

D. INTERNAL FRICTION AND MODULUS CHANGES DURING OXYGEN SATURATION AND VACUUM DESORPTION

Although it was not possible to make measurements while the crystal was being exposed to oxygen, Δ is observed to decrease to very low values ($\sim 2 \times 10^{-5}$) in times comparable to those required for oxygen to diffuse through the specimen. These low values are observed after saturation at temperatures from 715°K to 825°K. It is apparent that even at these relatively high temperatures the addition of as little as 20 ppm O_2 is effective in eliminating the majority of any dislocation contribution to internal friction. This conclusion is reinforced by the fact that a linear extra-

polation of the modulus data on an oxygen-saturated crystal at temperatures between 100°K and 340°K agrees to within 1 part in 10^4 with the modulus measured at 715°K immediately following saturation.

The series of standard desorption runs carried out on Specimen 34E are summarized in Table IV. Previous measurements on specimen 34C had assured us that the process of oxygen saturation and subsequent removal was completely reversible with respect to measurements of the damping, and that 24 hours at 1000°K in vacuum following saturation would assure this reproducibility.

The recovery of Δ during vacuum desorption was observed to occur by a multi-stage process, as is clearly seen in Fig. 30 for the run at 872°K. To allow for the possibility that a recovery stage may have been present which was completed before the first measurement was made, the initial level portions observed in the runs at 872°K, 898°K and 923°K were designated Stage I. This stage may, in fact, correspond to the damping level of fully saturated specimens. At these same three temperatures, Δ begins to rise at a relatively rapid rate soon after the measurements are started and eventually reaches a temporary plateau. This rise is designated stage II. At 975°K and 1000°K only the very end of stage II is observed. The remainder of the recovery has been designated stage III. The magnitude of the recovery in each stage was observed to be a function of

temperature, and is designated as Δ_R. In order to analyze the recovery curves we have followed the procedure described by Damask and Dienes[87]. If the same recovery stages are being observed at various temperatures, and if each separate stage does indeed correspond to a singly activated process, then a plot of Δ/Δ_R vs. ln(t) for each temperature should yield a series of parallel curves. Furthermore, the times required to recover some fixed fraction (Δ/Δ_R) of the damping in a given stage should be proportional to exp(H/KT), where H is the activation energy of the process. The data for both stage II and stage III have been analyzed in this fashion and are shown in Figs. 31 and 32 respectively. As can be seen, the curves at the various temperatures are reasonably parallel. The values of $\log(t_{1/2})$ vs. 1/T for a cross-cut at $\Delta/\Delta_R = 1/2$, shown in Figs. 41 and 42, yield good straight lines corresponding to activation energies of 0.67±0.06 eV for stage II and 2.63±0.4 eV for stage III. A similar analysis of the modulus data (Figs. 33 and 34) yields essentially identical activation energies for the two stages. The errors quoted correspond to the range of activation energies obtained by taking cross-cuts at various values of Δ/Δ_R.

We expect oxygen to interact strongly with any metallic impurities present in our samples to form internal oxide particles[63]. For the present low impurity concentrations

and relatively low saturation temperature (825°K) we expect the particles formed to be of atomic dimensions, i.e. oxygen impurity pairs. Since the strains associated with such pairs are large, their interaction with dislocations will be substantially greater than the interaction of either oxygen or the substitutional impurity alone. Since the pair must dissociate in order to diffuse, its mobility will be quite low, thus reducing its effectiveness in pinning dislocations. The increased magnitude of the interaction with dislocations can, however, lead to a larger number of pinning points than an equivalent substitutional impurity distribution, since the dislocations can gain more in binding energy than they lose in line energy by bowing out to include a larger number of pinning points[46]. In light of the model developed in the previous section we believe that pinning by such impurity-oxygen pairs accounts for the reduction in the decrement and modulus which is recovered in stage III.

From the solution to the diffusion equation for the specimen geometry we have found that the times required for the completion of stage II should correspond to the reduction of the average bulk oxygen concentration to less than 1 ppm. We therefore propose that the recovery of Δ in stage II corresponds to the removal of free oxygen from dislocations. As we saw from our discussion of the peak observed at 365°K (p.134ff), at intermediate concentrations individual oxygen

atoms can be expected to pin dislocations. At the highest temperatures at which stage II is observed (923°K), our criterion (Eq. IV-42) for pinning rather than breakaway from or diffusion with the dislocation is just satisfied at the highest strain amplitude ($2x10^{-6}$) utilized, assuming an oxygen dislocation binding energy of 0.25 eV. On the basis of this model we can now attempt to interpret the observed activation energies.

We will assume then that the initial level portion of the recovery curves (stage I) corresponds to those dislocations which are not effectively pinned by oxygen. We, therefore, subtracted this value from the values measured during stage II. In general we can write Δ or $\Delta E/E$ as the product of a function of temperature times a function of the number of variable pinning points, i.e. $\Delta = A(T).f(n_p)$. If we define $\Delta_R = A(T)\left[f(o) - f(n_o)\right]$ where n_0 is the initial number of variable pins, then $\Delta/\Delta_R = f(n_p)/\left[f(o) - f(n_0)\right]$. In the case of oxygen pinning we will have $f(o) \gg f(n_0)$, thus Δ/Δ_R is independent of n_0. Since stage II is complete well before stage III begins, and we do not expect the oxygen-impurity pairs to be mobile, f(o) should be independent of temperature. Thus a cross-cut made at a particular value of Δ/Δ_R should correspond to a constant value of n_p.

Since the times required for oxygen to diffuse out of

the specimen are long compared to those required to reach local equilibrium, the problem will be that of migration to the surface in the presence of traps. In this case, we expect that the activation energy determined will lie somewhere between[87] E_M (oxygen) and E_M (oxygen) + U_O, where U_O is the binding energy of oxygen to a dislocation. Since E_M (oxygen) is 0.50 eV, the observed activation energy of 0.67±0.06 eV leads us to a lower limit of 0.17±.06 eV for the binding energy of oxygen to a dislocation. At room temperature we expect this lower limit to be 0.22±.08 eV, which is within our estimate of 0.25±0.06 eV based on the interpretation of the peak observed at 365°K.

Stage III will correspond to the dissociation of oxygen-impurity pairs. For the expected large oxygen-impurity binding the observed activation energy should be equal to the sum of the binding energy and the migration energy of oxygen. Thus the observed activation energy (2.63±0.4 eV) indicates an oxygen-impurity binding energy of 2.13±0.4 eV. Since we have several impurities present, we might expect a number of such stages. In fact, the data would seem to indicate this is the case but that the spread in energies is fairly small. For Cu, however, additional experimental data on the dissociation is available.

Podgurski and Davies[62] have recently measured the equilibrium dissociation pressures of CuO in silver (<0.2wt%).

They found in particular that the reaction

$$CuO\ (s) \rightleftharpoons \underline{Cu} + \tfrac{1}{2}\ O_2$$

proceeds to equilibrium in silver in the temperature range of the present experiments with a heat of reaction of 1.86±0.01 eV. Within the present estimated error this agrees quite well with our estimate of 2.13±0.4 eV.

At high temperatures, then, we conclude that the internal friction and modulus defect due to dislocations are reduced by two mechanisms when oxygen is introduced. The initial reduction, which can amount to an order of magnitude, is due to the pinning of the dislocation network by internally oxidized trace impurities. A further reduction occurs from additional pinning by individual oxygen.

V. SUMMARY AND CONCLUSIONS

A. DISLOCATION CONTRIBUTIONS TO THE MODULUS AND INTERNAL FRICTION OF 6-9'S SILVER.

While our intended purpose was to measure the internal friction and modulus of well-annealed specimens at low as well as high temperatures, the relatively small amounts of handling involved in mounting or transfer were found to cause a transient, order of magnitude, increase in the internal friction, the majority of which is recovered in 24 hours at room temperature. We believe this increase and its subsequent recovery arise from deformation occurring near the knife edges on which the specimens are mounted. While the analysis[85] indicates the pinning of dislocations by the diffusion of point defects is responsible for the observed time dependence, we were not able, on the basis of our somewhat limited observations, to derive a value for the migration energy of the pinning defect. The additional decrease observed (in times of the order of several weeks at room temperature) would appear to be associated with small changes in the dislocation (and/or pinning point) configuration in the bulk of the specimen.

The uncertainties resulting from the room temperature transfer notwithstanding, it would appear that the dislocation contribution to the internal friction of well-annealed 6-9's

silver initially increases with temperature reaching a broad maximum near 100°K, decreases to temperatures of 400-500°K, and then increases up to the maximum temperature of the observations (1000°K). Superimposed on this overall behavior a number of small peaks are observed, primarily below 300°K. On the other hand, the modulus defect increases with increasing temperature over the entire temperature range (4.2-1000°K).

At high temperatures (i.e., above the observed minimum) the observed temperature and strain amplitude dependence of both the internal friction and modulus defect are very satisfactorily explained on the basis of the vibrating string (KGL) model, when the purity of the present material is taken into account. The scattering of thermal phonons would appear to provide enough drag on moving dislocations to account for the magnitude of the observed damping. The application of the KGL model leads to a value of the damping constant, B, about three times larger than Leibfried's theoretical estimate[95], and a dislocation density for the cyclic annealed specimens of $\Lambda = 3\text{-}5 \times 10^{-6}$. In addition, the measurements indicate that the binding energy of trace impurities (Cu, Bi, or Pb) to dislocations is 0.17-0.20 eV. Although we are not able to explain the somewhat complex behavior observed during cyclic annealing, it appears such treatment reduces the dislocation density by a factor of

from three to six. There is also some indication that this treatment results in larger fraction of dislocations which lie near the close-packed $\langle 110 \rangle$ directions.

At low temperatures it does not appear possible to come to any definite conclusion as to the mechanism or mechanisms responsible for the observed internal friction and modulus defect. This is particularly true as regards the origin of the observed structural features (peaks). We wish, however, to emphasize the following observations: 1) In the temperature range normally associated with the so-called Bordoni peak, at least three and as many as five separate peaks occur; 2) the peak observed here at 42°K does not appear to correspond to any previously reported peaks in this temperature range, and 3) at higher temperatures ($T > 120$°K) at least three additional peaks occur which are not appreciably affected by room temperature annealing.

Although the magnitude of the modulus steps associated with the peaks would indicate that they contribute only 10-20 per cent of the observed internal friction and modulus defect, we cannot rule out the possibility that what we have termed the 'background' internal friction is just the sum of a large number of discrete peaks. We have shown, however, that the temperature dependence of the 'background', the observed effect of room temperature annealing, and the differences between the as-grown and cyclic annealed specimens at

low temperatures could arise as result of a finite Peierls barrier to the motion of intrinsic kinks. The application of the kink-diffusion model[102, 114] to the present results would require that the activation energy for kink diffusion be 0.020±0.002 eV.

The amplitude dependence of the internal friction and modulus does not appear to be the result of a static hysteresis mechanism, although the results at low temperatures can be fitted by two Granato-Lücke[36] components. The observed behavior would seem to arise from an increase in the effective loop length at higher amplitudes due to thermal depinning[56] of dislocations.

B. THE INFLUENCE OF OXYGEN.

The addition of as little as 40 ppm of oxygen reduces the internal friction of 6-9's silver by two orders of magnitude below 800°K and by at least an order of magnitude above 800°K. While we can understand that the effectiveness of oxygen in pinning dislocations at low temperatures arises from its high room temperature mobility, this same high mobility would be expected to drastically reduce its effectiveness at high temperatures, since one would expect oxygen to be able to follow the motion of the dislocation by diffusion.

We have developed a model for the dragging of interstitial impurities by dislocations which is essentially an

extension of the model proposed by Schoeck[30] to explain the cold work peak observed in b.c.c. metals containing interstitial impurites to relatively high interstitial concentrations along the dislocation. The model leads to a relaxation loss in which the strength of the relaxation as well as the relaxation time depend on the interstitial concentration along the dislocations. We believe the peak observed here at 365°K is the result of the proposed mechanism. Application of the model to the present observations and those of Papazian[59] on this peak leads to a value for the binding energy of oxygen to a dislocation of 0.25±0.04 eV. Furthermore, with this value for the oxygen-dislocation binding energy we expect on the basis of the model that 40 ppm of oxygen will be effective in pinning the majority of dislocations up to temperatures of the order of 800°K.

A study of the rates at which the modulus and internal friction return to the pre-oxygen saturation levels during vacuum desorption indicated the recovery occurred in two stages, characterized by activation energies of 0.67±0.06 eV and 2.6±0.4 eV. We believe the initial recovery stage corresponds to the elimination of oxygen pinning points from the dislocations. The observed activation energy would then indicate that a lower limit to the oxygen dislocation binding energy at room temperature is 0.22±0.07 eV. The slower

recovery stage we believe corresponds to the elimination of pinning points resulting from the internal oxidation of trace impurities present in these specimens. The observed activation energy would indicate that the dissociation of oxygen-impurity pairs requires 2.1±0.4 eV in reasonable agreement with the observed dissociation energy of CuO in silver[62] of 1.86±0.02 eV.

While we have been able to arrive at a value for the binding energy of oxygen to dislocations of 0.25±0.04 eV, the precision with which we know this energy leaves much to be desired. On the other hand, it appears that the introduction of oxygen to silver can be of considerable value in a study of dislocation contributions to the internal friction, since its elimination of such contributions allows us to determine a base against which the modulus changes associated with dislocations can be measured.

ACKNOWLEDGEMENTS

The author wishes to express his appreciation to Dr. Lawrence Himmel for his advice and help during the course of this work, to Mr. Mitchell Nakamura for the design of the transistorized decay gate, and to the author's wife for her help in preparing the manuscript. This work was done under the auspices of the U.S. Atomic Energy Commission through the Inorganic Materials Research Division of the Lawrence Radiation Laboratory.

REFERENCES

1. C. Zener, Elasticity and Anelasticity of Metals (Chicago, 1948).
2. T. A. Read, Phys. Rev. 58, 371 (1940).
3. W. T. Read, Dislocations in Crystals (McGraw-Hill, 1953).
4. A. H. Cottrell, Dislocations and Plastic Flow in Crystals (Oxford, 1953).
5. J. Friedel, Les Dislocations (Gauthier-Villars, Paris, 1956). Dislocations (Addison-Wesley, 1964).
6. A. S. Nowick, Prog. Metal Phys. 4, 1 (1953).
7. K. Lücke and A. Granato, Dislocations and Mechanical Properties of Crystals (Wiley, 1957).
8. W. P. Mason, Physical Acoustics and the Properties of Solids (van Nostrand, 1958).
9. H.G. Van Bueren, Imperfections in Crystals (North-Holland, 1960).
10. D. H. Niblett and J. Wilks, Adv. in Physics 9, 1 (1960).
11. K. M. Entwistle, Metallurgical Reviews 7, 175 (1962).
12. P. G. Bordoni, Ric. Sci. 19, 851 (1949).
13. R. H. Chambers and J. Schultz, Acta Met. 10, 466 (1962).

14. R. Tsui, Thesis, Cornell Univ. (1962).

15. R. Chang, J. Appl. Phys. 32, 1127 (1961).

16. R. E. Peierls, Proc. Phys. Soc. London 52, 34 (1940).

17. W. P. Mason, J. Acous. Soc. Amer. 28, 1207 (1956).

18. A. Seeger, Phil. Mag. 1, 651 (1956).

19. H. Donth, Zeit. für Physik 149, 111 (1957).

20. A. Seeger, H. Donth, and F. Pfaff, Disc. Faraday Soc. 23, 19 (1957).

21. J. Lothe and J. P. Hirth, Phys. Rev. 115, 543 (1959).

22. A. Seeger and P. Schiller, J. Phys. Soc. Japan 18, 178, Supp. I (1963).

23. V. K. Paré, Thesis, Cornell University, AFOSR-TR-58-92 (1958); J. Appl. Phys. 32, 332 (1961).

24. see H. S. Sack, Acta Met. 10, 455 (1962); also Ref. 10 and several papers relating to the Bordoni peak in Proc. Int. Conf. Cryst. Latt. Def (1962), J. Phys. Soc. Japan 18, Supp. I (1963).

25. A. D. Brailsford, Phys. Rev. 122, 778 (1961).

26. J. J. Gilman, J. Phys. Soc. Japan 18, 172, Supp. I (1963).

27. R. R. Hasiguti, N. Igata, and G. Kamoshita, Acta Met. 10, 442 (1962).

28. R. R. Hasiguti, J. Phys. Soc. Japan 18, 114, Supp. I (1963).

29. D. P. Petarra, Thesis, Columbia Univ. (1962).

30. G. Schoeck and M. Mondino, J. Phys. Soc. Japan 18, Supp. I, 149 (1963). G. Schoeck, Acta Met. 11, 617 (1963).

31. D. Boone, Thesis, Univ. of Illinois (1962).

32. W. Köster, L. Bangert, and R. Hahn, Arch. Eisenhütten W. 25, 569 (1954).

33. T. Mura, J. Tamura, and J. O. Brittain, J. Appl. Phys. 32, 92 (1961).

34. G. Schoeck and A. Seeger, Acta Met. 7, 469 (1959).

35. D. H. Boone and C. Wert, J. Phys. Soc. Japan 18, Supp. I, 141 (1963).

36. A. Granato and K. Lücke, J. Appl. Phys. 27, 583 (1956).

37. J. S. Koehler, Imperfections in Nearly Perfect Crystals (Wiley, 1952), 197.

38. R. B. Gordon, Acta Met. 10, 339 (1962).

39. D. O. Thompson and D. K. Holmes, J. Appl. Phys. 27, 191 (1956).

40. R. Truell and R. Bayer, Phys. Rev. 110, 1206 (1958).

41. V. K. Paré and D. O. Thompson, Acta Met. 10, 327 (1962); also D. O. Thompson, J. Phys. Soc. Japan 18, Supp. I, 104 (1963).

42. J. Wilks, Phil. Mag. 4, 1379 (1959).

43. J. Weertman and E. I. Salkovitz, Acta Met. 3, 1 (1955).

44. J. Weertman, J. Appl. Phys. 26, 202 (1955).

45. J. Weertman, J. Appl. Phys. 28, 193 (1957).

46. N. F. Mott, in Imperfections in Nearly Perfect Crystals Wiley, 1952).

47. J. C. Swartz and J. Weertman, J. Appl. Phys. 32, 1860 (1961).

48. J. M. Roberts and D. E. Hartman, J. Phys. Soc. Japan 18, 119 Supp. I (1963).

49. D. Gelli, J. Appl. Phys. 33, 1547 (1962).

50. H. K. Birnbaum and M. Levy, Acta Met. 4, 84 (1956).

51. J. Friedel, C. Boulanger, and C. Crussard, Acta Met. 3, 380 (1955).

52. H. S. Sack, Symp. Plastic Deform., Pittsburgh (1950).

53. L. A. Kamentsky, Thesis, Cornell Univ., AFOSR-TN-56-425 (1956).

54. W. P. Mason, Bell Syst. Tech. J. 34, 903 (1955).

55. G. Leibfried, in Dislocations and Mechanical Properties of Crystals (Wiley, 1957), 495.

56. L. Teutonico, A. Granato, and K. Lücke, J. Appl. Phys. 35, 220 (1964).

57. J. Friedel, in The Relation between the Structure and Mechanical Properties of Metals (London, HMSO, 1963) Vol. I, 409.

58. R. Busch, Thesis, Univ. of California, Berkeley UCRL-10816, June 1963 (unpublished).

59. J. M. Papazian, Thesis, Univ. of California, Berkeley UCRL-11017, Sept. 1963 (unpublished).

60. S. Gupta, Thesis, Univ. of California, Berkeley (forthcoming).

61. W. Eichenauer and G. Müller, Z. Metallk. 53, 321 (1962).

62. H. H. Podgurski and F. N. Davis, Trans. AIME 230, 731 (1964).

63. J. L. Meijering and M. F. Druyvestyn, Philips Res. Rep. 2, 81, 200 (1947).

64. Y. Quèrè, J. Phys. Soc. Japan, 18, Supp. III, 91 (1963).

65. R. H. Chambers, Carnegie Inst. of Tech. Report, AT(30-1)-1193, (1957).

66. See Ref. 44.

67. D. N. Beshers, J. Appl. Phys. 30, 252 (1959).

68. N. F. Fiore and C. L. Bauer, J. Appl. Phys. 35, 2242 (1964).

69. W. Köster, Z. Metallk. 39, 9 (1948).

70. A. S. Nowick, in Metal Interfaces (ASM, Cleveland) 248.

71. S. Pearson and L. Rotherham, J. Metals 8, 894 (1956).

72. P. G. Bordoni, J. Acoust. Soc. Amer. 26, 495 (1954).

73. S. Okuda, J. Phys. Soc. Japan 18, Supp. I, 187 (1963).

74. R. M. Stern, "Untersuchungen der Resonanzdämpfung der Versetzungen" (Thesis), Technischen Hochschule, Aachen (1961).

75. See Ref. 27.

76. R. B. Jacobs and D. Bancroft, Rev. Sci. Inst. 9, 279 (1938).

77. P. D. Southgate, J. Sci. Inst. 36, 284 (1959).

78. See Ref. 23.

79. See Ref. 53.

80. M. E. Fine, Rev. Sci. Inst. 28, 643 (1957).

81. P. Morse, Vibration and Sound (McGraw-Hill, 1948).

82. R. L. Powell, M. D. Bunch, and R. J. Corruccini, Cryogenics 1, 139 (1961).

83. C. P. Bean, R. W. DeBlois, and L. B. Nesbitt, J. Appl. Phys. 30, 1976 (1959).

84. C. A. Wert, J. Appl. Phys. 20, 29 (1949).

85. A. Granato, A. Hikata, and L. Lücke, Acta Met. 6, 470 (1958).

86. J. D. Livingston, Acta Met. 10, 229 (1962).

87. A. C. Damask and G. J. Dienes, Point Defects in Metals (Gordon and Breach, 1963).

88. H. L. Caswell, Thesis, Cornell University, AFOSR-TR-57-69 (1957); J. Appl. Phys. 29, 1210 (1958).

89. A. J. Filmer, D. H. Rogers, and T. S. Hutchison, Proc. of Inter. Cong. of Refrig. (Copenhagen), 1959.

90. R. M. Stern and A. V. Granato, Acta Met. 10, 358, (1962).

91. G. de Wit and J. S. Koehler, Phys. Rev. 116, 1113 (1959).

92. A. J. E. Foreman, Acta Met. 4, 322 (1955).

93. J. R. Neighbors and G. A. Alers, Phys. Rev. 111, 707 (1958).

94. H. J. Levinstein and W. H. Robinson in The Relation between the Structure and Mechanical Properties of Metals, (HMSO, London, 1963).

95. G. Leibfried, Z. Phys. 127, 344 (1950).

96. A. S. Nowick in Creep and Recovery (Amer. Soc. Metals, Cleveland, 1957).

97. W. Köster, Z. Metallk. 32, 382 (1940).

98. A. H. Cottrell and B. A. Bilby, Proc. Phys. Soc. London A62, 49 (1949).

99. R. Hasiguti, N. Igata, and K. Tanaka, Comment to a paper presented by K. Lücke, J. Phys. Soc. Japan 18, Supp. I (1963).

100. A. D. N. Smith, Phil. Mag. 44, 453 (1953).

101. A. Howie and P. R. Swann, Phil. Mag. 6, 1215 (1961).

102. P. D. Southgate and A. E. Attard, J. Appl. Phys. 34, 855 (1963).

103. D. H. Niblett and J. Wilks, Conf. Phys. Basses Temp. Paris, P. 484 (1955).

104. D. O. Thompson and D. K. Holmes, J. Appl. Phys. 30, 525 (1959).

105. L. J. Bruner and B. M. Mecs, Acta Met. 10, 494 (1962).

106. Y. Hiki, J. Phys. Soc. Japan 13, 1138 (1958).

107. T. S. Hutchison, S. L. McBride, and D. H. Rogers, Acta Met. 10, 397 (1962).

108. A. Sosin, Acta Met. 10, 390 (1962).

109. A. H. Cottrell, Report of a conference on the strength of solids, Phys. Soc. London (1948).

110. A. Granato, K. Lücke, J. Schlipf, and L. Teutonico, J. Appl. Phys. 35, 2732 (1964).

111. G. Vineyard, J. Phys. Chem. Solids 3, 121 (1957).

112. A. Sawatzky and F. Jaumot Jr., Trans. Aime, 1207 (1957).

113. A. Cochardt, G. Schoeck, and H. Wiedersich, Acta Met. 3, 533 (1959).

114. A. D. Brailsford, Phys. Rev. 137, A1562 (1956).

115. J. Pittenger, Carnegie Institute of Technology Thesis (1951).

116. R. R. Stevens, Thesis, Cornell University AFOSR-TR-57-11 (1957).

117. T. Ninomiya, R. Thomson, and F. Garcia-Moliner, J. Appl. Phys. 35, 3607 (1964).

118. D. H. Rogers, J. Appl. Phys. 33, 781 (1962).

119. G. Alefeld, J. Appl. Phys. 36, 2642 (1965).

Table I. Summary of Measurements.

Specimen	Measurement	Temperature	Fig.
12A ⟨100⟩	Recovery after mounting	377°K	11
< 0.2 ppm Cu, Pb, Bi	Recovery after transfer	340°K, 372°K	--
23C ⟨111⟩	Δ_I vs. temperature one week after mounting	4°-300°K	19
< 0.2 ppm Cu, Pb, Bi	Δ_I vs. temperature	300°-1000°K	12
23AM ⟨100⟩ Ag - 1% Mg	Δ_I vs. temperature	4°-100°K	23
34D ⟨111⟩	Δ_I vs. temperature one day after mounting	4°-300°K	19
< 0.2 ppm Cu, Pb, Bi	Δ_I vs. temperature two mos. after mounting	4°-300°K	17, 19
	Δ vs. strain amplitude	4°-300°K	25, 29
	Recovery after transfer	294°K	---
	Δ_I vs. temperature	300°-1000°K	12

Continued on next page

Table I. (Cont'd.)

Specimen	Measurement	Temperature	Fig.
34C <111>	Recovery after mounting	293°K	10
$<$0.2 ppm Cu, Pb, Bi	Δ_I vs. temperature	300°-1000°K	12
	Cyclic annealing	500°-1000°K	13
	Δ_I vs. temperature	300°-1000°K	17
	Δ vs. strain amplitude	300°-1000°K	26, 27
	Oxygen saturation and desorption	750°-1000°K	---
	Specimen 34C was relabeled 34E following oxygen saturation and rapid cooling to room temperature.		
34E <111>	Δ_I vs. temperature	4°-300°K	16, 23, 24
40 ppm oxygen	Δ vs. strain amplitude	50°-300°K	28
	Δ_I vs. temperature	300°-390°K	16
	oxygen desorbed	1000°K	---
$<$0.2 ppm Cu, Pb, Bi	Cyclic annealing	500°-1000°K	---
	Δ_I vs. temperature	300°-1000°K	16
30 ppm oxygen	Desorption kinetics	875°-1000°K	30-35
$<$0.2 ppm Cu, Pb, Bi	Δ_I vs. temperature one week after transfer	4°-300°K	16, 21

Table II. Recovery after mounting or transfer.[d]

Specimen	T°K	$\Delta_R \times 10^3$	$\beta \times 10^3$	$\left(\frac{\Delta E}{E}\right)_R \times 10^3$	f_0	f_∞	$\Delta_\infty \times 10^3$	$\Lambda \times 10^{-5}$	$L_0 \times 10^{+4}$	Fig.
34C[a]	293	10.7	3.75[e]	10.4	26754	26895	5.60	3.2	3.1	10
12A[a]	377	6.5	11.2	----	-----	-----	3.00	---	---	11
12A[b]	372	7.85	10.5	18.0	15925	16072	2.00	6.8	2.6	--
12A[b]	340	6.7	7.8	-----	-----	-----	4.40	---	---	--
34D[c]	294	11.9	3.50	16.5	26561	26782	3.40	6.7	2.6	--

[a]Recovery after mounting.

[b]Recovery after transfer.

[c]Recovery after transfer following 8 weeks at room temperature.

[d]The values of Λ and L_0 appearing in the table are calculated from Eqs. I-2 and I-3 using the measured values of Δ_R and $(\Delta E/E)_R$.

[e]β is in units of $(\text{minutes})^{-2/3}$.

Table III. Structure at low temperatures. ($T < 300°K$)

Specimen	23C	23AM	34D	34D	34E	34E
Annealing[a]	1 week	1 week	1 day	2 mos.	1 week	1 day
Composition	6-9's Ag	Ag-1%Mg	6-9's Ag	6-9's Ag	6-9's Ag	40ppm O_2
'Background'	$\sim 10^{-3}$	$\sim 10^{-5}$	$\sim 10^{-3}$	$\sim 10^{-3}$	$\sim 10^{-3}$	$\sim 10^{-5}$
Temp.						
7°K	------	------	7×10^{-4} m	------	------	------
10°K	------	------	------	------	------	2×10^{-5} p[b]
22°K	1×10^{-4} p 2×10^{-4} m	------	2×10^{-4} p 5×10^{-4} m	1×10^{-4} p	2×10^{-4} m	------
37°K	------	------	3×10^{-4} m	------	------	------
41°K	------	2×10^{-5} p	------	1×10^{-4} p	------	------
42°K	2×10^{-4} p 1×10^{-4} m	------	5×10^{-4} p	------	------	1×10^{-5} p
44°K	------	------	3×10^{-4} m	------	4×10^{-4} p 3×10^{-4} m	------
54°K	------	------	------	------	4×10^{-4} p 4×10^{-4} m	------
62°K	3×10^{-4} p 2×10^{-4} m	------	3×10^{-4} p 3×10^{-4} m	2×10^{-4} p	------	5.10^{-6} p
67°K	------	------	------	------	3×10^{-4} m	
72°K	2×10^{-4} p 3×10^{-4} m	------	2×10^{-4} p 5×10^{-4} m	2×10^{-4} p	------	
75°K	------	------	------	------	------	
82°K	3×10^{-4} m	------	6×10^{-4} p	------	4×10^{-4} m	

Continued on next page

Table III. (Continued)

Specimen	23C	23AM	34D	34D	34E	34E
Temp. 92°K	3×10^{-4} p 2×10^{-4} m	------	7×10^{-4} p 2×10^{-3} m	------	4×10^{-4} m	------
110°K	------	------	4×10^{-4} p 2×10^{-4} m	------	------	------
130°K	peak	------	------	peak	peak	------
140°K	specimen lost	------	------	------	------	2×10^{-5} p
148°K		------	------	------	------	3×10^{-5} p
160°K		------	------	------	------	5×10^{-6} p
170°K		------	------	peak	peak	------
200°K		broad peak	broad peak	peak	------	------
210°K				------	peak	------
237°K				------	------	4×10^{-5} p[c]
245°K				peak	------	------
255°K				------	peak	------
280°K		------	------	peak	peak	------

[a]Recovery time at room temperature after mounting or transfer.

[b]Plateau extending to lowest temperature of measurement.

[c]Additional structure at both higher and lower temperatures. (See Fig. 24)

[m]Indicates the observed value of the modulus defect $\Delta E/E$.

[p]Indicates the height of peak or irregularity above 'background.'

Table IV. Summary of results obtained during oxygen desorption.

Stage	H(eV)	872°K		898°K		923°K		975°K		1000°K	
		Δ_R[a]	$t_{1/2}$[b]	Δ_R	$t_{1/2}$	Δ_R	$t_{1/2}$	Δ_R	$t_{1/2}$	Δ_R	$t_{1/2}$
I	----	1.3	---	2.8	---	5.3	---	15.0	---	15.5	---
II	0.67	0.7	254	6.0	196	18.0	151		---		---
III	2.63	40.0	15800	15.0	cont'd at 1000°K	18.0	2480	34.0	379	41.5	195
After 24 hrs at 1000°K	----	53.5	---	53.5	---	52.0	---	52.0	---	57.0	---

[a] Δ_R = magnitude of damping recovered in units of 10^{-4}.

[b] $t_{1/2}$ = time in minutes required to recover 1/2 Δ_R.

Table V. Analysis of amplitude dependent internal friction[a] (specimen 34D).

		$\Delta^{b}_{H_1}$			$\Delta^{b}_{H_2}$	
T°K	$\Delta_0 x10^3$	$C_1 x10^{10}$	$C_2 x10^7$	r^c	$C_1 x10^{10}$	$C_2 x10^7$
4.2	0.24	1.0	1.41	0.64	22	5.75
49	1.74	6.4	1.73	0.40	48	6.15
77	4.05	7.7	1.54	0.32	56	5.7
104	3.88	11.0	1.41	0.51	49	5.4
155	3.57	4.6	1.11	0.65	19	5.1
210	3.59	2.2	0.92	0.87	12	4.6
265	3.09	6.0	1.55	1.35	33	7.5
299	1.56	4.2	1.52	1.08	10	5.6

[a]The internal friction has been separated into three components, viz., $\Delta = \Delta_0 + \Delta_{H_1} + \Delta_{H_2}$

[b] Δ_{H_1} and Δ_{H_2} are both of the form $\Delta_H = (C_1 / \epsilon_0)\exp(-C_2/\epsilon_0)$

[c] $r = (\Delta E / E)_H / \Delta_H$

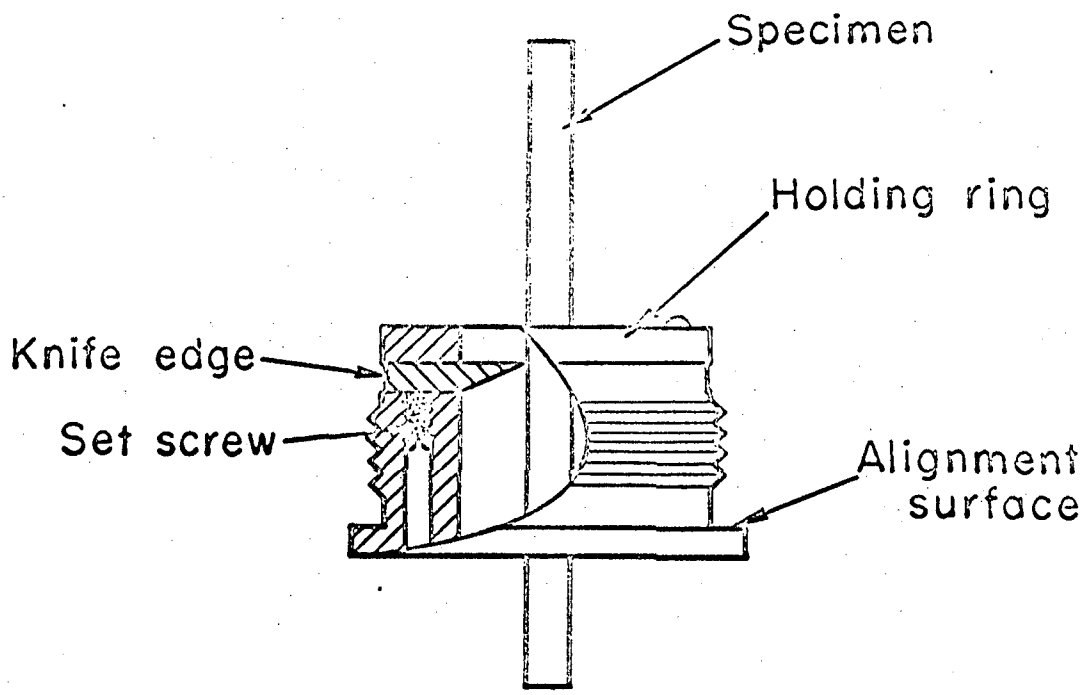

MU-34065

Fig. 1. Specimen Holder

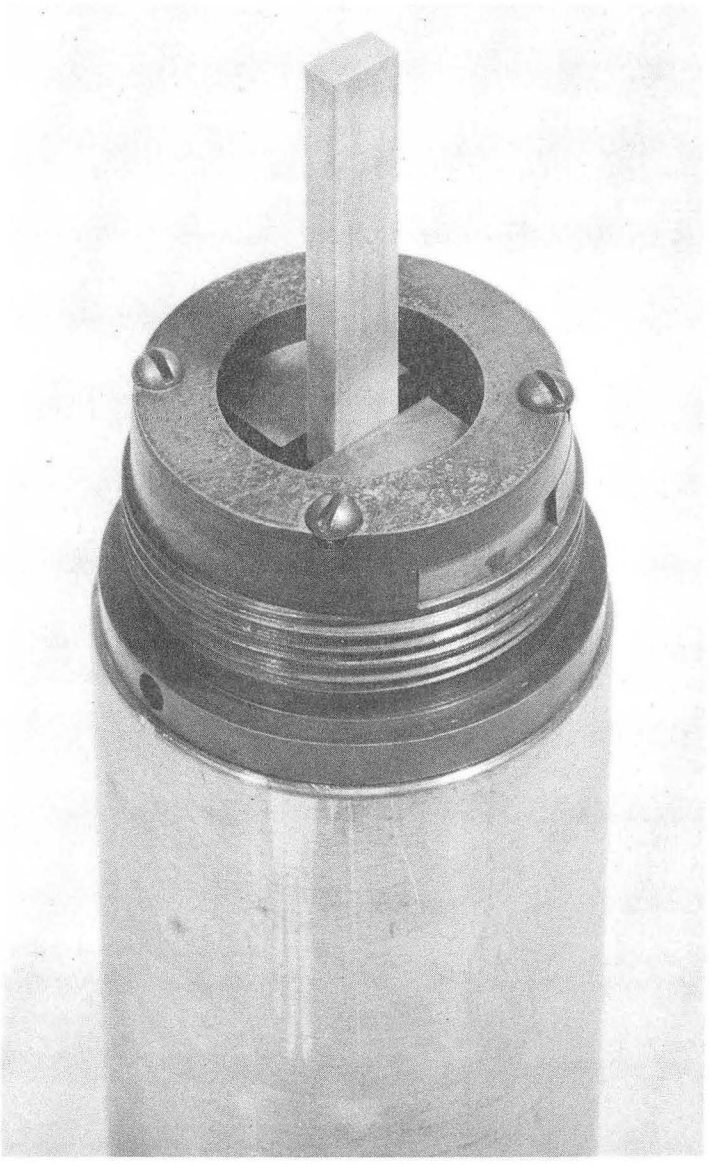

ZN-5979

Fig. 2. Photograph of Mounted Specimen

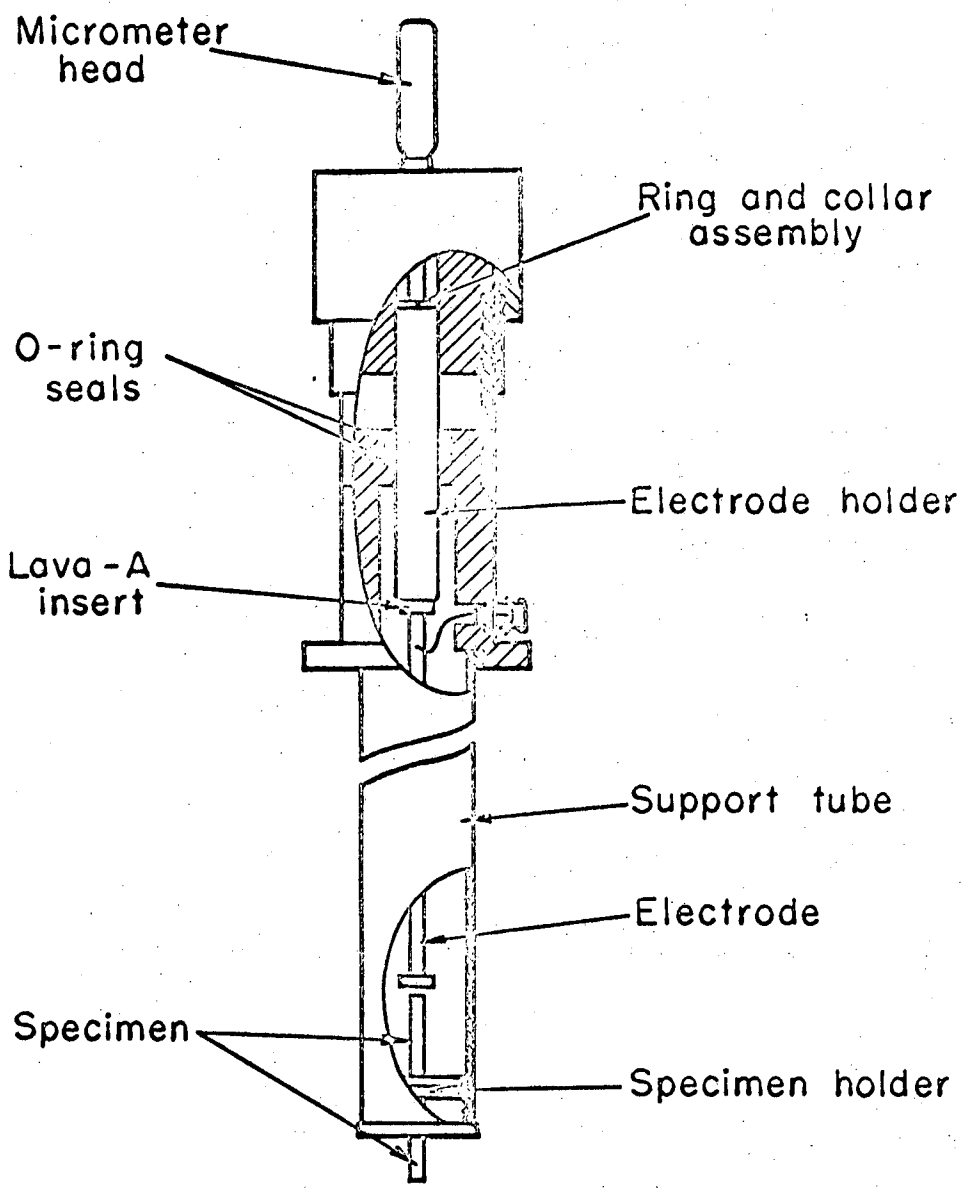

Fig. 3. Electrode Assembly and Support Tube

MU-34066

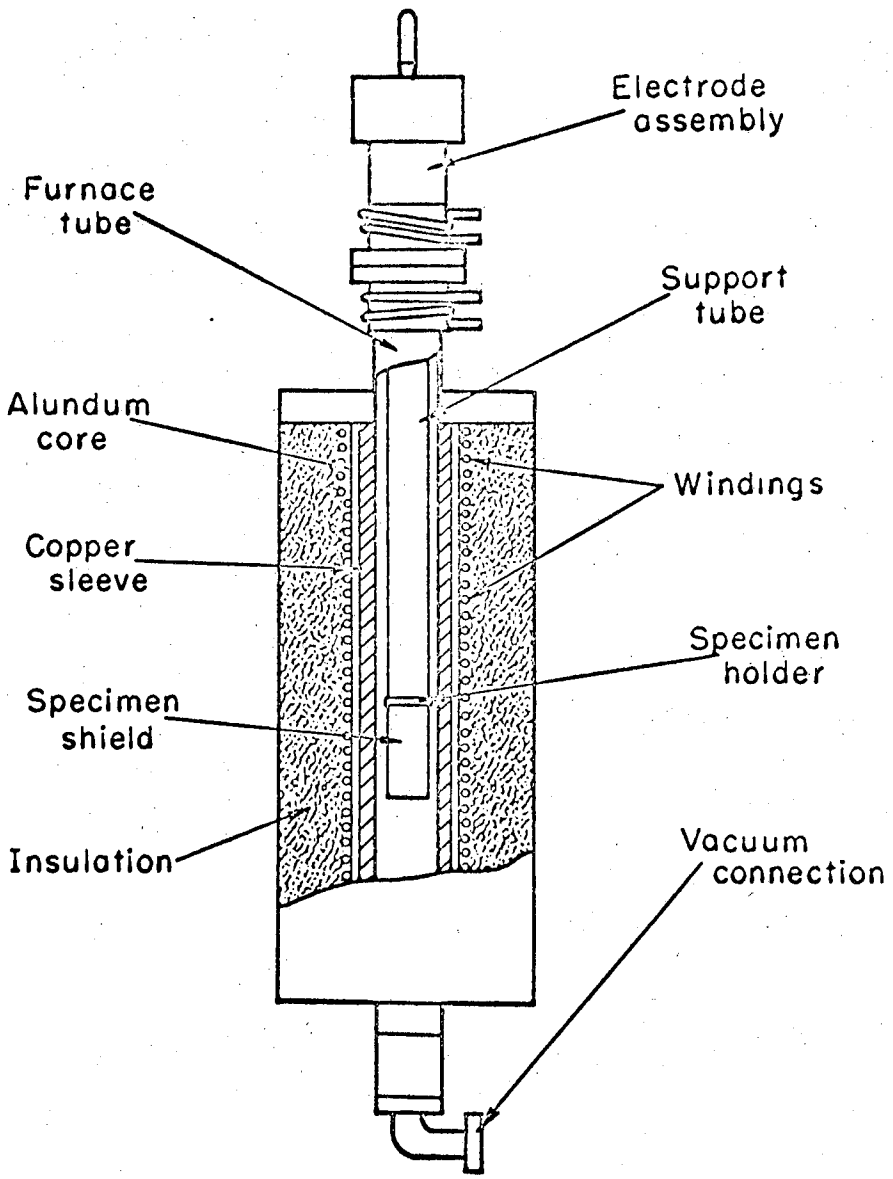

MU-34067

Fig. 4. High Temperature Apparatus

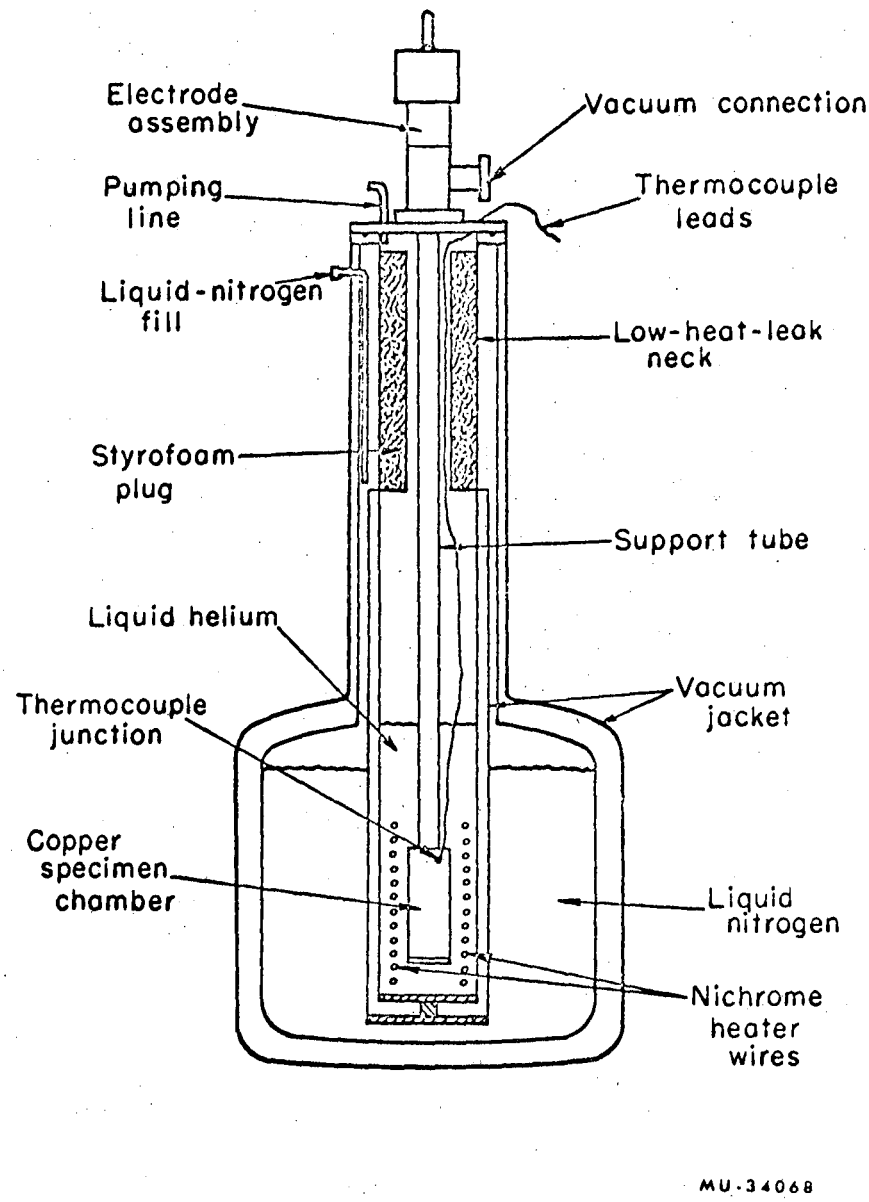

Fig. 5. Low Temperature Apparatus

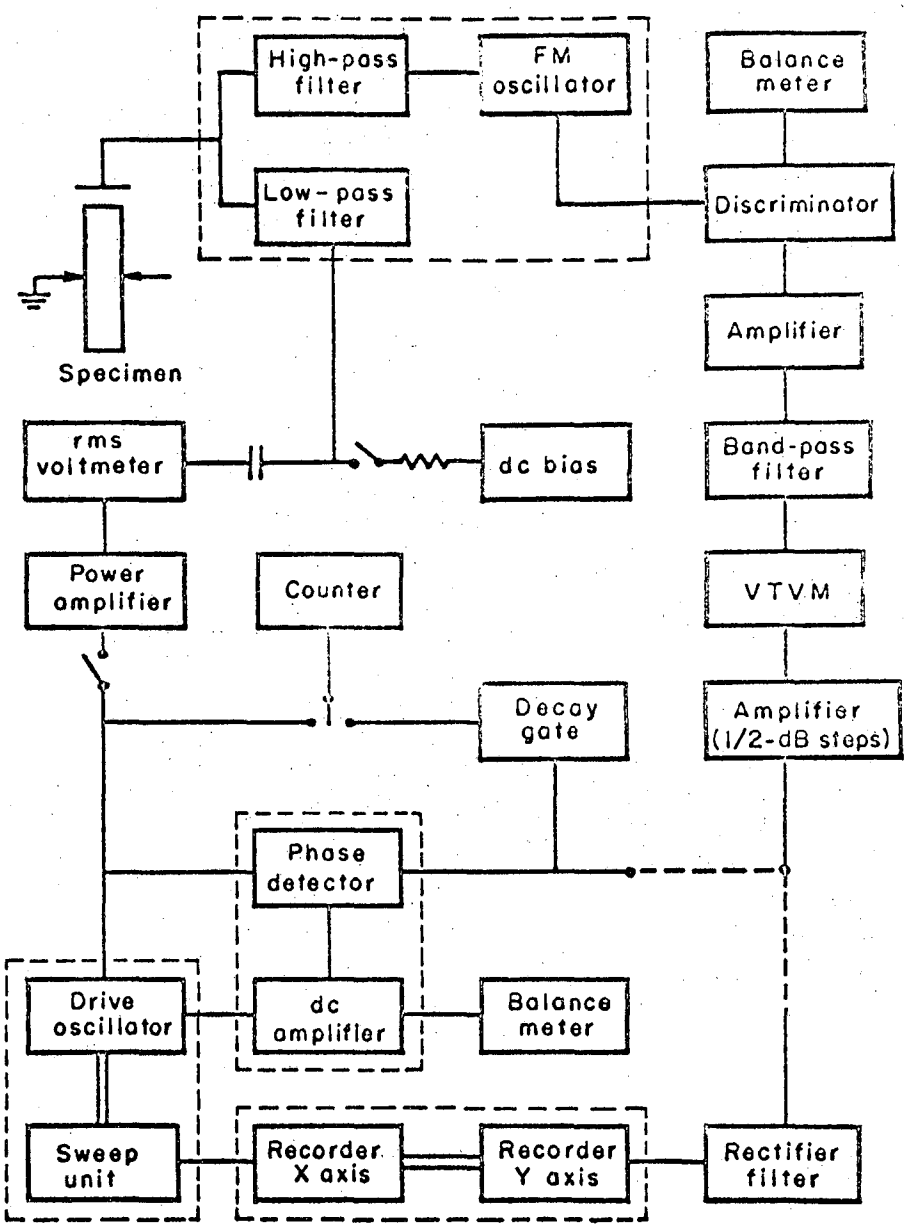

MU-34069

Fig. 6. Block Diagram of the Electronic Measuring System

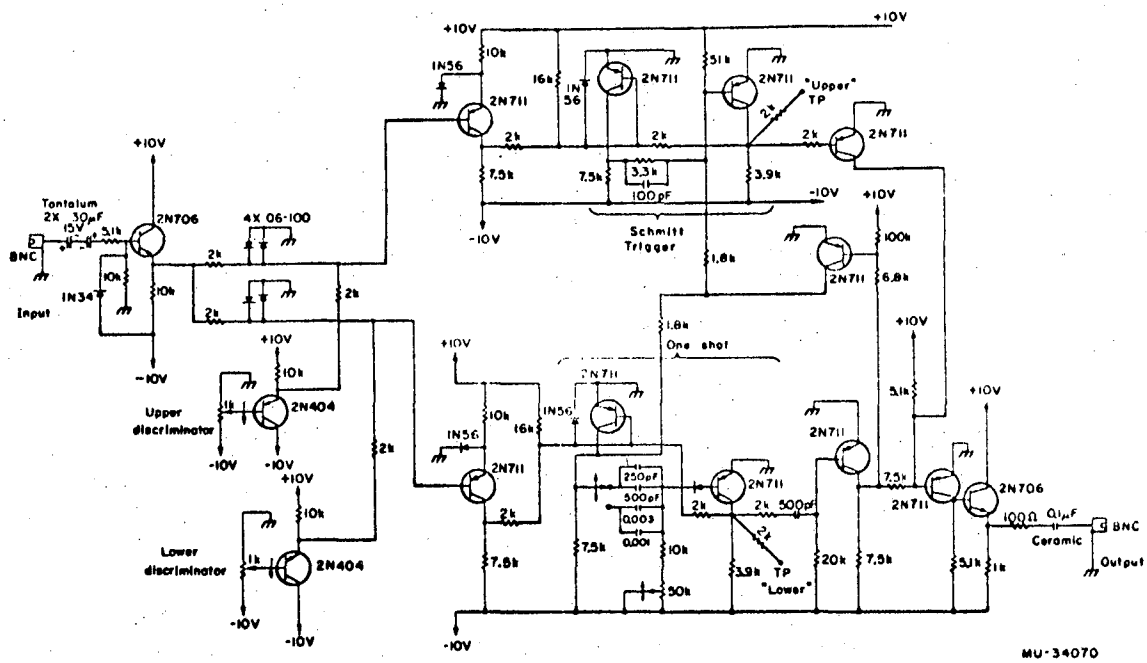

Fig. 7. Circuit Diagram of the Transistorized Decay Gate (All resistors are 1/2 Watt, and all capacitors are silver mica unless otherwise specified.)

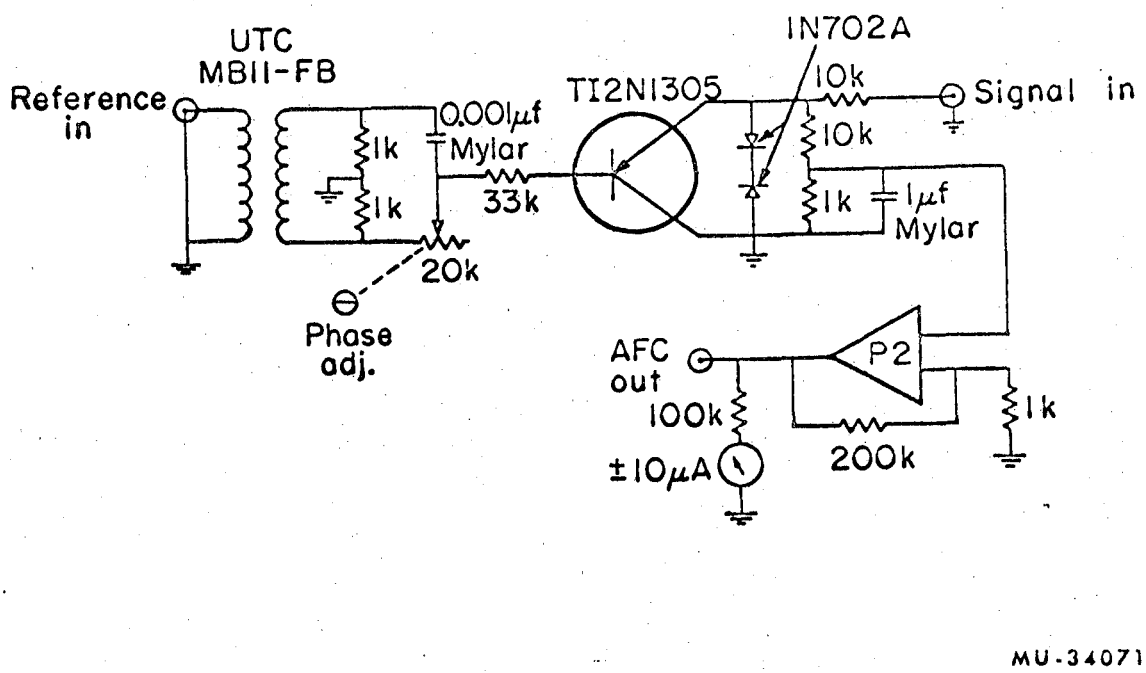

Fig. 8. Circuit Diagram of the Phase Detector Used to Maintain Resonance

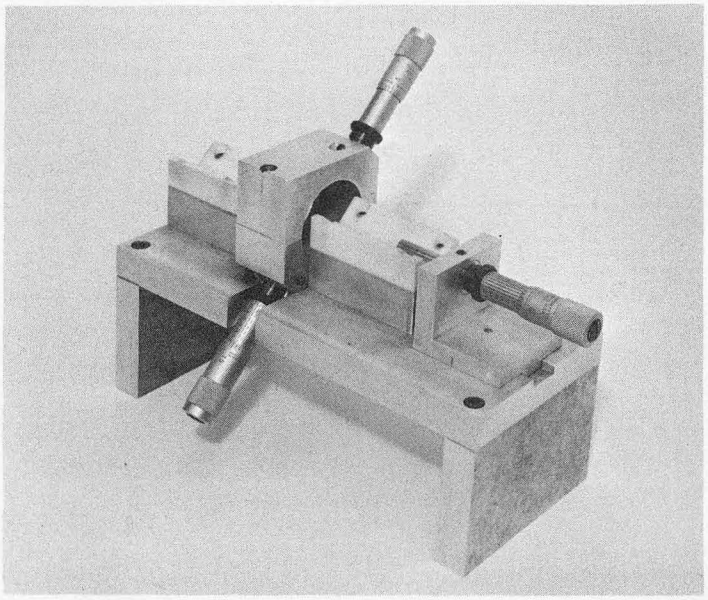

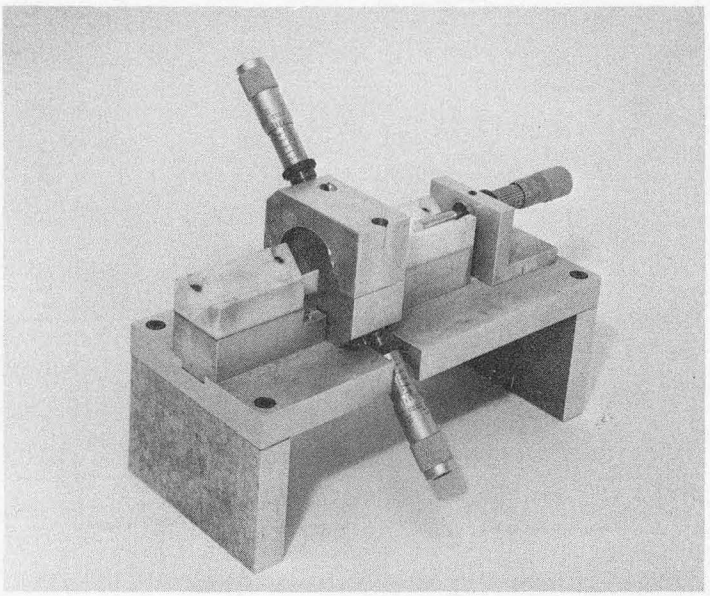

ZN-5977

Fig. 9. Photograph of the Specimen Mounting Jig (two views)

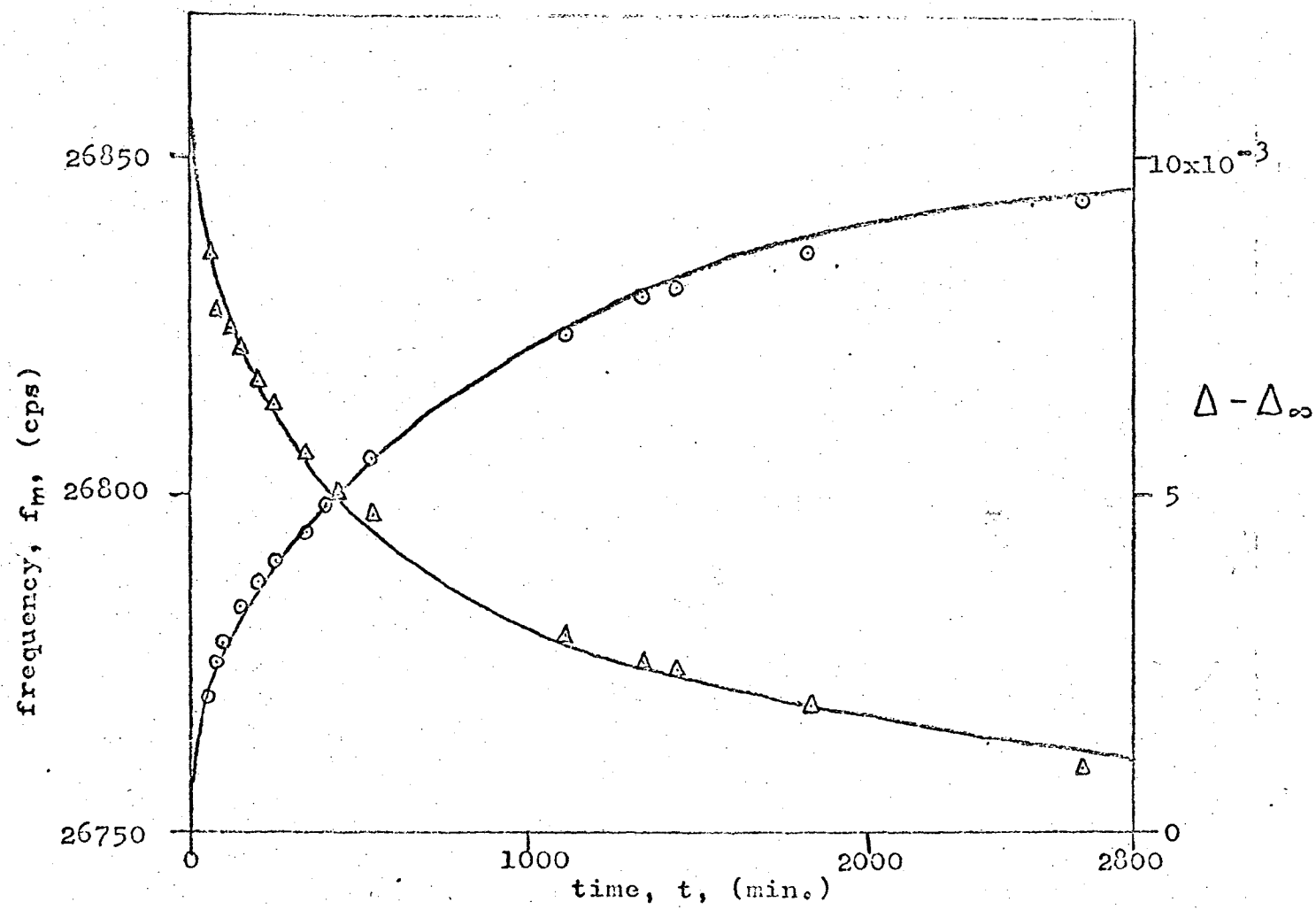

Fig. 10. Recovery of the Decrement (Δ) and Resonant Frequency (⊙) after Mounting at 293°K for Specimen 34C. (The solid lines shown correspond to the time dependence predicted by theory.)

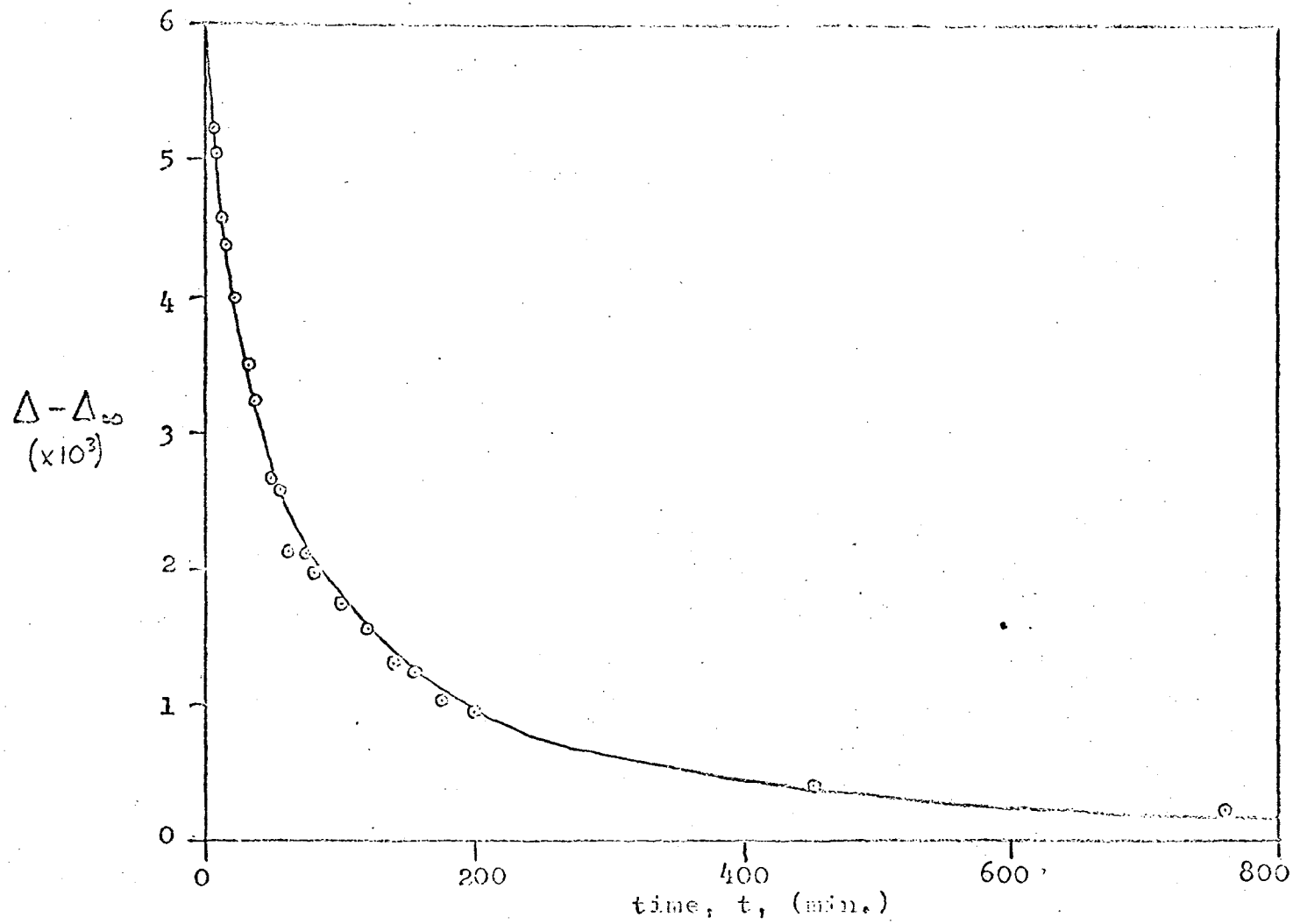

Fig. 11. Recovery of Decrement after Mounting at 377°K for Specimen 12A. (The solid lines shown correspond to the time dependence predicted by theory.)

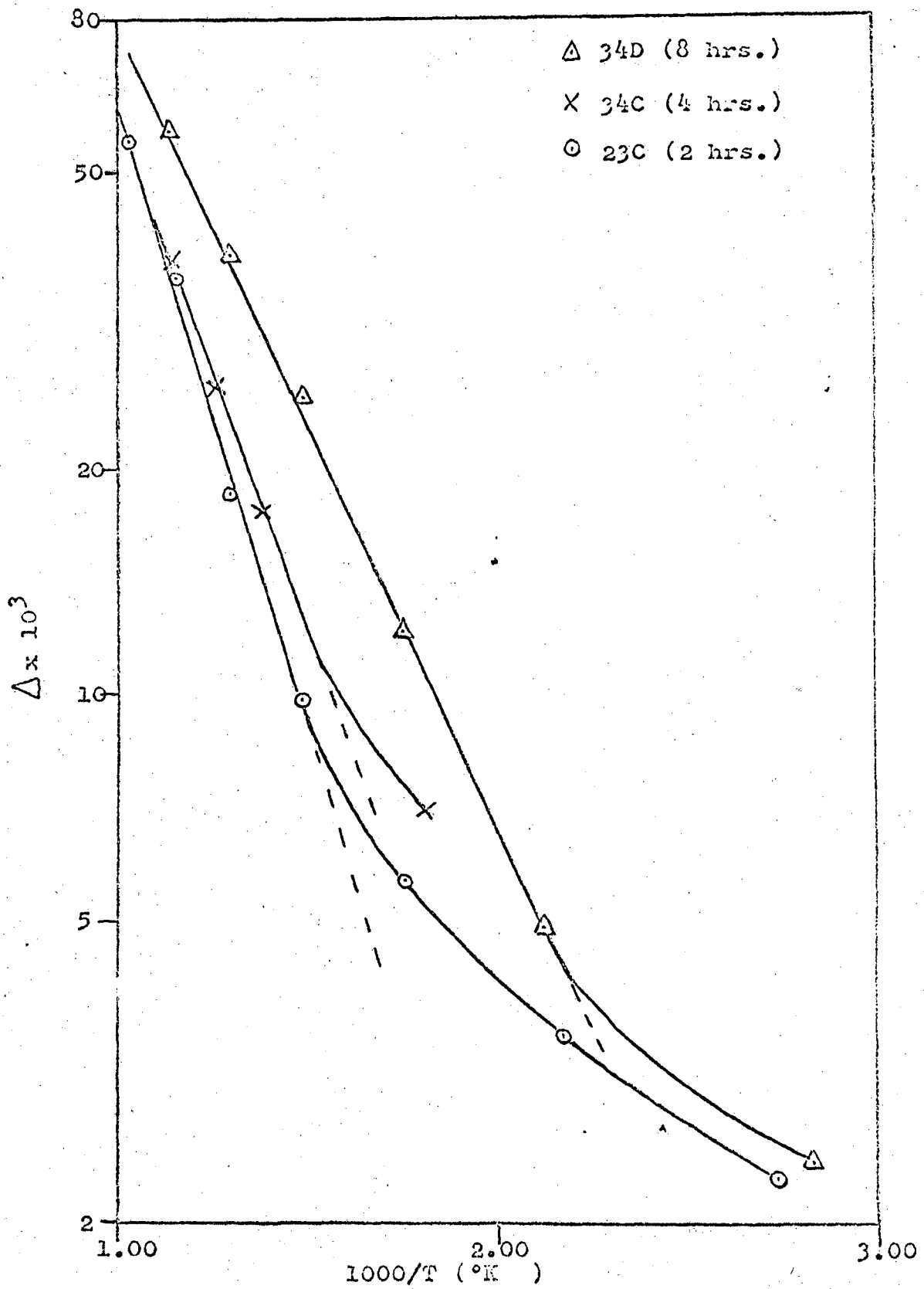

Fig. 12. The Decrement during Initial Warmup for Several Specimens as a Function of 1/T (°K). (The times indicated in the figure are the equilibration times at each temperature.)

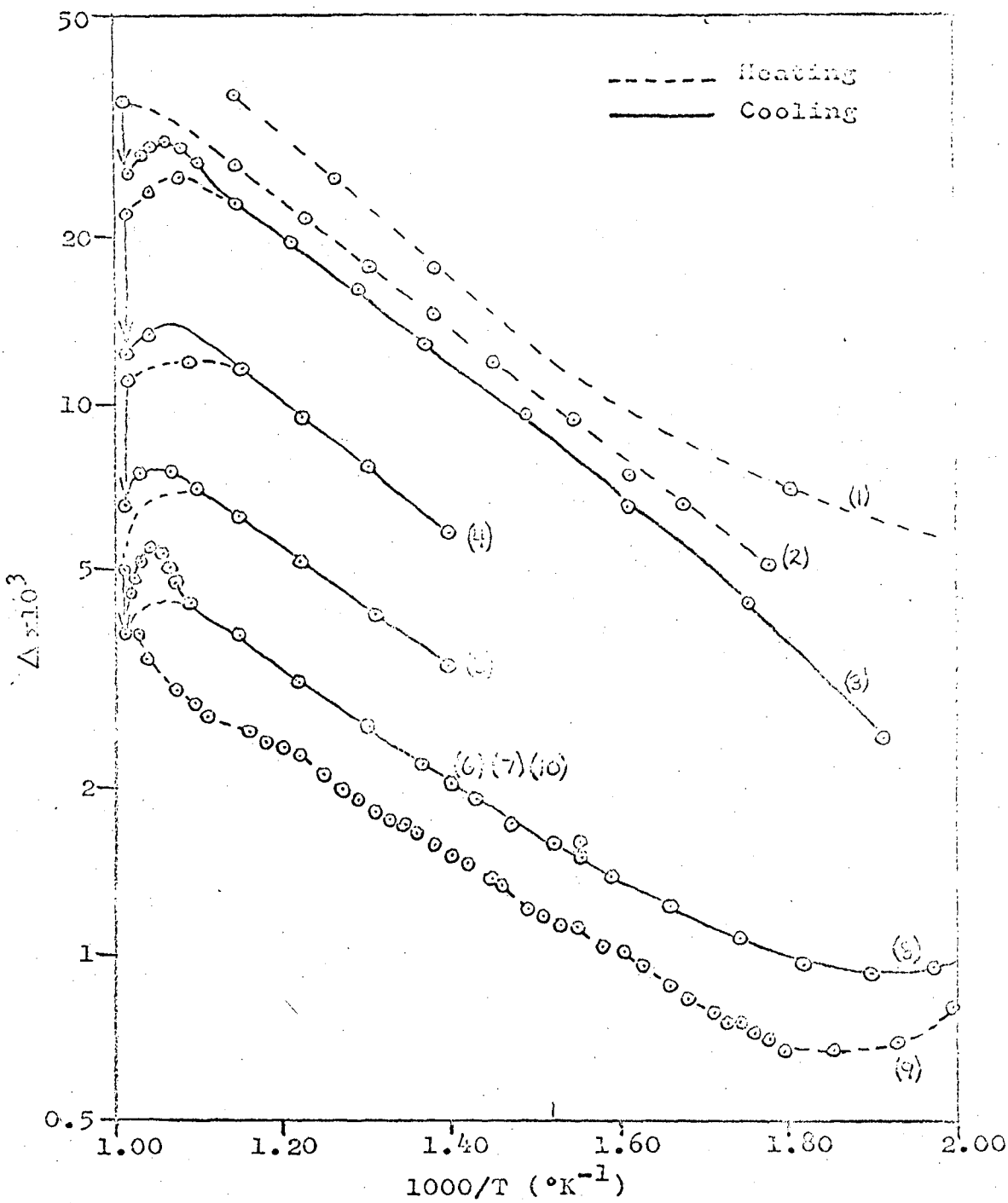

Fig. 13. The Decrement during Cyclic Annealing of Cyclic Annealing of Specimen 34C. (Successive cycles are labeled in sequence following the initial warmup (1).)

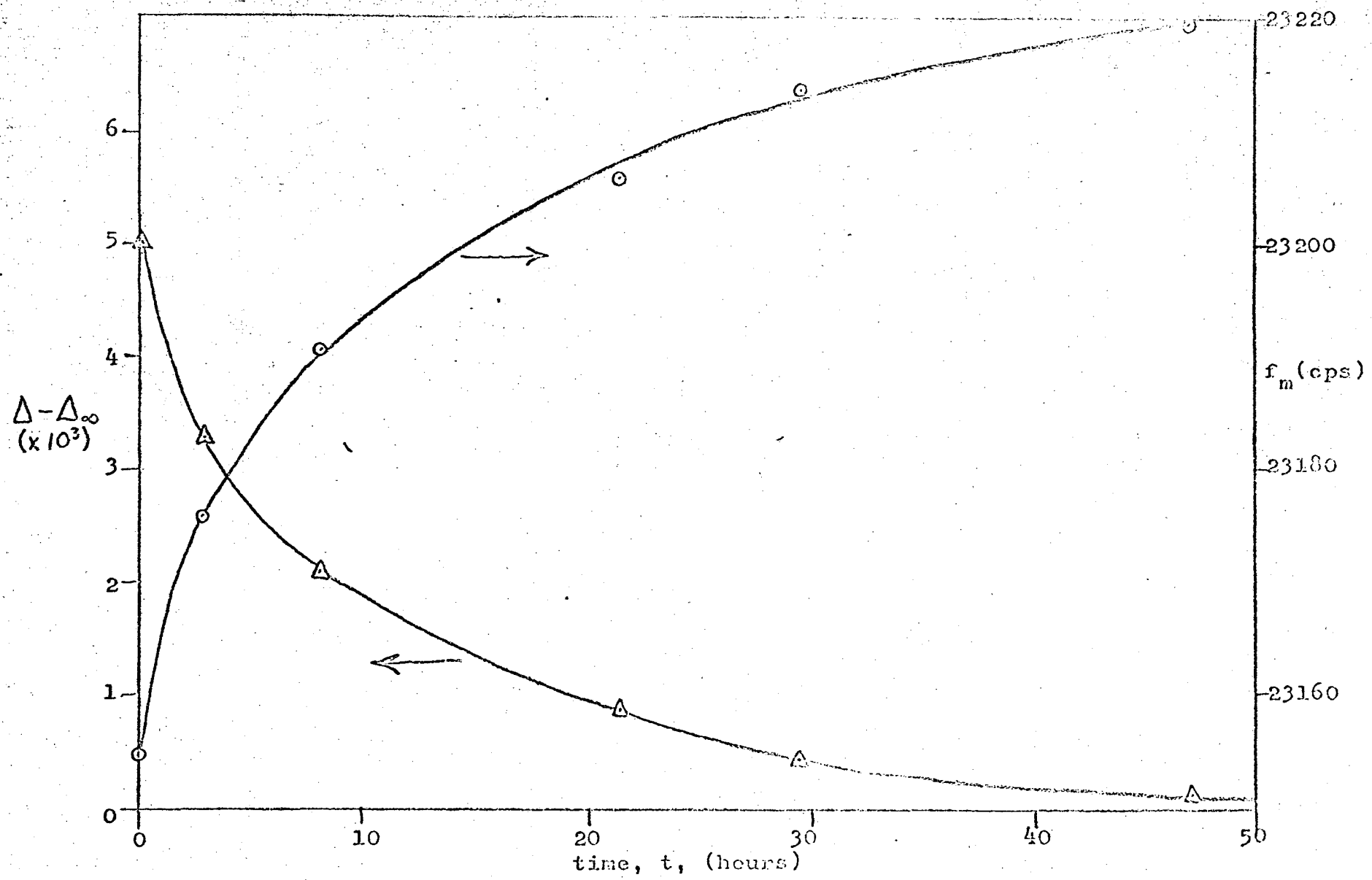

Fig. 14. The Time Dependence of the Decrement and Resonant Frequency at 994°K after Cycle (3) in Fig. 13.

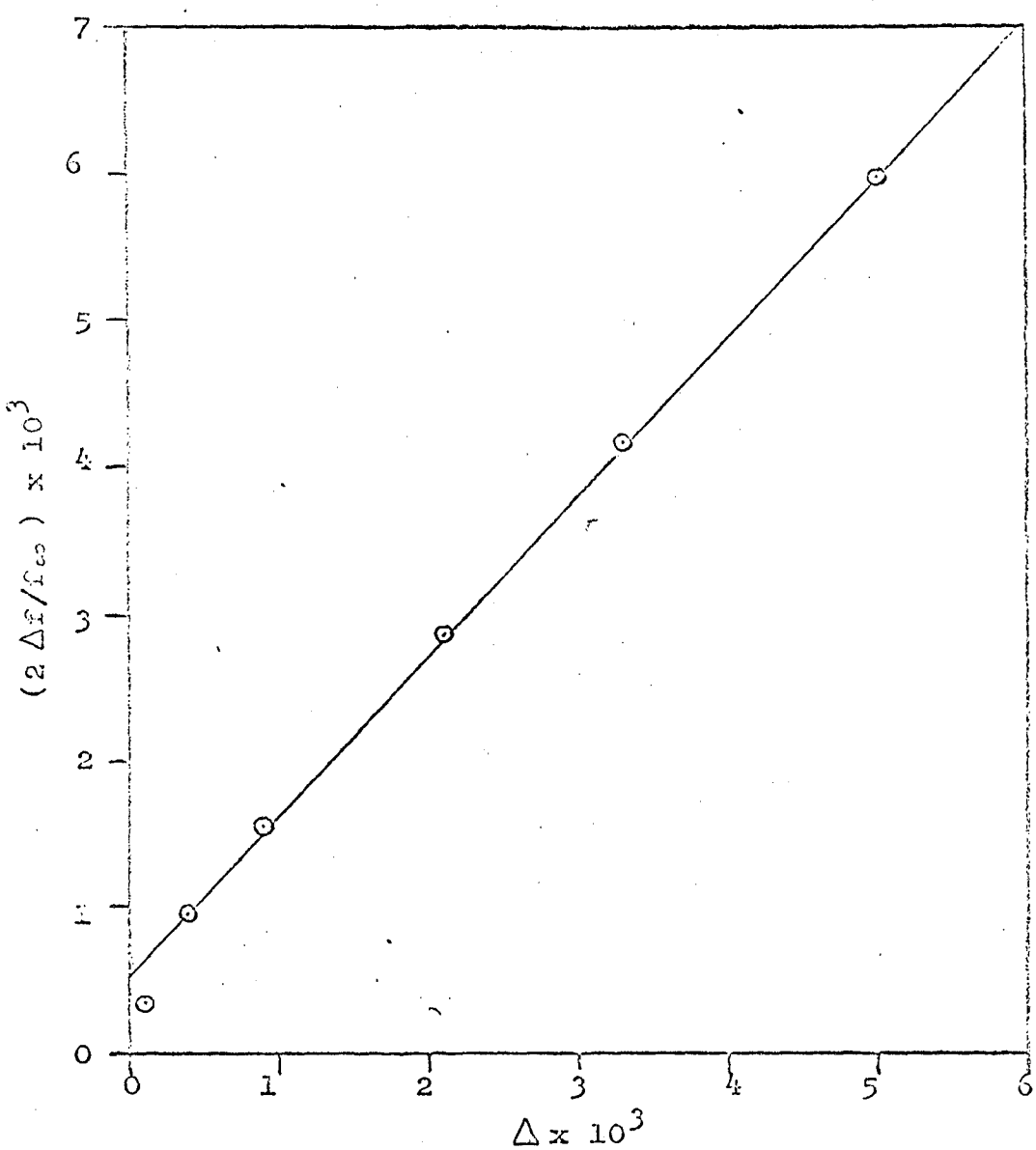

Fig. 15. The Change in the Modulus as a Function of the Change in the Decrement for the Data of Fig. 14.

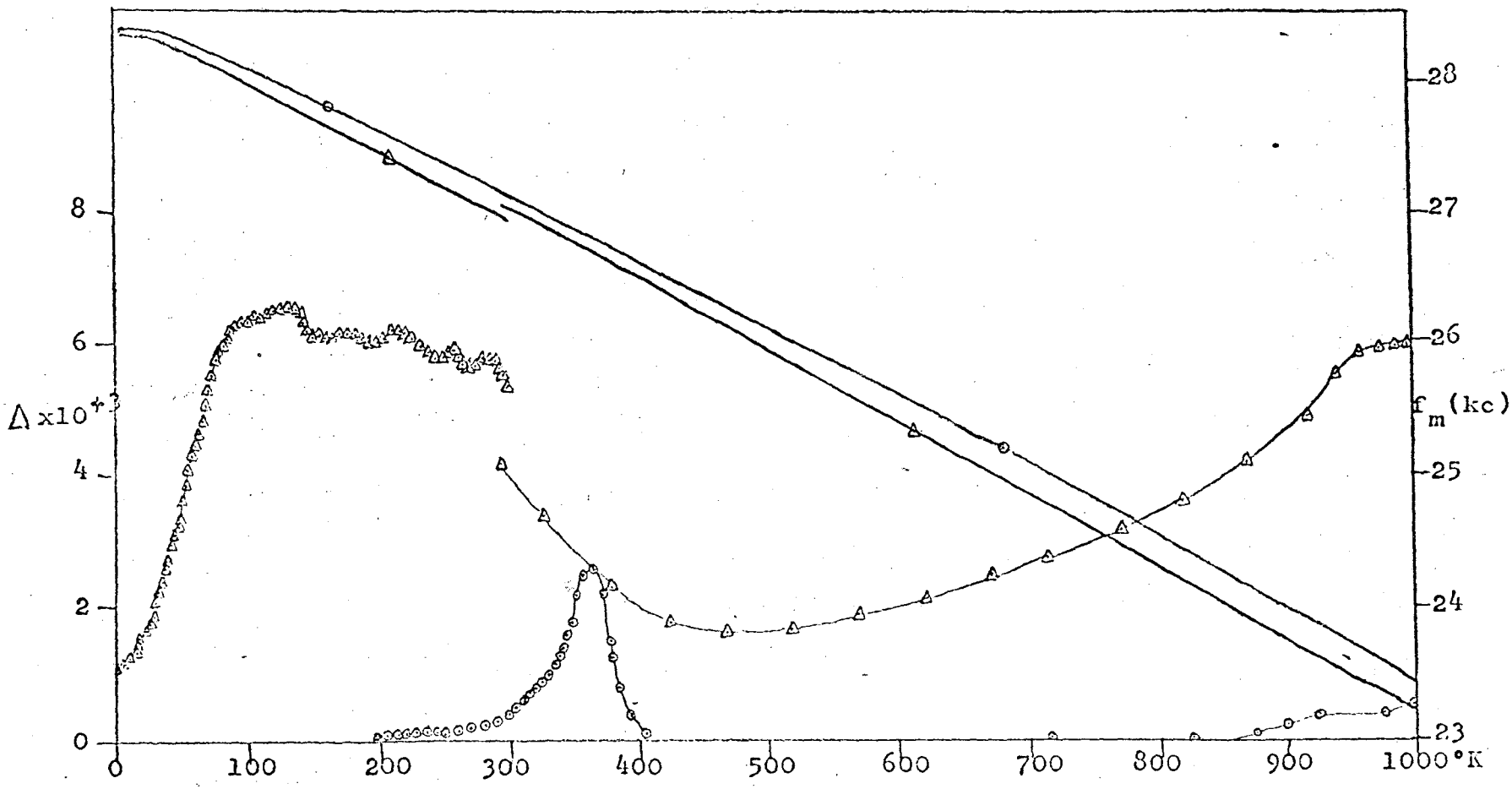

Fig. 16. The Decrement and Resonant Frequency for Specimen 34E (△) and 34E Containing 40 ppm O_2 (⊙) as a Function of Temperature.

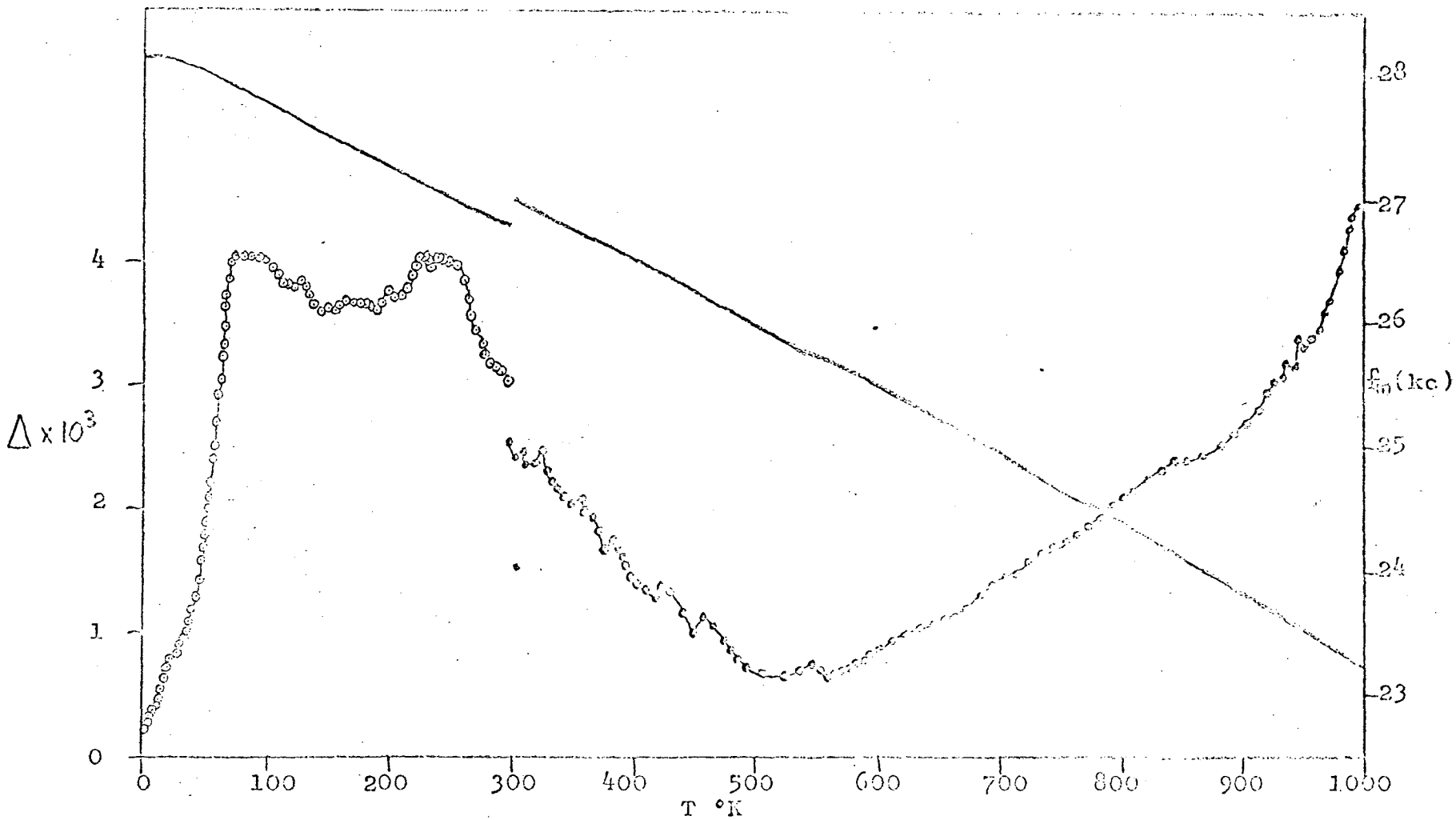

Fig. 17. The Decrement and Resonant Frequency for Specimen 34D (T<300°K) and Specimen 34C (T>300°K) as a function of Temperature. (The measurements were made on continuous warmup at ~20°K/hour.)

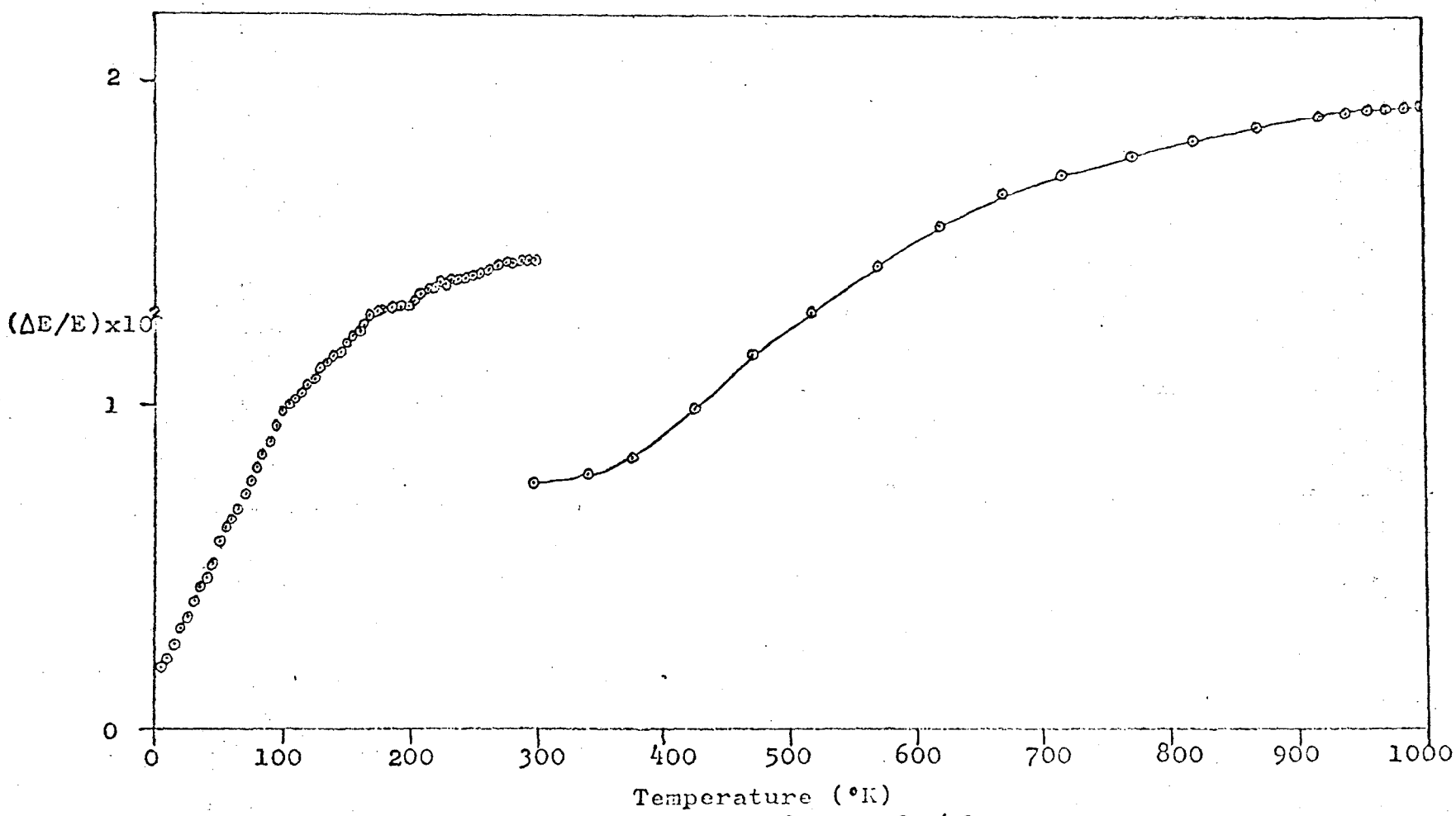

Fig. 18. The Modulus Defect, $\Delta E/E = (f_{0x}^2 - f_M^2)/f_{0x}^2$ as a function of Temperature for Specimen 34E. (See Fig. 16 for corresponding decrement measurements.)

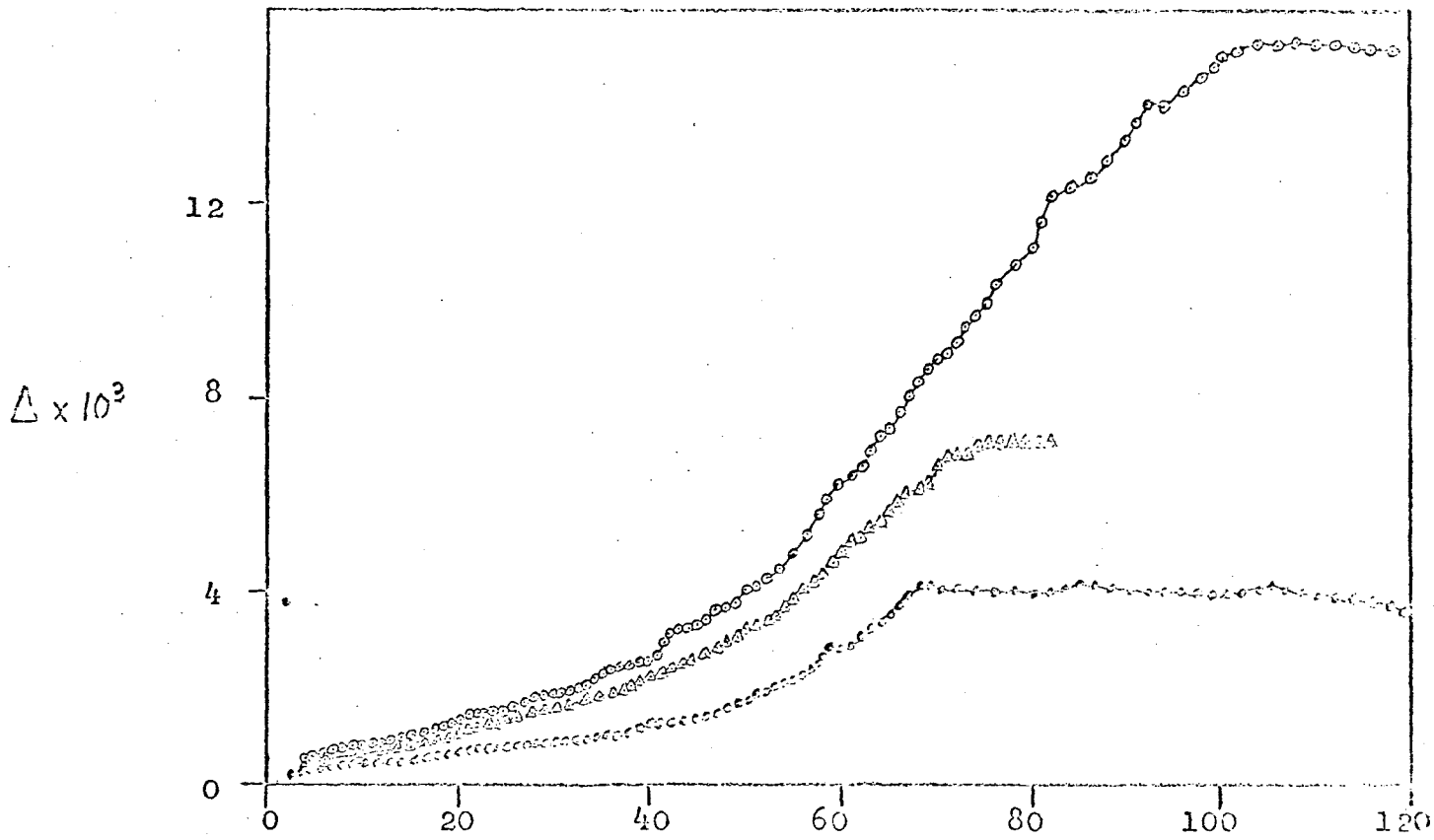

Fig. 19. The Effect of Room Temperature Annealing on the Decrement at Low Temperatures. (The curves correspond to measurements made one day (⊙), one week (Δ), and two months (○) after room temperature mounting.)

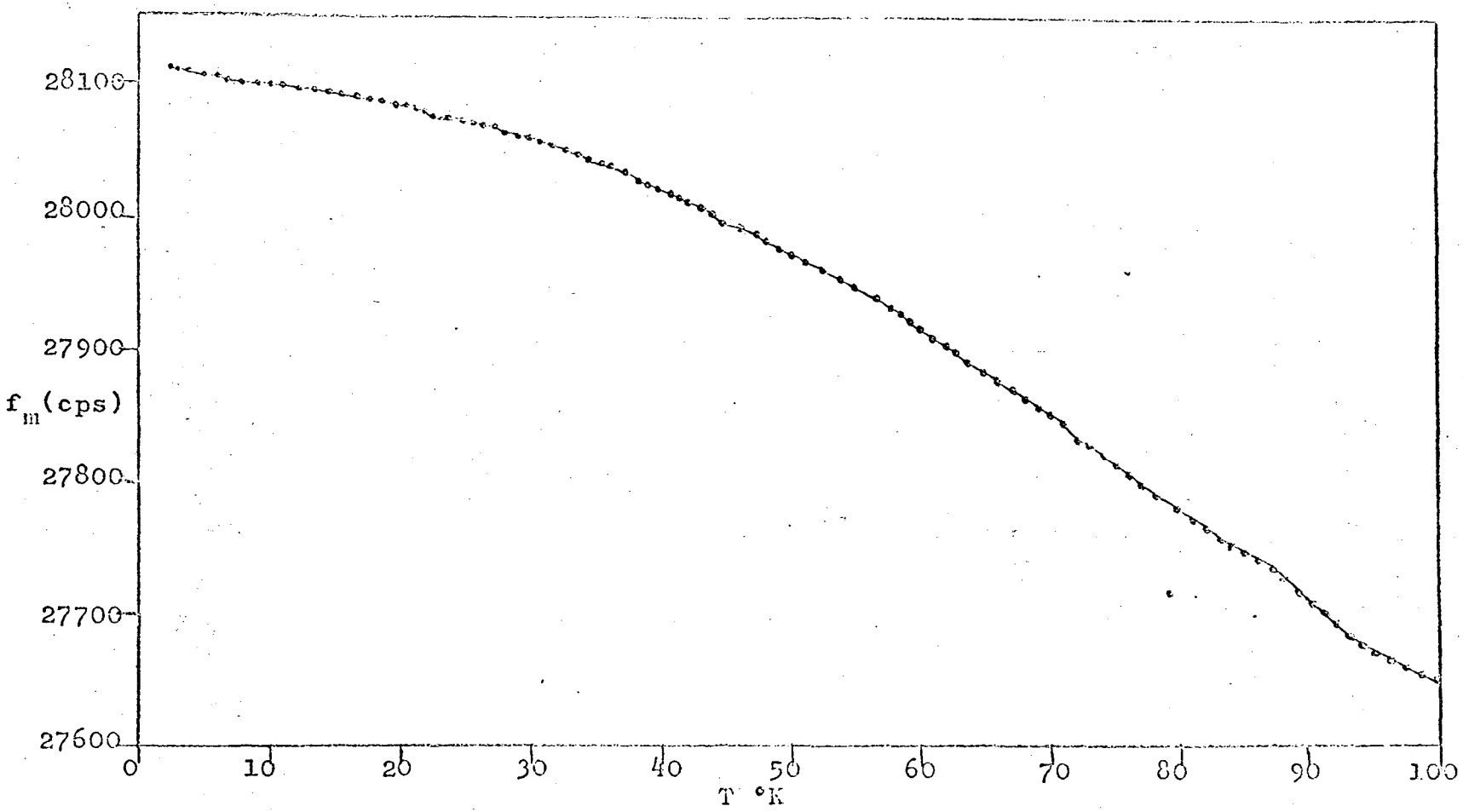

Fig. 20. The Resonat Frequency for Specimen 34D below 100°K. (The resonant frequencies shown here correspond to the decrement data of Fig. 19 taken after one day of room temperature annealing.)

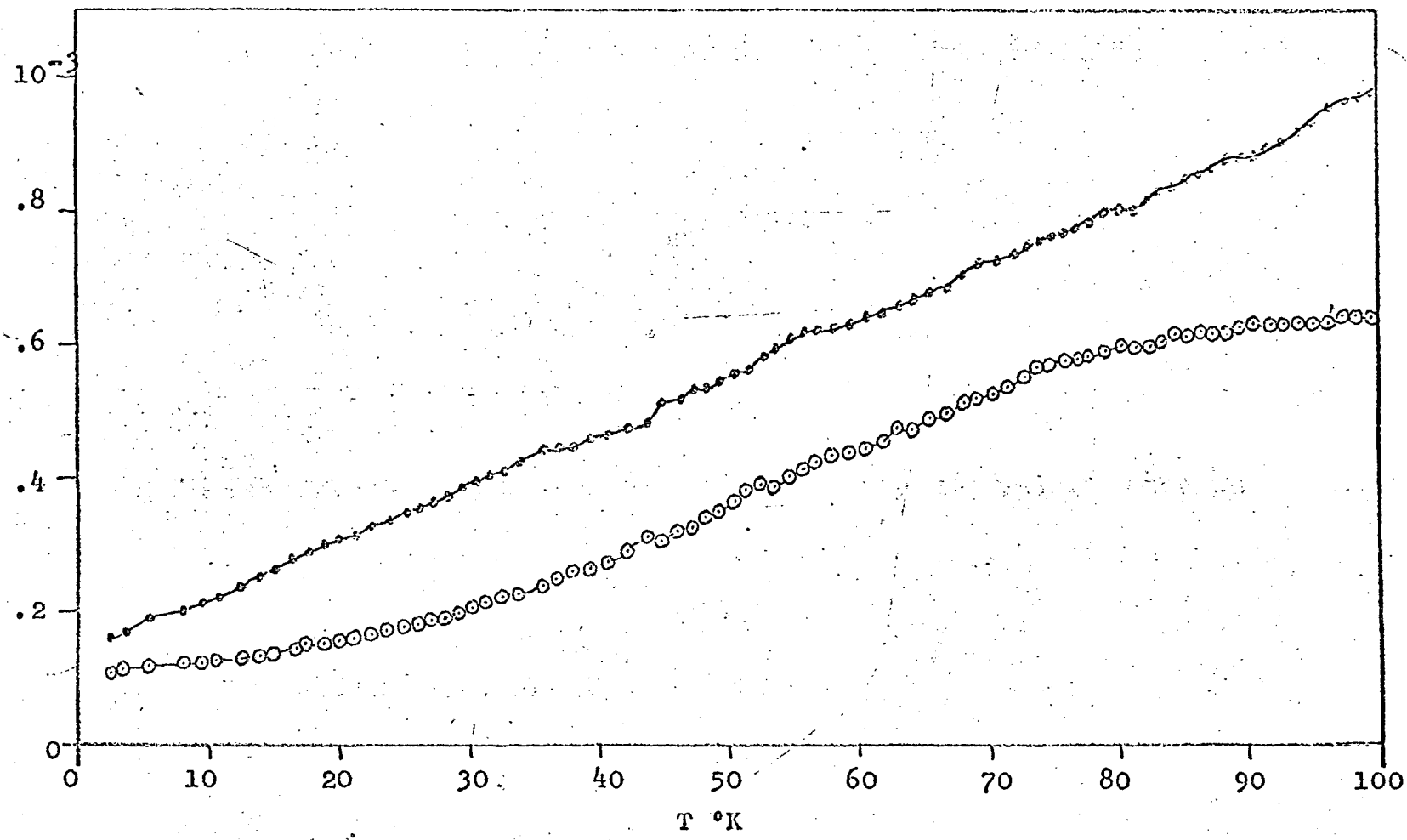

Fig. 21. The Decrement (⊙) and Modulus Defect (●), $(f_{0x}^2 - f_m^2) / f_{0x}^2$, for Specimen 3/4E at Low Temperatures.

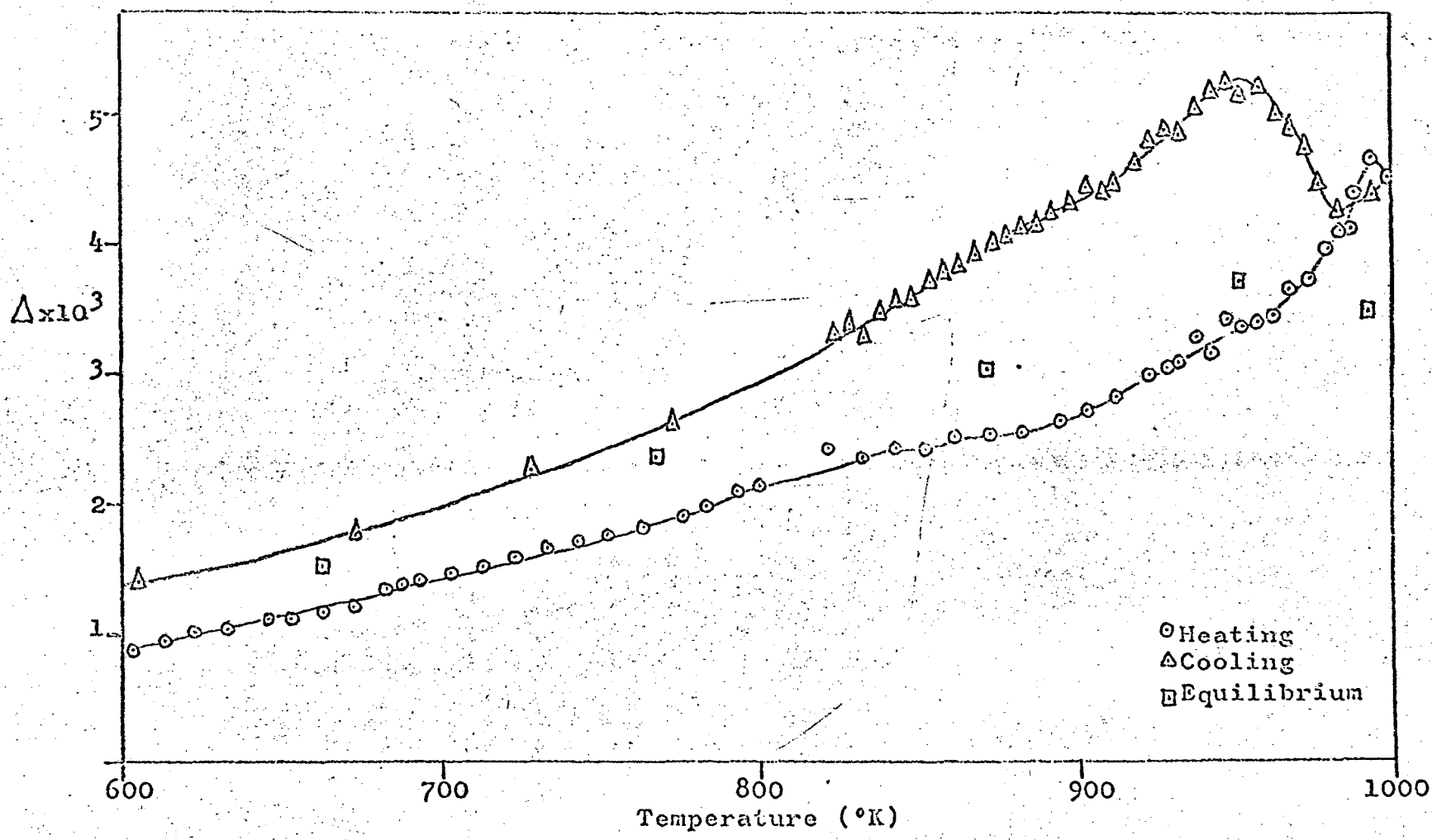

Fig. 22. The Decrement as a Function of Temperature for a Continuous Heating and Cooling Cycle at 30°K/hour. (The equilibrium points correspond to measurements made after 12 hours at temperature.)

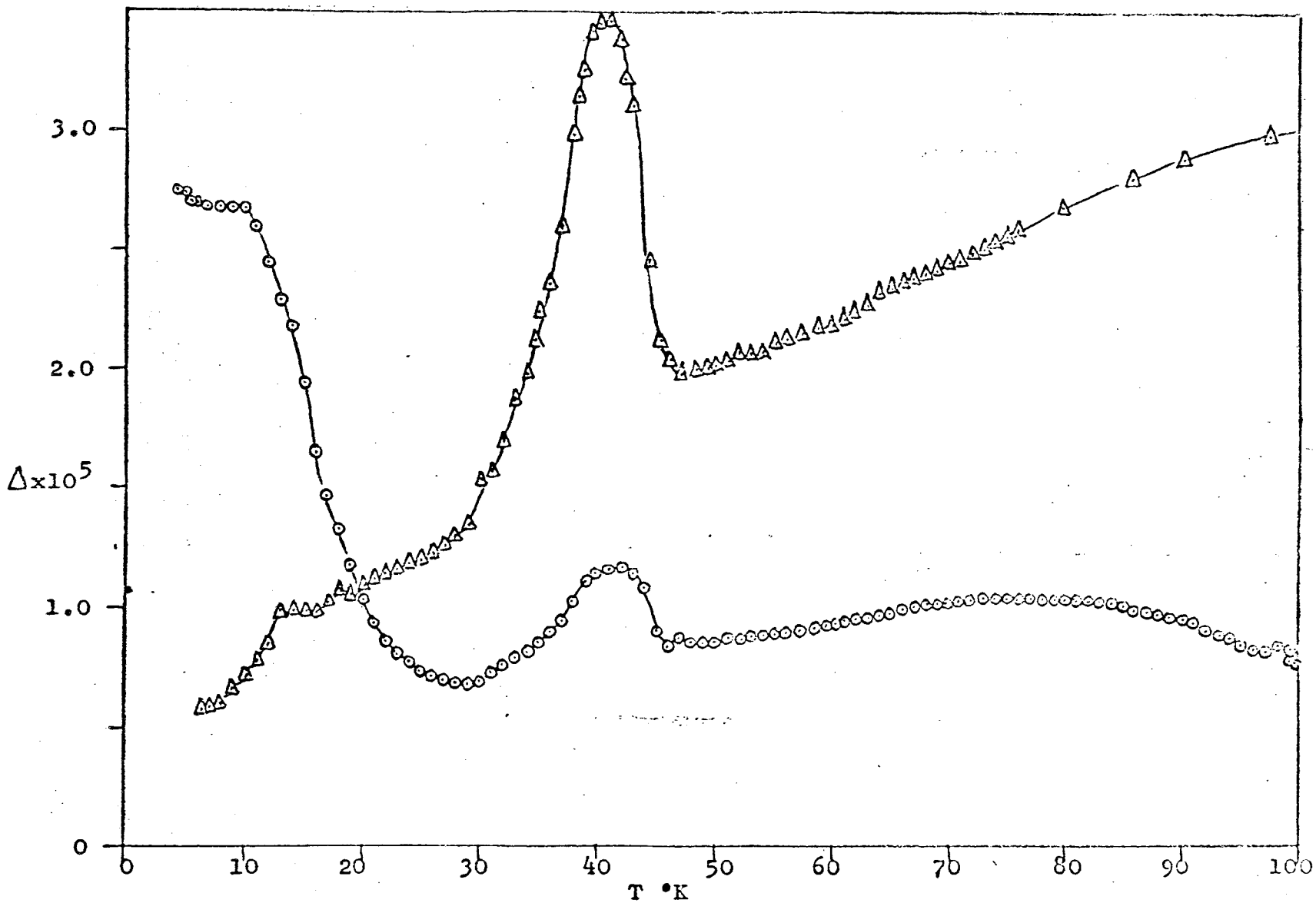

Fig. 23. Decrement at Low Temperatures for Specimen 34E Containing 40 ppm O_2 (⊙) and Specimen 23 AM (1% Mg) (△).

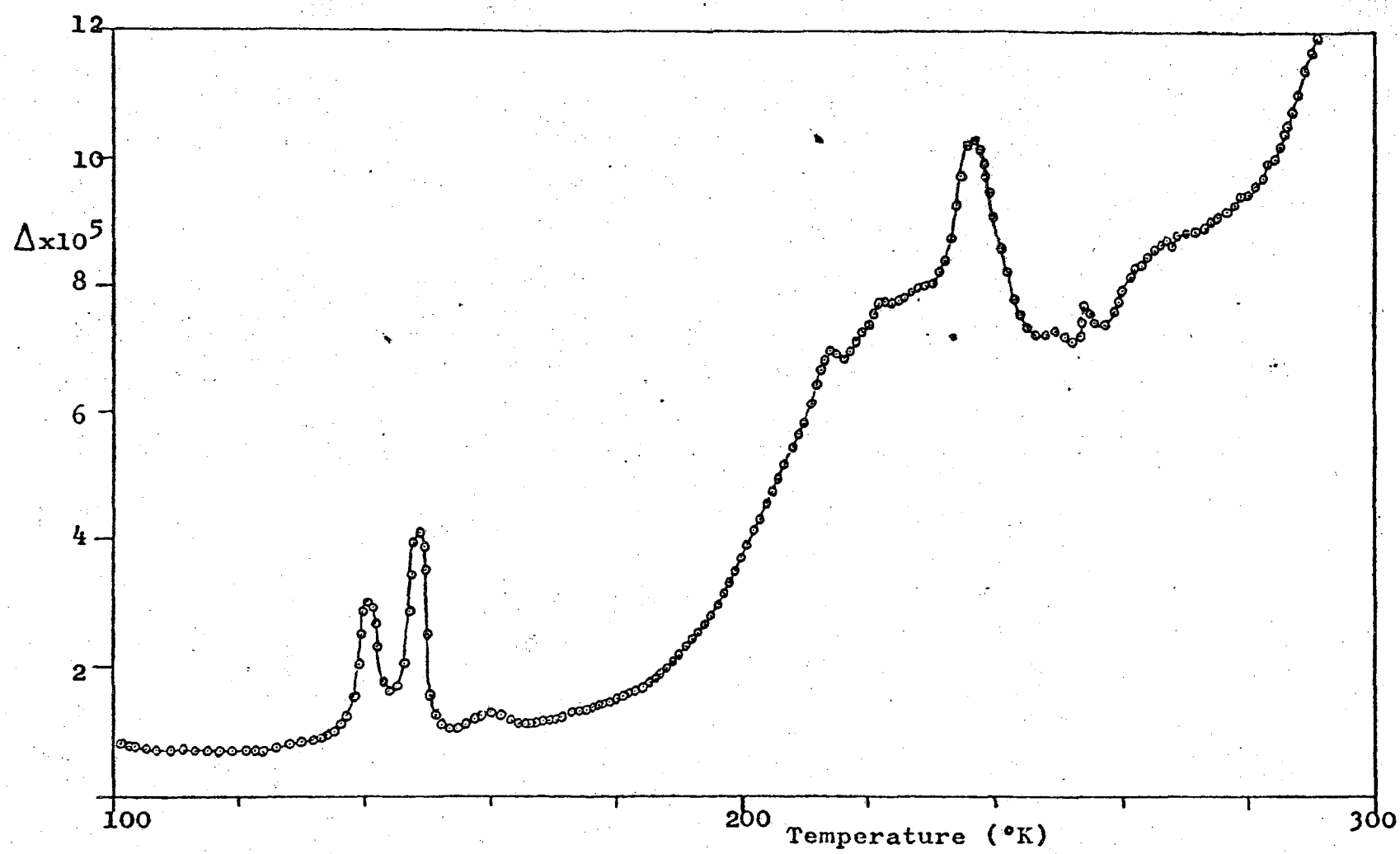

Fig. 24. The Decrement for 34E Containing 40 ppm O_2 from 100°K - 300°K. (Note scale change wrt Fig. 23.)

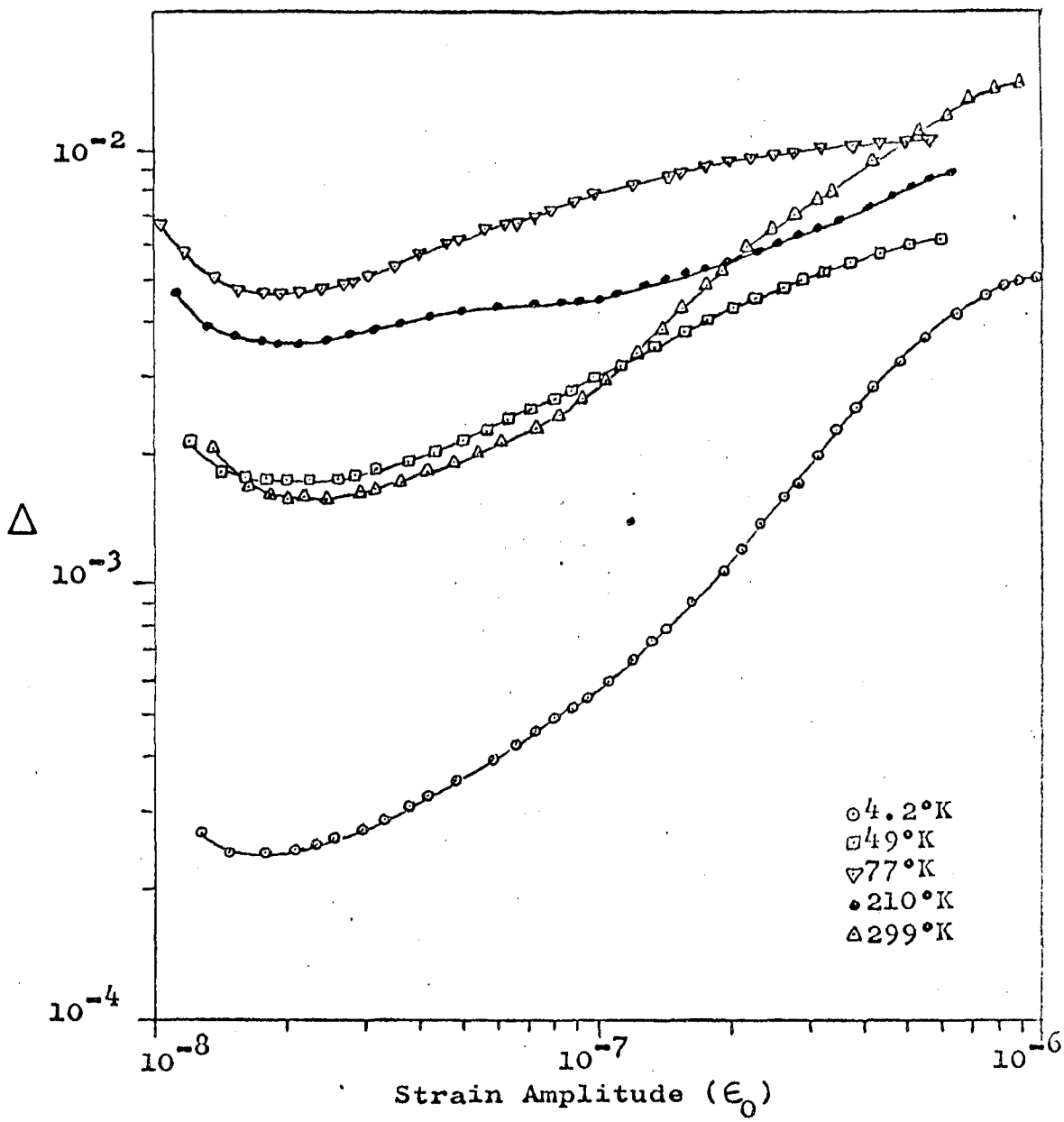

Fig. 25. The Decrement as a Function of Strain Amplitude for 34D at Various Temperatures between 4.2°K and 294°K.

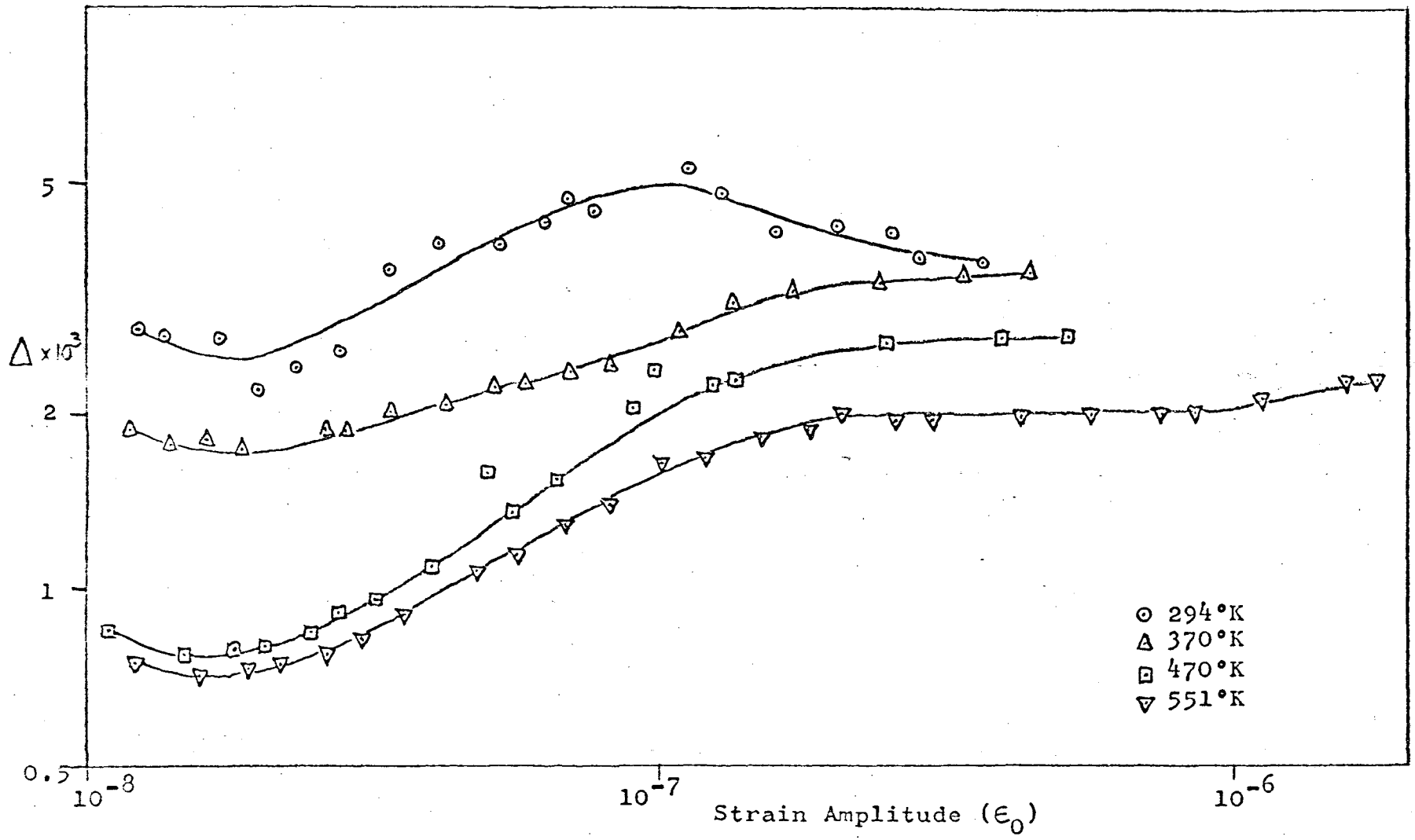

Fig. 26. The Decrement as a Function of Strain Amplitude for Specimen 34C below 600°K.

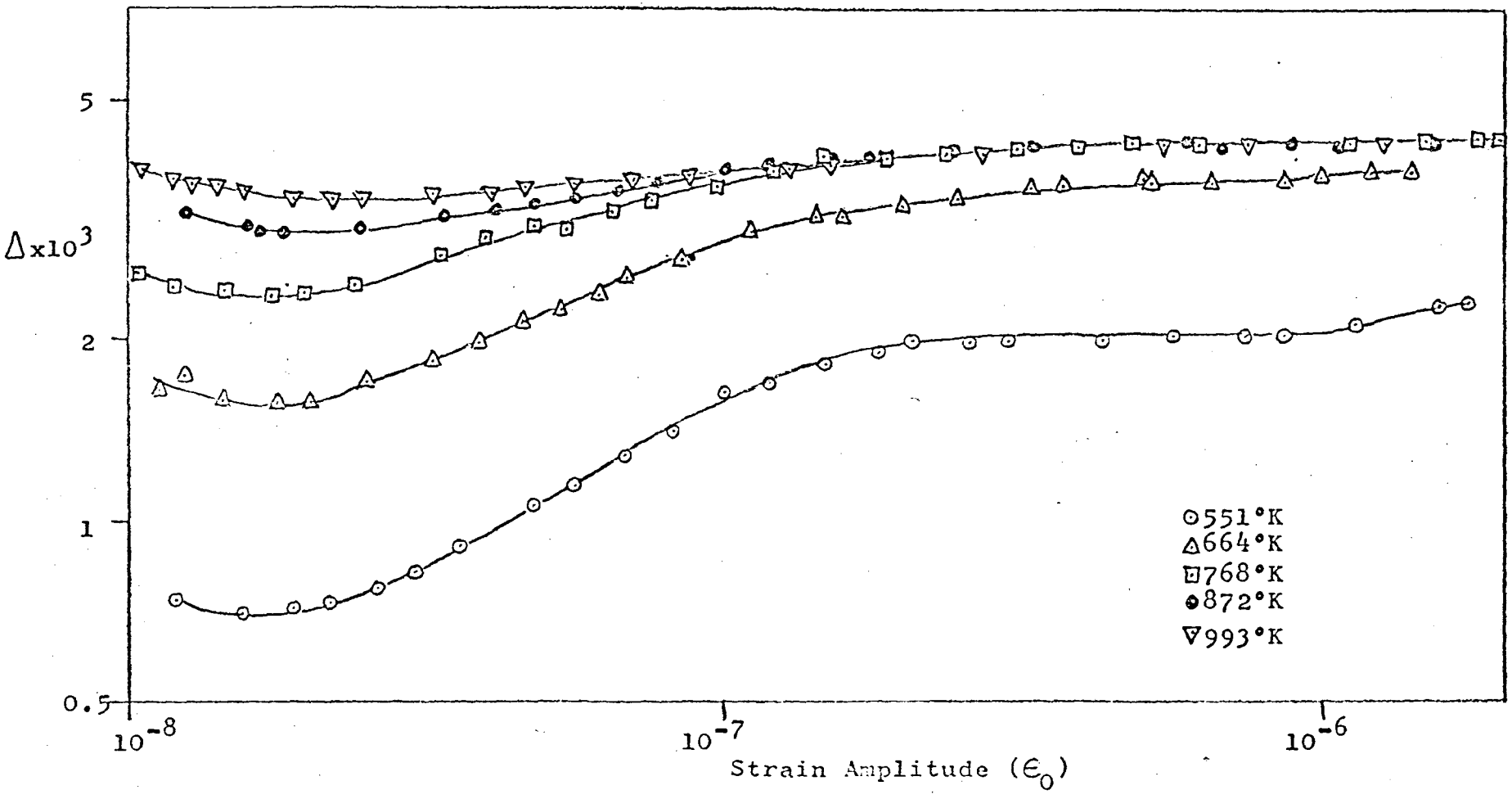

Fig. 27. The Decrement as a Function of Strain Amplitude for 34C above 500°K).

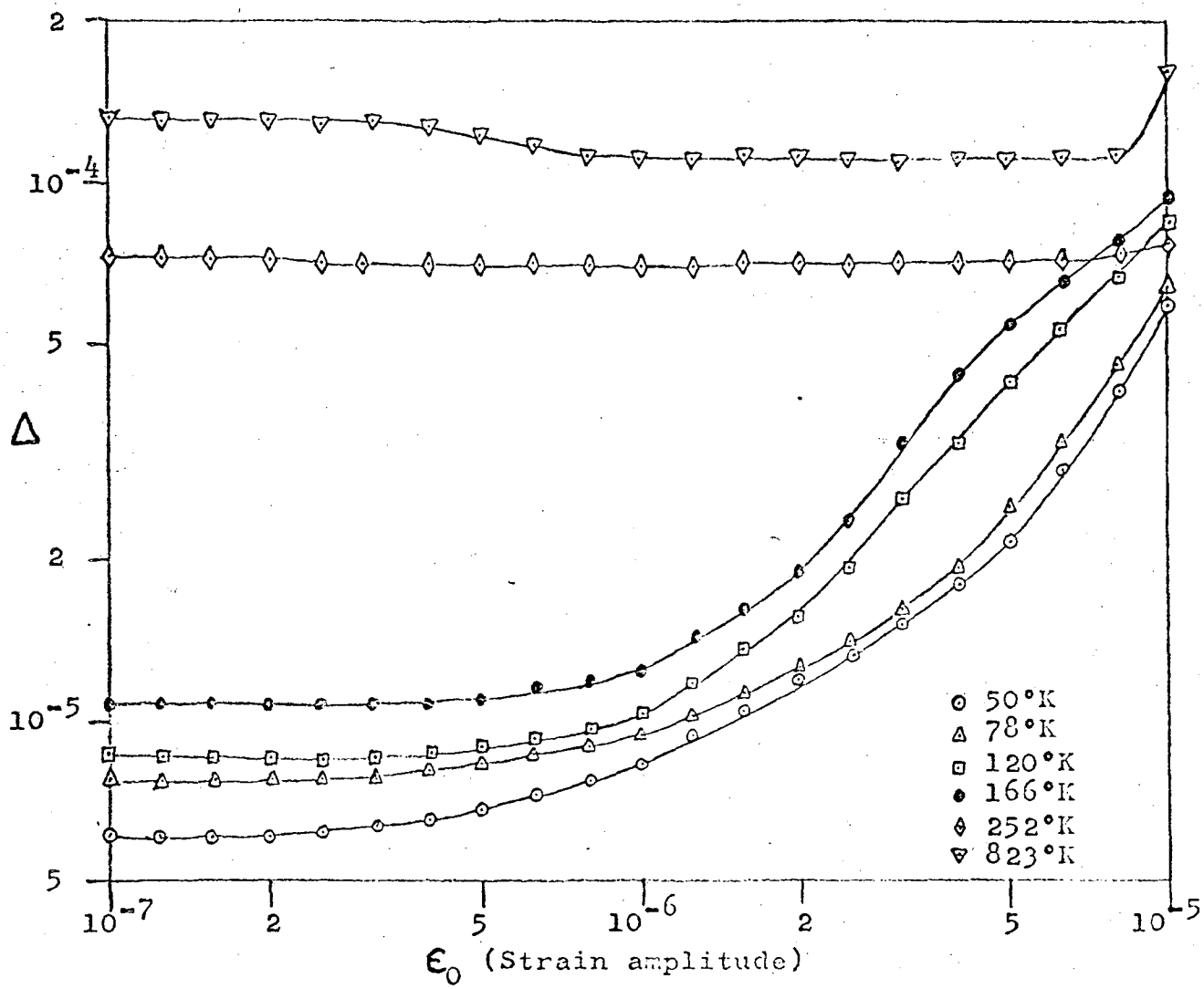

Fig. 28. The Decrement as a function of Strain Amplitude for Specimen 34E Containing 40 ppm O_2 at Various Temperatures.

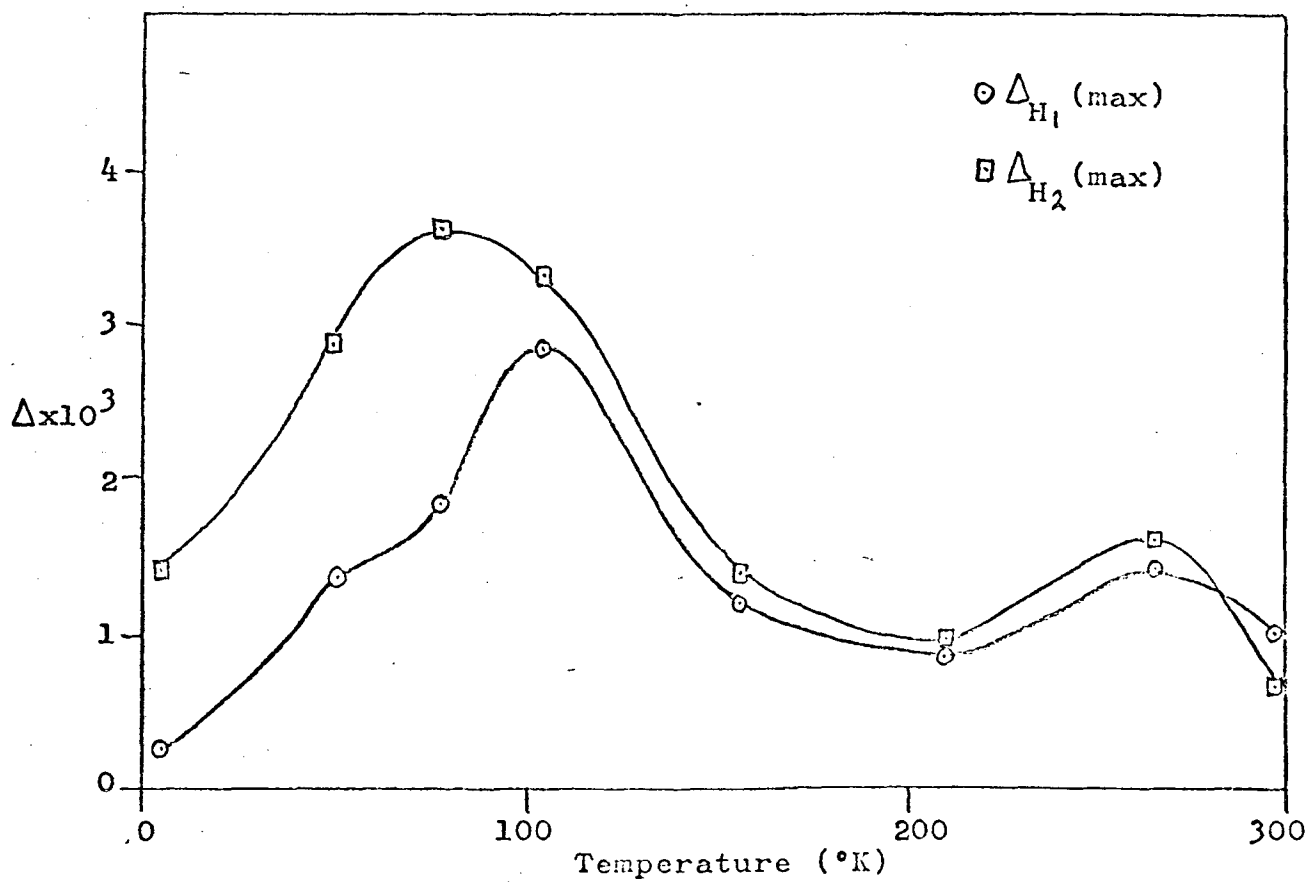

Fig. 29. The Magnitude of the Amplitude Dependent Decrement, Δ_H, as a Function of Temperature for Specimen 34D at Low Temperatures.
The separation of Δ_H into two components is described in the text (122 ff).

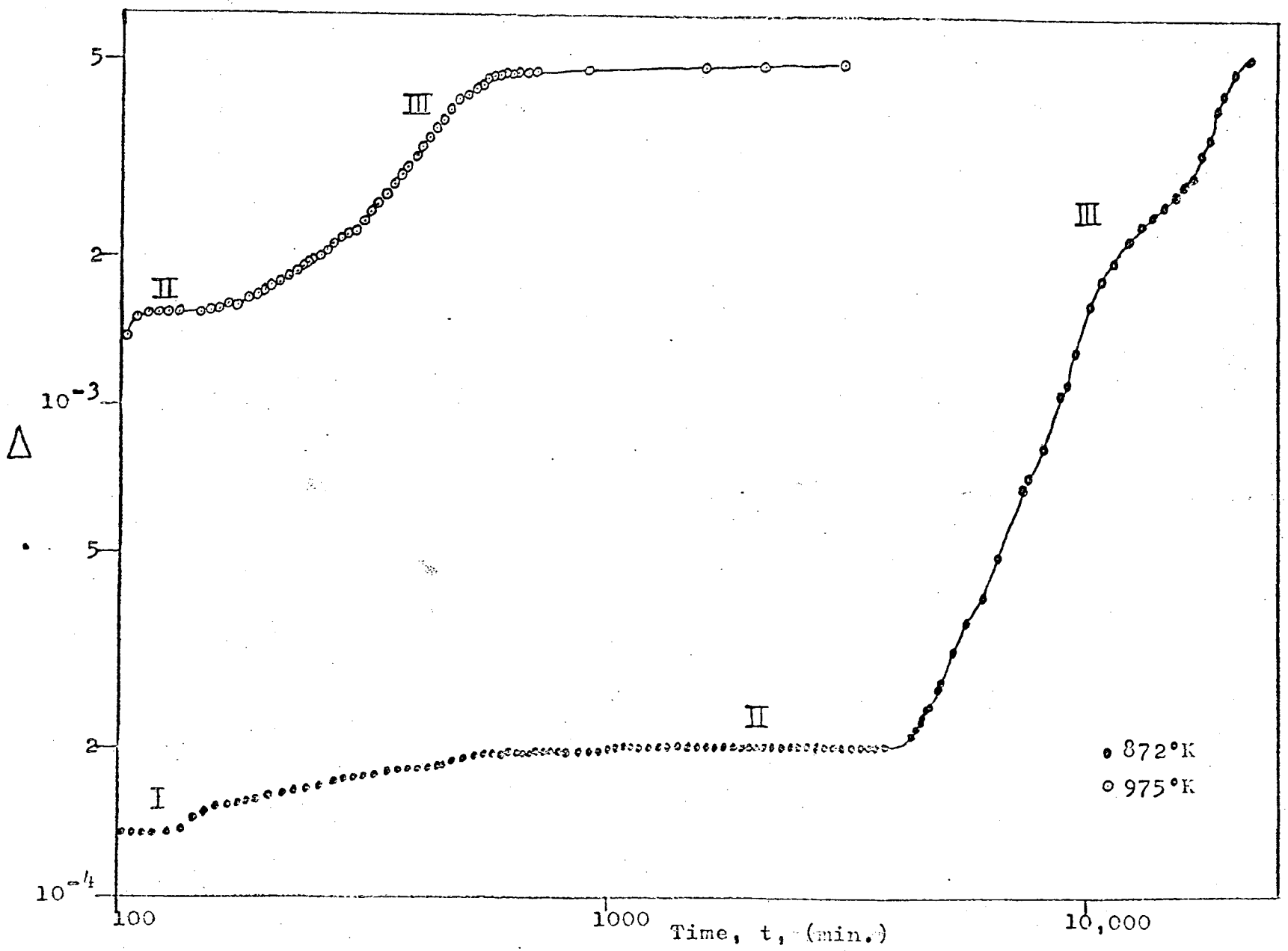

Fig. 30. Recovery of the Decrement during Oxygen Desorption at 872°K and 975°K.

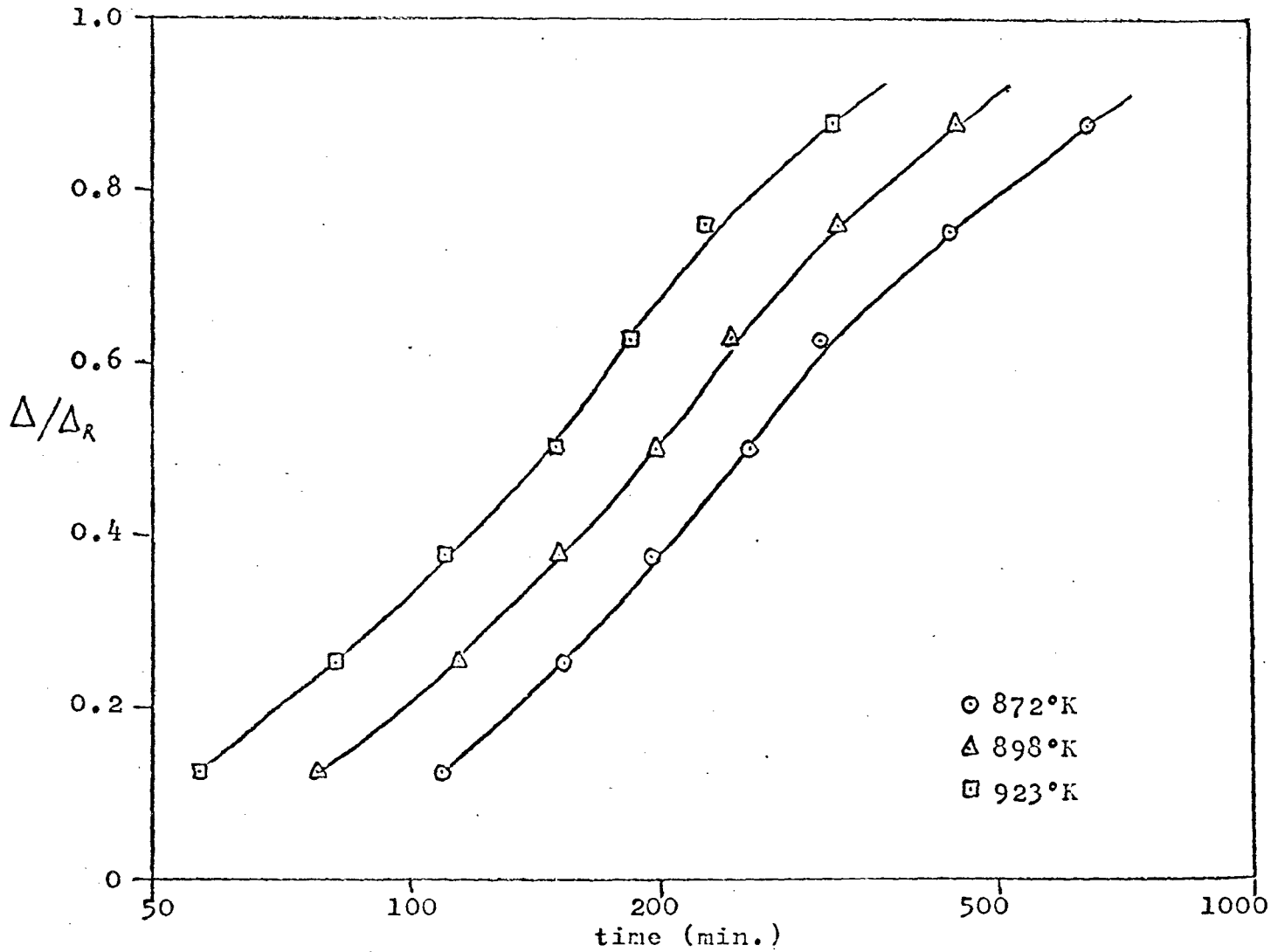

Fig. 31. Recovery of the Decrement during O_2 Desorption. Stage II. (The fraction of the decrement recovered in Stage II is plotted as a function of log t for several temperatures.)

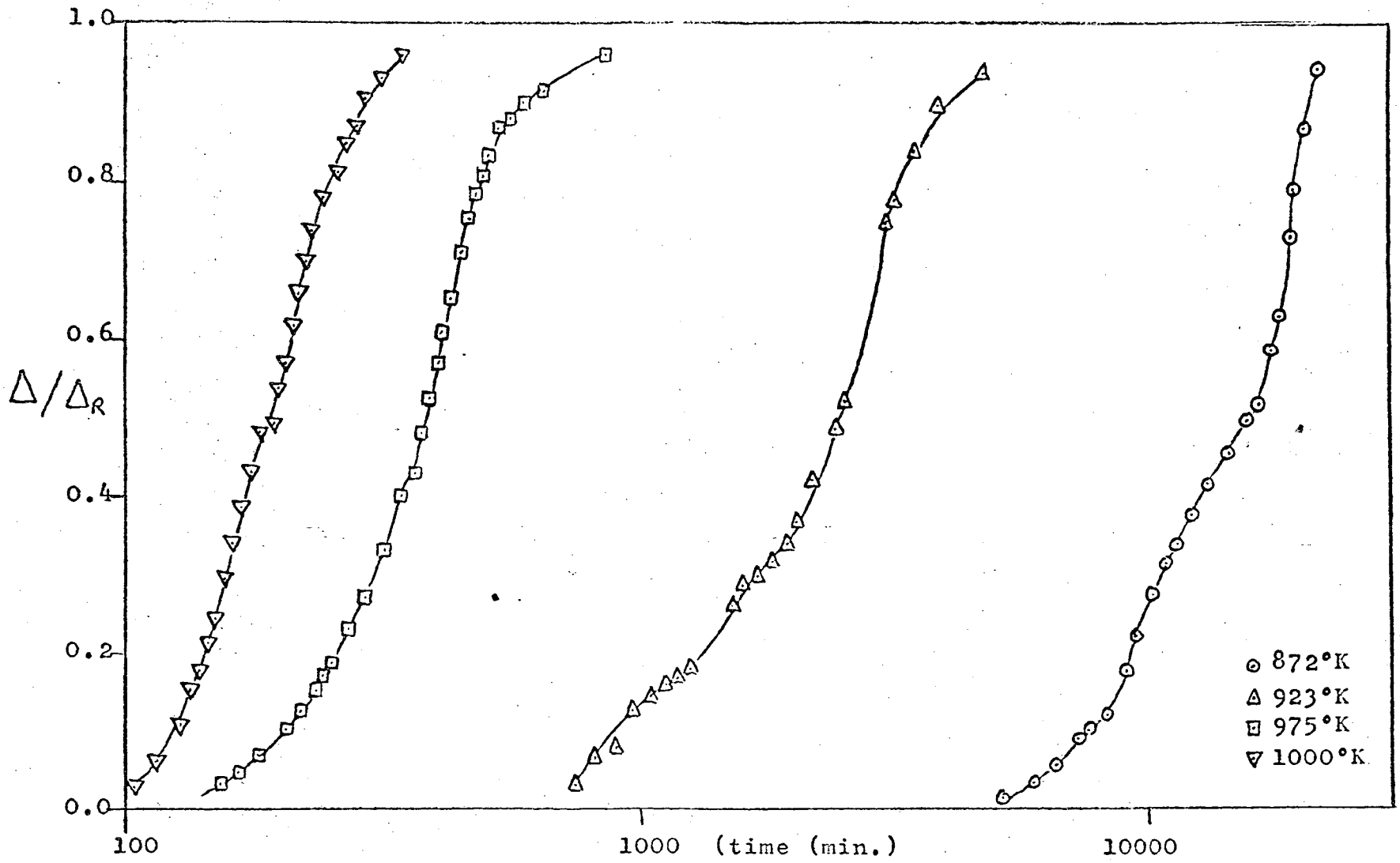

Fig. 32. Recovery of the Decrement during O_2 Desorption. Stage III. (The fraction of the decrement recovered in Stage III is plotted as a function of log t for several temperatures.)

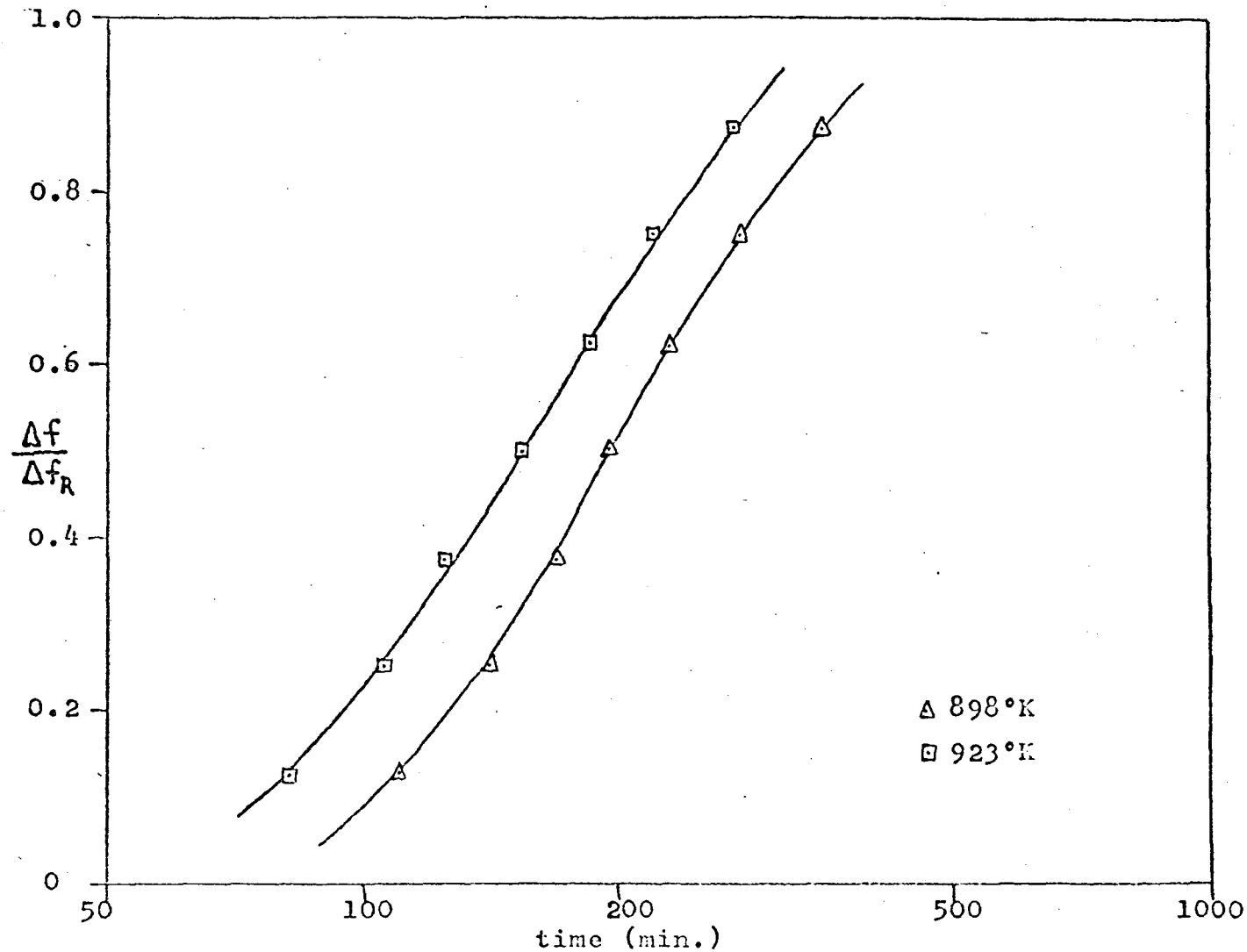

Fig. 33. Recovery of the Modulus Defect during O_2 Desorption. Stage II. (The fraction of the modulus defect recovered in Stage II is plotted as a function of log t for several temperatures.)

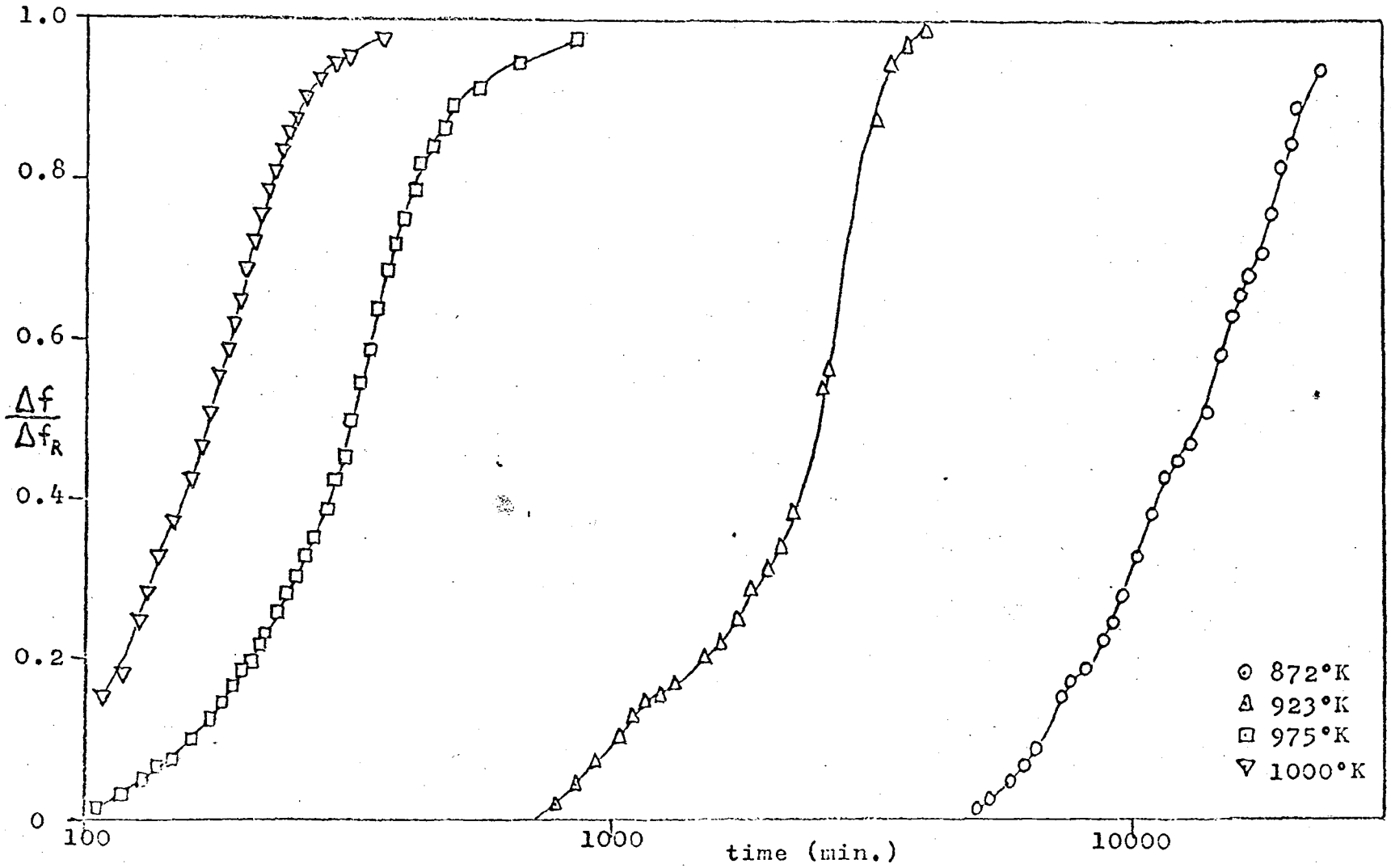

Fig. 34. Recovery of the Modulus Defect during O_2 Desorption. Stage III. (The fraction of the modulus defect recovered in Stage III is plotted as a function of log t for several temperatures.)

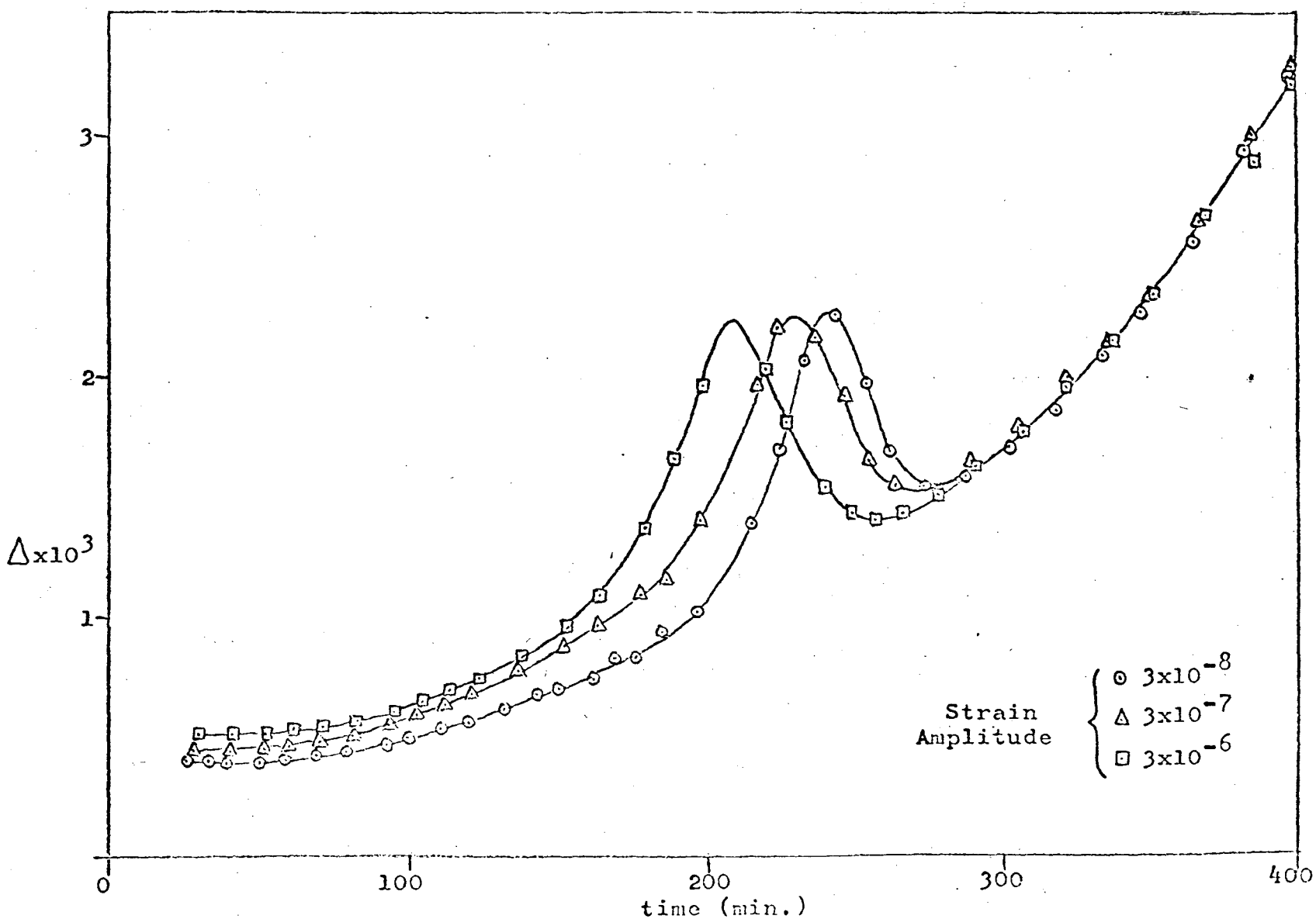

Fig. 35. The Decrement during O_2 Desorption at Three Different Strain Amplitudes (T = 975°K).

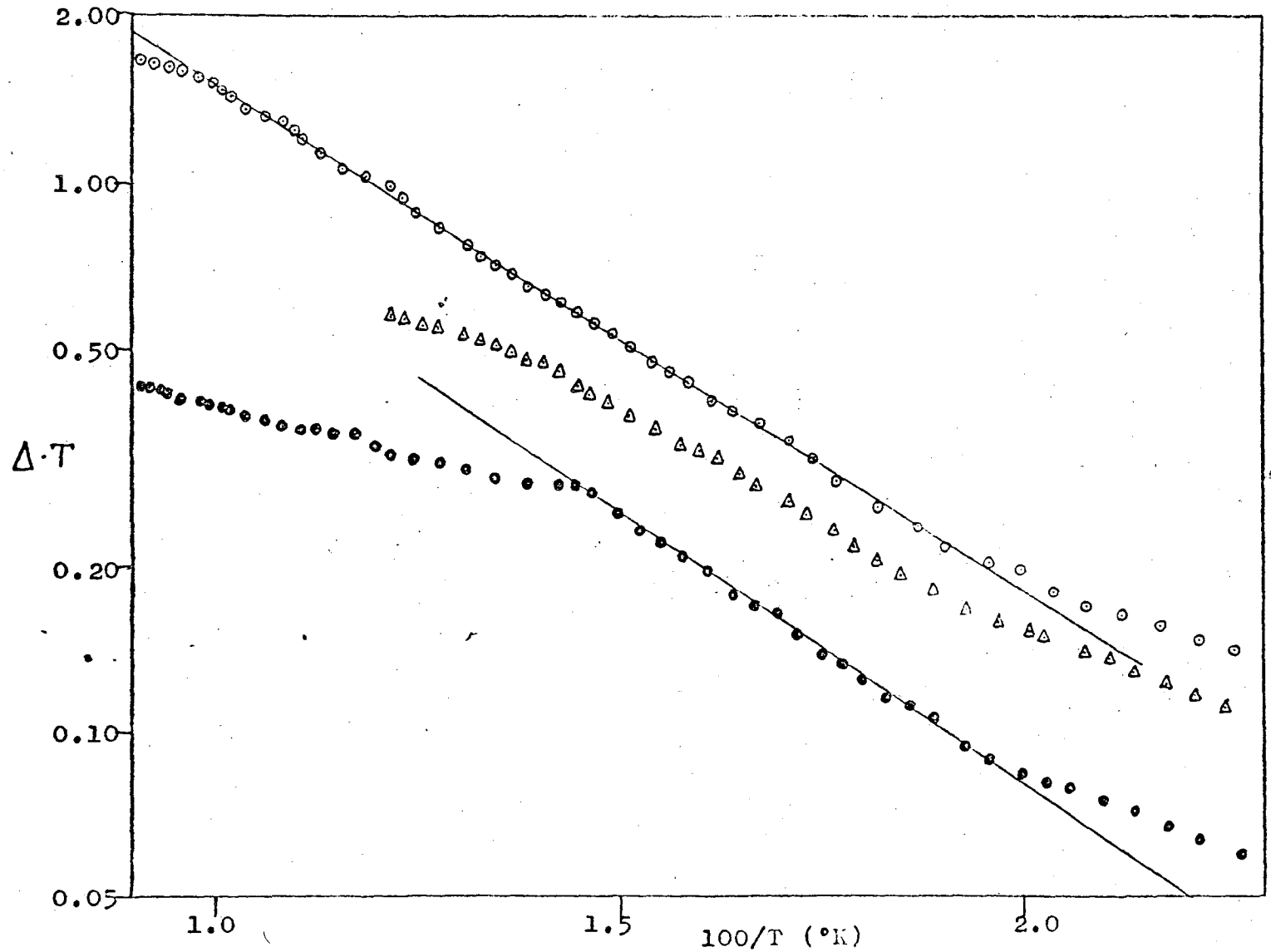

Fig. 36. Analysis of the Low Temperature 'Background' Internal Friction. (The quantity ln(Δ×T) is plotted as a function of 1/T (°K) for the low temperature measurements of Fig. 19.)

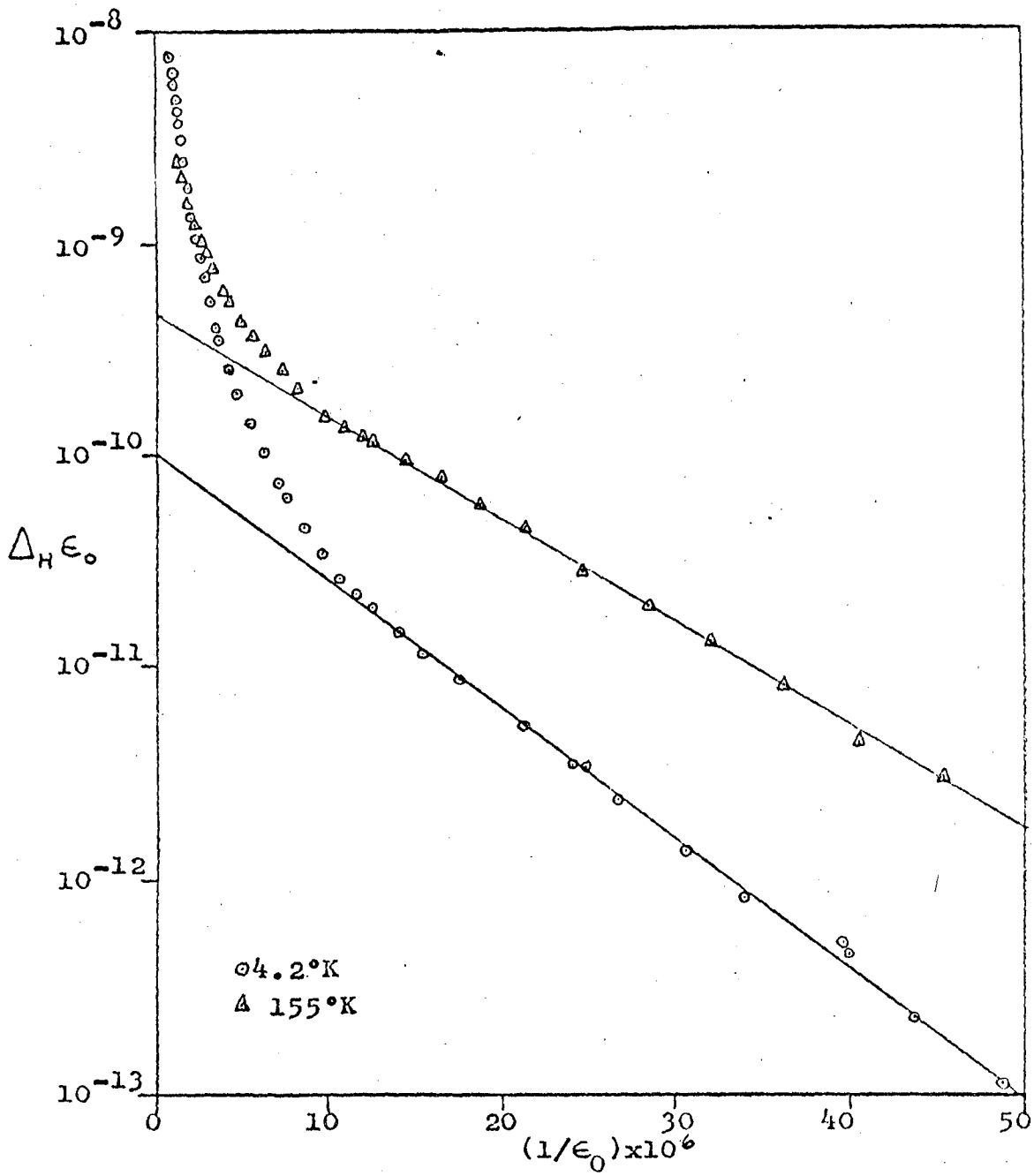

Fig. 37. Typical Granato-Lücke Plots for the Amplitude Dependent Component of the Decrement. (The plots $\log(\Delta_H \cdot \epsilon_0)$ vs. $1/\epsilon_0$ correspond to the data of Fig. 25.)

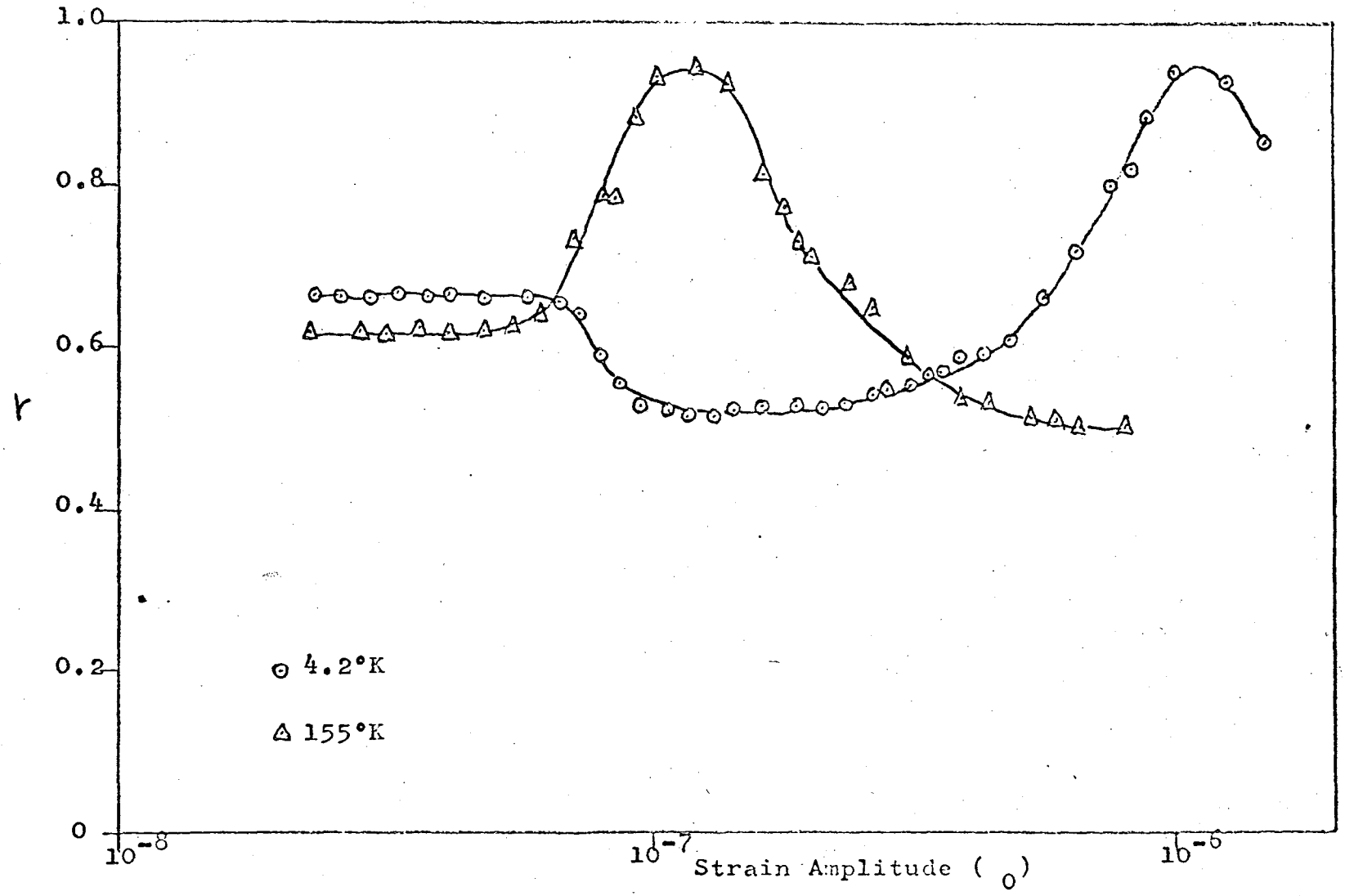

The ratio, γ, of the Amplitude Dependent Modulus Change, $(\Delta E/E)_H$, to the Amplitude Dependent Decrement, Δ_H, as a Function of Strain Amplitude for the Data of Fig. 37.

Fig. 38

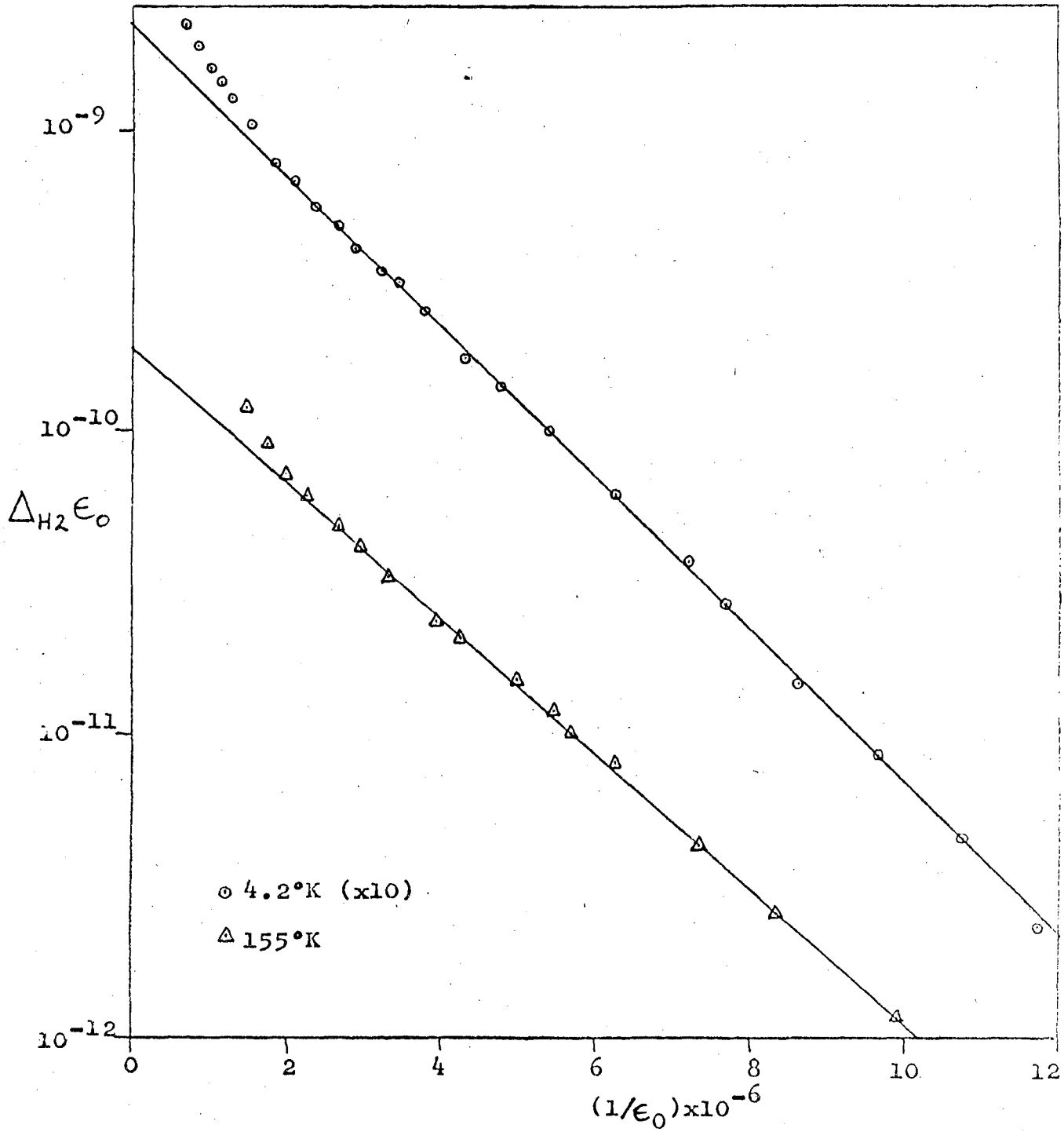

Fig. 39. Granato-Lücke Plot of the Remaining Amplitude Dependent Decrement, Δ_{H2}, after Subtracting the Maximum Contribution Expected from Δ_{H1} in Fig. 37.

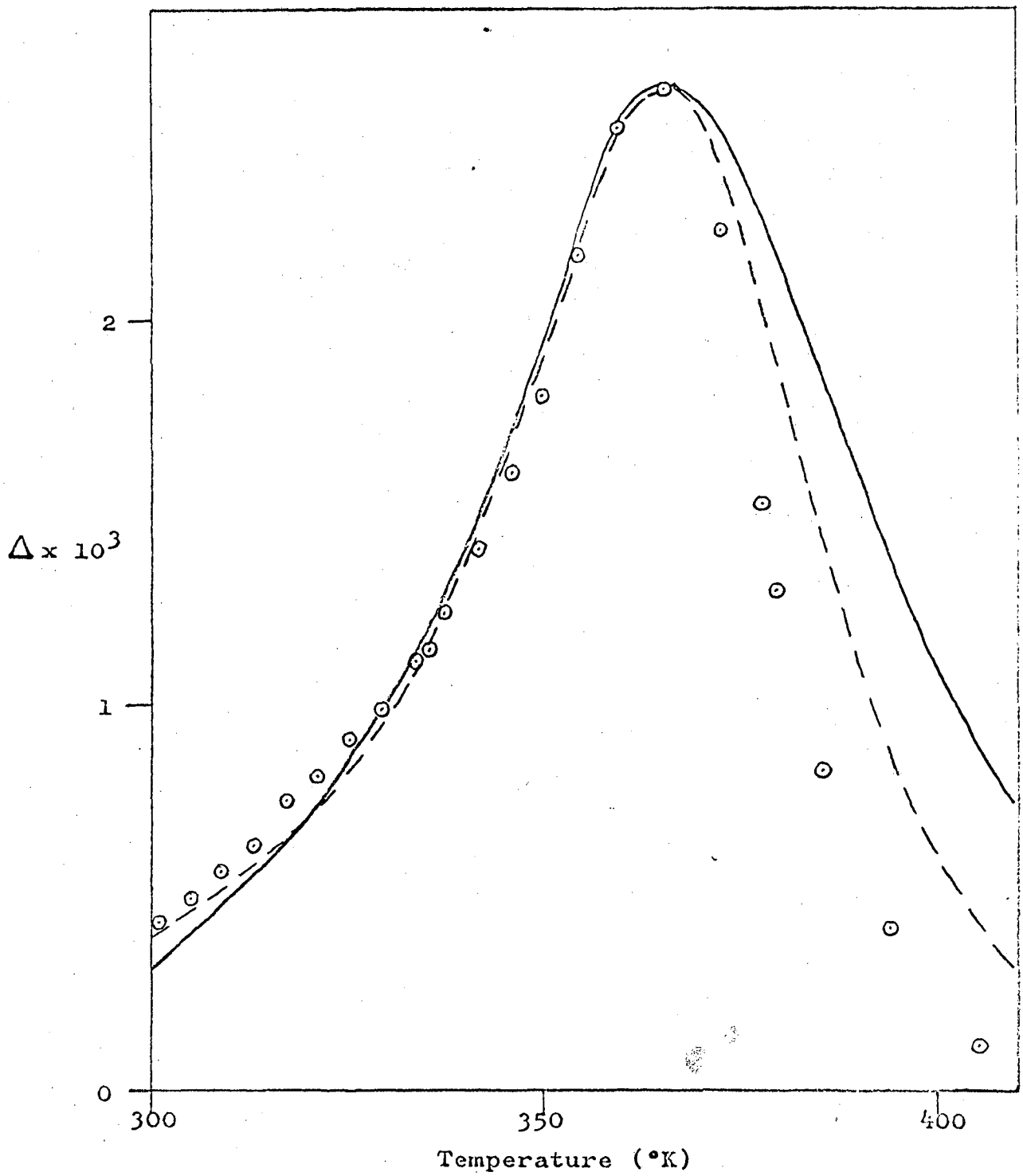

Fig. 40. Comparison of 365°K Peak Observed in 6-9's Silver Containing 40 ppm O_2 with the Theory Given in the Text (P. 134 ff). (The solid line corresponds to Eq. IV-49, while the dashed line is an approximation to Eq. IV-49 given by Eq. IV-50.)

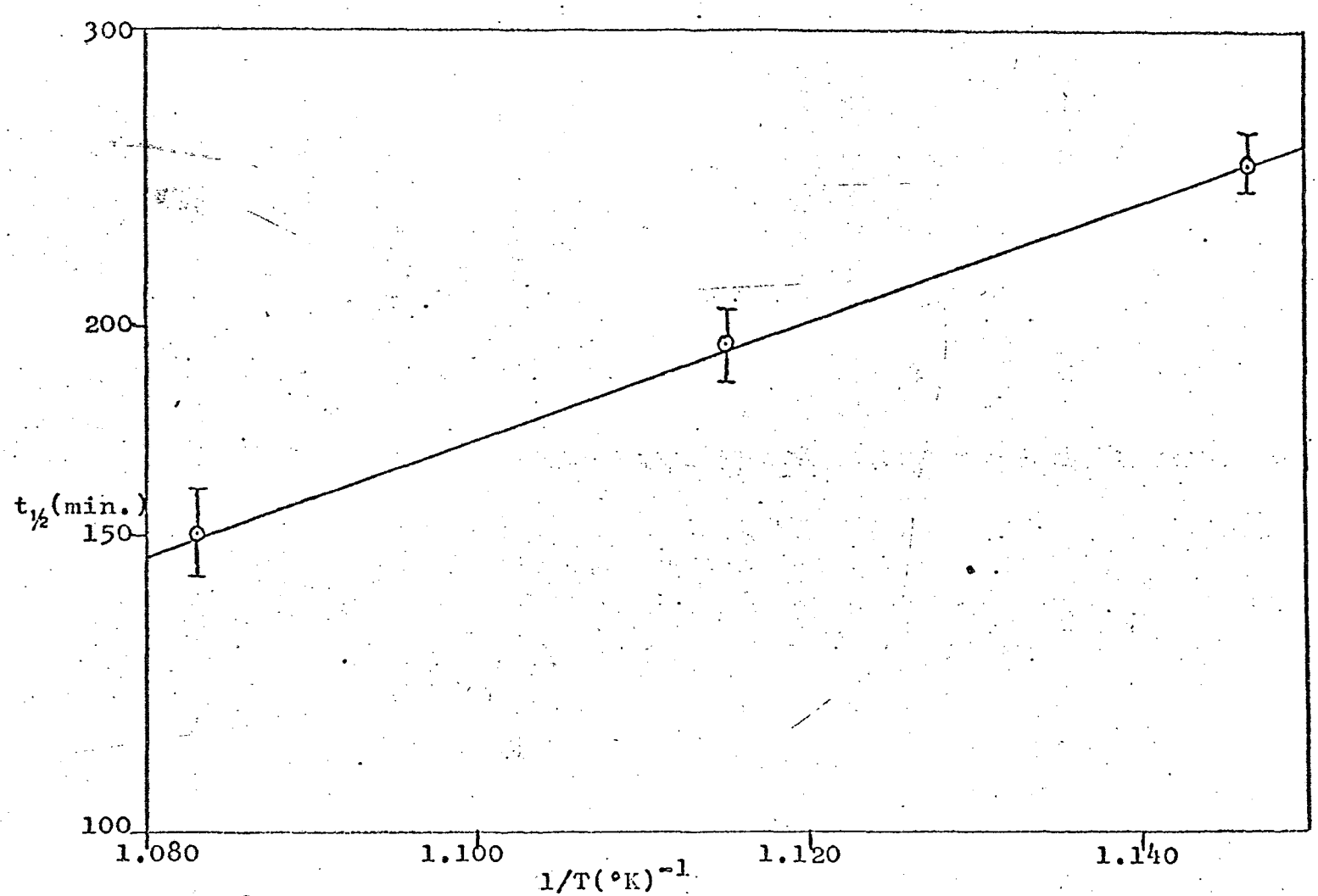

Fig. 41. Determination of the Activation Energy for Stage II. (The log of the time required to recover one-half the decrement is plotted as a function of 1/T (°K).)

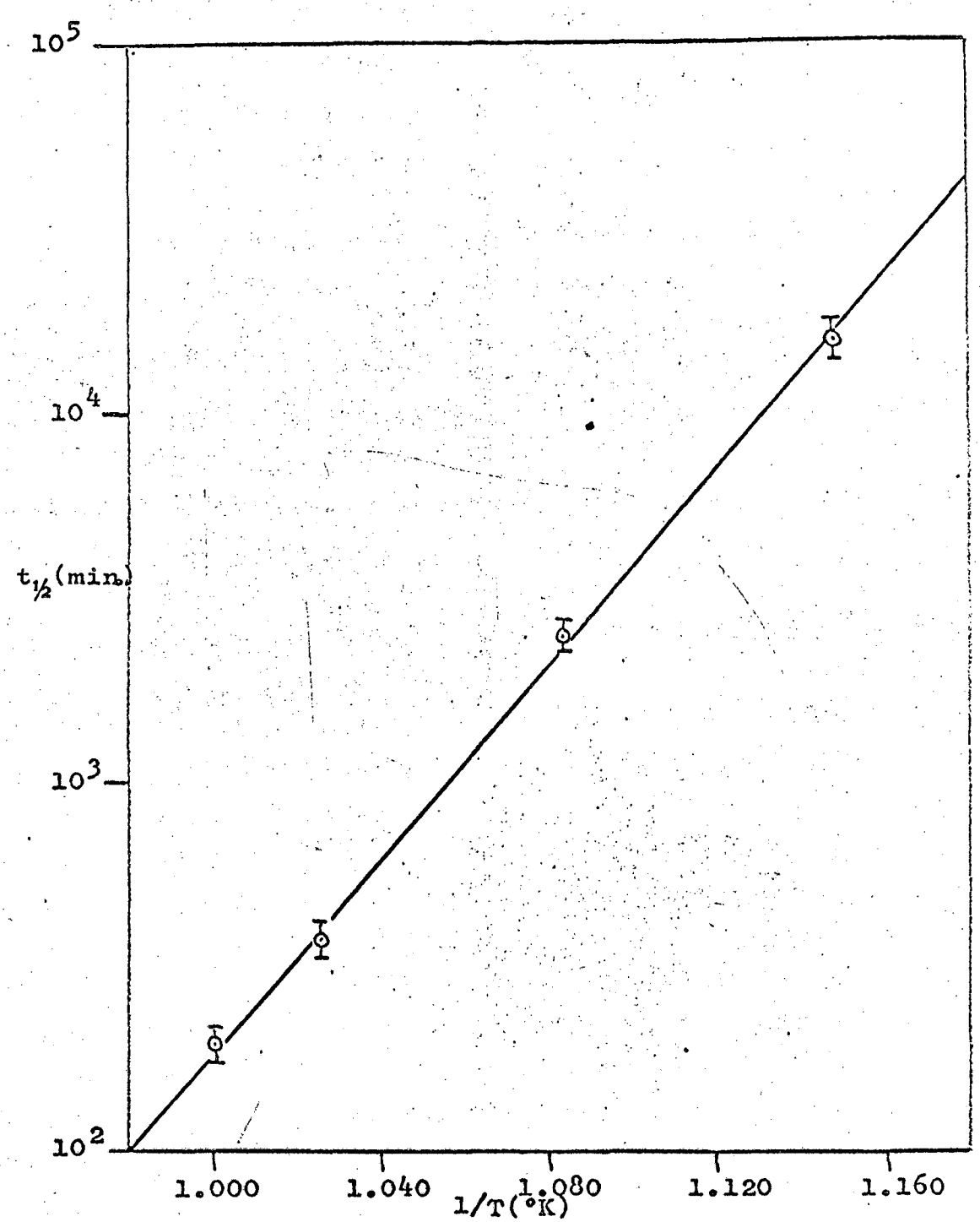

Fig. 42. Determination of the Activation Energy for Stage III. (The log of the time required to recover one-half the decrement is plotted as a function of 1/T (°K).)

This report was prepared as an account of Government sponsored work. Neither the United States, nor the Commission, nor any person acting on behalf of the Commission:

A. Makes any warranty or representation, expressed or implied, with respect to the accuracy, completeness, or usefulness of the information contained in this report, or that the use of any information, apparatus, method, or process disclosed in this report may not infringe privately owned rights; or

B. Assumes any liabilities with respect to the use of, or for damages resulting from the use of any information, apparatus, method, or process disclosed in this report.

As used in the above, "person acting on behalf of the Commission" includes any employee or contractor of the Commission, or employee of such contractor, to the extent that such employee or contractor of the Commission, or employee of such contractor prepares, disseminates, or provides access to, any information pursuant to his employment or contract with the Commission, or his employment with such contractor.